

# Lower Diamondoids and Their Derivatives as Molecular Building Blocks

BY

YONG XUE

B. S., Sichuan University, 2005

M. S., University of Illinois at Chicago, Chicago, 2008

THESIS

Submitted as partial fulfillment of the requirements  
for the degree of Doctor of Philosophy in Physics  
in the Graduate College of the  
University of Illinois at Chicago, 2012

Chicago, Illinois

Defense Committee:

G Ali Mansoori, Chair and Advisor  
Lahsen Assoufid, Argonne National Laboratory  
Serdar Ogut  
Mark Schlossman  
Michael Stroscio

## ACKNOWLEDGMENTS

I would like to thank my thesis committee—Professor G Ali Mansoori, Dr. Lahsen Assoufid, Professor Serdar Ogut, Professor Mark Schlossman, and Professor Michael Stroschio—for their unwavering support and assistance. They provided guidance in all areas that helped me accomplish my research goals and enjoy myself in the process.

A number of individuals who I encountered in the graduate training were especially helpful, here list some but not all my friends and colleagues at UIC who supported me with their thorough explanations of the experimental equipment and assistance for technical issues, special thanks to Dr. Jun Yin for the advice in the UHV (ultra-high vacuum) system, Dr. Yuanli Song and Dr. Boyang Wang for the suggestions in the MD simulation for nanoscale systems, Dr. Ling Wu for the help in (ATR) FT-IR-spectrometer.

I also would like to acknowledge the researchers in the Argonne National Laboratory who mentored me in the past years: Dr. Seth Darling for the Ambient AFM/STM system, Dr. Rula Diva for preparing the experimental samples, Dr. Nathan Guisinger for UHV STM systems and Dr. Brandon Fisher for 4-probe system.

The computer facility staff at UIC also assisted me a lot in my computational research.

I am extremely grateful to my family members who have always been supportive of me, without whom this project would never have been accomplished.

# TABLE OF CONTENTS

CHAPTER 1	INTRODUCTION .....	1
1.1	THE FASCINATING IDEA OF BOTTOM-UP FABRICATION .....	1
1.1.1	<i>Coming of Nano Era.....</i>	<i>1</i>
1.1.2	<i>General steps and fundamental questions of the nanoscience .....</i>	<i>2</i>
1.1.3	<i>The outline of thesis.....</i>	<i>4</i>
1.2	MOLECULAR ELECTRONICS AND SELF-ASSEMBLY .....	5
1.2.1.	<i>The development of Molecular Electronics devices and their theoretical studies .....</i>	<i>5</i>
1.2.2.	<i>Towards the fabrication of molecular IC's .....</i>	<i>5</i>
1.3	DIAMONDOIDS AS MOLECULAR BUILDING BLOCKS .....	6
1.3.1	<i>Diamondoids family and their applications .....</i>	<i>6</i>
1.3.2	<i>Lower Diamondoids and their Derivatives .....</i>	<i>8</i>
1.4	GENERAL METHODS FOR MOLECULAR SCALE STUDIES .....	9
CHAPTER 2 ELECTRONIC STRUCTURES OF THE SEVEN DIAMONDIDS-----		
QUANTUM COMPUTATION STUDIES .....		11
2.1	THE FRAMEWORK OF THEORIES .....	11
2.1.1	<i>Hartree-Fock Theory and Self-consistent method.....</i>	<i>12</i>
2.1.2	<i>Introduction to Density functional Theory and exchange-correlation functions .....</i>	<i>15</i>
2.1.3	<i>Basis sets, atomic orbitals, molecular orbitals, and total wave functions .....</i>	<i>17</i>
2.2	QUANTUM COMPUTATIONAL STUDIES OF DIAMONDID MOLECULES .....	19
2.2.1	<i>Computation results comparison and methods validation .....</i>	<i>19</i>
2.2.2	<i>HOMO and LUMO for seven lower diamondoids.....</i>	<i>20</i>

2.2.1 Optimized geometries and atomic charge in molecules .....	22
CHAPTER 3 QUANTUM CONDUCTANCE OF THE SEVEN DIAMONDOIDS----- AB	
INITIO NEGF STUDIES.....	23
3.1 THEORETICAL FRAMEWORK .....	23
3.1.1 Introduction to Non-Equilibrium Green's Functions (NEGF).....	24
3.1.2 NEGF formalism for transportation in two-probe system.....	27
3.1.3 <i>ab initio</i> NEGF with DFT.....	30
3.2 TWO PROBE SYSTEM WITH SEVEN DIAMONDIODS .....	36
3.2.1 Calculation tools and System setups .....	36
3.2.2 Computation settings .....	38
3.3 CALCULATION PROCEDURES, RESULTS AND DISCUSSIONS .....	39
3.3.1 Quantum conductance calculations.....	39
3.3.2 Adamantane and Diamantane .....	41
3.3.3 Memantine, Rimantadine and Amantadine .....	41
3.3.4 ADM•Na and DIM•Na.....	45
3.3.5 I-V and G-V characteristics.....	47
3.4 CONCLUSIONS .....	48
CHAPTER 4 SELF-ASSEMBLY AND PHASE TRANSITIONS-----MD STUDIES .....	
4.1 SELF-ASSEMBLY AND MD SIMULATIONS OF DIAMONDODS .....	50
4.1.1 Self-assembly researches of diamondoids .....	50
4.1.2 Phase transition MD simulations .....	51
4.2 INTRODUCTION TO MOLECULAR DYNAMICS SIMULATIONS.....	52
4.2.1 Molecular interaction, Quantum mechanics and Force fields in nutshell. ....	52

4.2.2 OPLS-AA force field. ....	54
4.2.3 Temperature, temperature couplings and simulated annealing in MD.....	56
4.2 MD SIMULATION PROCEDURES AND RESULTS .....	58
4.2.1 Settings of simulation system and the validations .....	58
4.2.2 Hydrogen-bonds distribution of Group 2 .....	65
4.3 RADIAL DISTRIBUTION FUNCTIONS (RDFs) AND STRUCTURE FACTORS (SFs) ANALYSIS .....	67
4.3.1. Adamantane and ADM•Na .....	67
4.3.2. Diamantane and ADM•Na: .....	69
4.3.3. Amantadine, Rimantadine and Memantine .....	70
4.3.4 Density dependence studies of phase transition points .....	73
4.4 CONCLUSION .....	75
REFERENCES .....	76
APPENDIX A.....	86
APPENDIX B .....	93
VITA.....	100

## LIST OF TABLES

### TALBESPAGE

TABLE 1. MOLECULAR FORMULAS AND STRUCTURES OF ADAMANTANE, DIAMANTANE, MEMANTINE, RIMANTADINE, AMANTADINE, OPTIMIZED ADM•NA AND OPTIMIZED DIM•NA MOLECULES. IN THESE FIGURES BLACKS REPRESENT –C, WHITES REPRESENT –H, BLUES REPRESENT –N AND PURPLES REPRESENT –NA.....	8
TABLE 2. LUMO AND HOMO OF ADAMANTANE WITH DIFFERENT BASIS UNDER DFT CALCULATIONS. ....	20
TABLE 3 LUMO AND HOMO OF ADAMANTANE IN VARIOUS HF METHODS WITH 6-311++G(D, P) BASIS .....	20
TABLE 4. HOMO AND LUMO OF THE THREE GROUPS. (FERMI ENERGY=0 eV) .....	21
TABLE 5 HOMO AND LUMO OF SEVEN MOLECULES IN CC-PVQZ BASIS. ....	22
TABLE 6. QUANTUM CONDUCTANCE ( $G$ ), IN [ $\mu S$ ], AND CENTRAL REGION WIDTH, IN [ $\text{\AA}$ ], OF THE THREE DIAMONDDOIDS GROUPS UNDER ZERO BIAS AND THE CORRESPONDING ORIENTATIONS.....	40

## LIST OF FIGURES

### FIGURESPAGE

FIGURE 1. SEMI-INFINITE TWO PROBE SYSTEM .....	27
FIGURE 2. SCHEME OF AB INITIO NEGF FOR TWO PROBE SYSTEM.....	35
FIGURE 3. THE TWO SEMI-INFINITE LINEAR AND 2×2 GOLD (AU) CHAIN ELECTRODES .....	37
FIGURE 4. TRANSMISSION SPECTRUM IN AU LINEAR ELECTRODES CASES. (A)TRANSMISSION SPECTRUM OF GROUP 1. (B)TRANSMISSION SPECTRUM OF GROUP 2 CORRESPONDING TO “ORIENTATION 1” IN TABLE 4. (C) TRANSMISSION SPECTRUM OF GROUP 3 CORRESPONDING TO “ORIENTATION 1” IN TABLE 4.....	43
FIGURE 5. TRANSMISSION SPECTRUM IN AU 2X2 UNIT CELL CASES. (A)TRANSMISSION SPECTRUM OF GROUP 1. (B) TRANSMISSION SPECTRUM OF GROUP 2 CORRESPONDING TO “ORIENTATION 1” IN TABLE 4. (C) TRANSMISSION SPECTRUM OF GROUP 3 CORRESPONDING TO “ORIENTATION 1” IN TABLE 4.....	44
FIGURE 6. $G [\mu S]$ vs. $V [V]$ AND $I [\mu A]$ vs. $V [V]$ CHARACTERISTICS OF ADM•NA AND DIM•NA IN LINEAR ELECTRODES CORRESPONDING TO THEIR HORIZONTAL ORIENTATIONS (ORIENTATIONS 2 IN TABLE 4). .....	47
FIGURE 7. SNAPSOTS FROM MD SIMULATIONS USING VARIOUS NUMBERS OF ADAMANTINE MOLECULES ( $2^3, 3^3, 4^3, 5^3, 6^3, 7^3, 8^3, 9^3$ ) .....	60
FIGURE 8. STAGES OF SIMULATION PROCEDURE: (A) INITIAL 5x5x5 MD SIMULATION BOX; (B) MOLECULES RELAXED IN VACUUM AT 100 K AFTER A SHORT MD SIMULATION; (C) BOXED SIMULATION SYSTEM WITH OVERALL GAS DENSITY; (D) GAS PHASE AS A RESULT OF EQUILIBRATING SIMULATION IN THE NVT ENSEMBLE; (E) THE LIQUID STATE; (F) FINAL SELF-ASSEMBLY OF MOLECULES TO SOLID STATE. ....	61
FIGURE 9. SELF-ASSEMBLY SNAPSOTS OF 125 MOLECULES OF THE SEVEN COMPOUNDS (FROM TOP: ADAMANTANE, DIAMANTANE, AMANTADINE, RIMANTADINE, MEMANTINE, ADM•NA., ADM•NA) AS TEMPERATURE [K] IS DECREASED.....	63

FIGURE 10. MD SNAPSHOTS OF (FROM TOP TO BOTTOM) AMANTADINE, RIMANTADINE AND MEMANTINE AND AT 50K HYDROGEN BONDS LOCATION .....	65
FIGURE 11. THE NUMBER OF HYDROGEN BONDS FOR AMANTADINE, MEMANTINE AND RIMANTADINE VS. TEMPERATURE. AS TEMPERATURE DECREASES THE NUMBERS OF H-BONDS INCREASE, AND TEND TO MAXIMUM NUMBERS FOR THE THREE DERIVATIVES. ....	66
FIGURE 12. HYDROGEN-BOND DISTANCE DISTRIBUTION (LEFT) AND HYDROGEN-BOND ANGLE DISTRIBUTION (RIGHT) AT 60K FOR AMANTADINE, RIMANTADINE AND MEMANTINE. THE MOST POSSIBLE HYDROGEN-BOND LENGTHS ARE AROUND 0.3 NM FOR THE THREE MOLECULES. THE HYDROGEN-BOND ANGLES SEEM RANDOMLY DISTRIBUTED.....	66
FIGURE 13. RADIAL DISTRIBUTION FUNCTIONS (LEFT) AND STRUCTURE FACTORS (RIGHT) OF ADAMANTANE AT 450K, 300K AND 150K FOR GAS, LIQUID AND SOLID STATES, RESPECTIVELY. ....	68
FIGURE 14. RADIAL DISTRIBUTION FUNCTIONS (LEFT) AND STRUCTURE FACTORS (RIGHT) OF ADM•NA AT 600K, 450K AND 200K FOR GAS, LIQUID AND SOLID STATES, RESPECTIVELY. ....	68
FIGURE 15. RADIAL DISTRIBUTION FUNCTIONS (LEFT) AND STRUCTURE FACTORS (RIGHT) OF DIAMANTANE AT 500K, 400K AND 300K FOR GAS, LIQUID AND SOLID STATES, RESPECTIVELY. ....	69
FIGURE 16. RADIAL DISTRIBUTION FUNCTIONS (LEFT) AND STRUCTURE FACTORS (RIGHT) OF ADM•NA AT 600K, 500K AND 400K FOR GAS, LIQUID AND SOLID STATES, RESPECTIVELY. ....	70
FIGURE 17. RADIAL DISTRIBUTION FUNCTIONS (LEFT) AND STRUCTURE FACTORS (RIGHT) OF AMANTADINE AT 450K, 370K AND 300K FOR GAS, LIQUID AND SOLID STATES, RESPECTIVELY. ....	71
FIGURE 18. RADIAL DISTRIBUTION FUNCTIONS (LEFT) AND STRUCTURE FACTORS (RIGHT) OF RIMANTADINE AT 500K, 430K AND 250K FOR GAS, LIQUID AND SOLID STATES, RESPECTIVELY .....	71
FIGURE 19. RADIAL DISTRIBUTION FUNCTIONS (LEFT) AND STRUCTURE FACTORS (RIGHT) OF MEMANTINE AT 500K, 430K AND 250K FOR GAS, LIQUID AND SOLID STATES, RESPECTIVELY. ....	72
FIGURE 20. RADIAL DISTRIBUTION FUNCTIONS OF THE SEVEN COMPOUNDS (FROM LEFT: ADAMANTANE, DIAMANTANE, AMANTADINE, RIMANTADINE, MEMANTINE, ADM•NA., ADM•NA) IN THE SELF-ASSEMBLED (SOLID) STATE. ....	72



FIGURE 21. STRUCTURE FACTORS OF THE SEVEN COMPOUNDS (FROM LEFT: ADAMANTANE, DIAMANTANE, AMANTADINE, RIMANTADINE, MEMANTINE, ADM•NA., ADM•NA) IN THE SELF- ASSEMBLED (SOLID) STATE. ....	73
FIGURE 22. POTENTIAL ENERGY VS. TEMPERATURE RAW SIMULATION DATA OF 125 ADAMANTANE MOLECULES ENSEMBLE SYSTEM AT DIFFERENT DENSITY FROM 5, 10, 20, 25 AND 40G/L SIMULATED ANNEALING FROM 500K-200K, SHOWING DENSITY DEPENDENCE OF PHASE TRANSITION POINTS. ...	74
FIGURE 23. TOTAL POTENTIAL ENERGY VS. TEMPERATURE RAW SIMULATION DATA OF 64 ADAMANTANE MOLECULES ENSEMBLE SYSTEM AT DIFFERENT DENSITIES (5, 10, 20, 25 AND 40G/L) USING SIMULATED ANNEALING TECHNIQUE SHOWING DENSITY DEPENDENCE OF PHASE TRANSITION POINTS. .....	74

## LIST OF ABBREVIATIONS AND SYMBOLS

ADM	Adamantane
ATK	Atomistix ToolKit
DFT	Density functional theory
DIM	Diamantane
DZP	Double zeta polarization
HOMO	Highest occupied molecular orbital
LDA-PZ	Perdew-Zunger local density approximation
LUMO	Lowest unoccupied molecular orbital
MED	Molecular Electronic Devices
NEGF	Non-equilibrium Green's functions
Ry	Rydberg
VNL	Virtual Nanolab
$e$	Electron charge
E	Energy
$g$	Conductance
$g_0$	Quantum conductance $g_0 = \frac{2e^2}{h} = 77.5 \mu S$
H	Hamiltonian
I	Current
T	Transmission
$V_b$	Bias potential
$\mu S$	$10^{-6}$ Siemens

## SUMMARY

Diamondoid molecules are cage-like, ultra-stable, saturated hydrocarbons (known as cage-hydrocarbons). These molecules have a diamond-like structure consisting of a number of six-member carbon rings fused together, and these carbon-carbon framework constitutes the fundamental repeating unit in the diamond lattice structure. Due to their six or more linking groups, highly symmetrical and strain free structures, controllable nanostructural characteristics and non-toxicity, diamondoids have found major applications as templates or molecular building blocks (MBBs) in molecular manufacturing, polymer synthesis, drug delivery, drug targeting, DNA-directed assembly, DNA-amino acid nanostructure formation, and host-guest chemistry. In addition to the structural traits, diamondoid derivatives show interesting electronic properties and have excellent potential for building diamondoid-based molecular electronic devices, nano-electro-mechanical systems (NEMS) and micro-electro-mechanic system (MEMS). Diamondoid molecules and their derivatives have been recognized as promising MBBs candidates in the field of nanotechnology.

In this project, electronic, phase-transition and self-assembly properties of seven molecules are studied, which are two lower diamondoids: adamantane ( $C_{10}H_{16}$ ), diamantane ( $C_{14}H_{20}$ ); three adamantane derivatives: amantadine ( $C_{10}H_{17}N$ ), memantine ( $C_{12}H_{21}N$ ), rimantadine ( $C_{11}H_{20}N$ ); and two organo-metallic derivatives of adamantane molecules: ADM•Na ( $C_{10}H_{15}Na$ ), DIM•Na ( $C_{14}H_{19}Na$ ).

The integration of Non-Equilibrium Green's Function (NEGF) theory with Density functional theory (DFT) allows the first-principle calculations of quantum conductances and other essential electronic properties for these seven molecules. ATK and VNL software, which comprise of

TRANSTA-C package, are used to construct semi-infinite linear Au and  $2\times 2$  Au probe systems for the calculations. The results show that the quantum conductance of adamantane and diamantane are very small as predicted from the large HOMO-LUMO gap, while the derivatives of these diamondoids have considerable conductance at certain particular orientations and show interesting electronic properties. The nontrivial conductance indicates that residues like nitrogen and sodium atoms have great effects on the conductance and electronic properties of single molecule. Moreover, the quantum conductances of such molecules are significantly different at various molecule orientations and at different distances between electrodes. The various conductances confirm the influence of system structures on electronic properties. In addition, when conductance is calculated, the central region considered includes a few layers of the electrodes and there are more atoms in the  $2\times 2$  case, as a result, in the case of Au  $2\times 2$  Electrodes the conductance is generally greater than the linear case.

Self-assembly and phase transition properties can be studied by Molecular Dynamics (MD) Simulation using simulated annealing methods in 125-molecule simulation systems. DFT calculations are applied to optimize the molecular geometries and obtain atomic electronic charges for the corresponding MD simulations. The nature of self-assembly in these molecules is a structure-dependent phenomenon, and the final self-assembly structures depend on the different bonding types present in the molecular structure of these various molecules. Radial distribution functions and structure factors studies show different effects of -Na and -NH<sub>2</sub> groups on the final structures, while the potential energy vs. temperature curves manifest that these residues can increase phase transition temperatures.

## **Chapter 1 INTRODUCTION**

### **1.1 The fascinating idea of bottom-up fabrication**

#### **1.1.1 Coming of the Nano Era**

Mankind being able to stand on the top of the food chain of the ecosystem is essentially due to the special capabilities to create and utilize complicated tools to change their environments. Building novel apparatus has been the crucial element of social and industrial revolutions since the very beginning of human history. Now, in the second decade of 21st century, we are at the entrance of Nano Era in which one can fabricate instruments from atoms and molecules. Although the words ‘atom’ and ‘molecule’ have been coined long time ago from Greek and Latin, only until the first a few decades in the 20th century, after the establishments of the Special Relativity and Quantum Mechanics, the fundamental principles of the atoms and molecules were finally revealed to human beings. Many passionate scientists have started to harness their knowledge and technologies to fulfill the vision of manufacture everything from atomic/molecular building blocks, since the launch of nanoscience and nanotechnology by Richard Feynman who pointed that there was no physical limit of building things from the ‘bottom’ at the end of 1959.<sup>1</sup>

Although in the sense of Quantum Mechanics electrons are ‘indistinguishable’ to us,<sup>2-4</sup> we have been able to ‘see’ and ‘feel’ individual atoms and molecules experimentally after the invention of two power tools Scanning Tunneling Microscope (STM) and Atomic Force

Microscope (AFM).<sup>5-7</sup> Their successful stories approved at least three points about the philosophy of Nanoscience: 1. atoms and molecules theoretically can be the building blocks for the purpose of the bottom-up nanofabrication among many other evidences, such as X-ray, neutron and electron diffractions;<sup>8</sup> 2. We can treat atoms/molecules as mass point classically but with special caveat to the quantum effect of electrons and subatomic particles, which is also one of the justifications of Molecular Dynamics Simulations;<sup>9</sup> 3. Innovative instruments are the necessities to any scientific and technological breakthrough. Therefore, a brand new scheme of fabrication could and should appear based on the understanding of the atomic/Molecular Building Blocks (MMBs) and the competence to manipulate them. We already know almost all the fundamental physics principles that are necessary for 'bottom-up' fabrication, and no limitation is imposed for that; however, there are complications arise largely due to the intricate nature of many-body nano systems which make obtaining exact mathematical solutions impractical and novelties of nano fabrication that may demand original engineering processes. As researches in any other fields, there should be many 'trial and error' in nanoscience investigations whose intensity determines the overall progress.<sup>10</sup>

### 1.1.2 General steps and fundamental questions of the nanoscience

If we intend to build things in the bottom-up fashion, then the rudimental questions we should ask could be: 1.what structures can we construct for practical purpose? 2. What are the building-blocks for those structures? 3 Through what methods and processes do we fabricate the desired structures? At molecular level, the same questions rise, however, accompanied with tremendous scientific and engineering novelties and difficulties, which lays the possibilities and challenges of nanoscience and nanotechnology.

To answer the first question- the market demand, the main driven force is from the semiconductor industry which has been the largest application area of condensed matter physics for decades; according to the Morse's law,<sup>11, 12</sup> the traditional top-down manufacturing processes in microelectronics will reach its limit(mainly due to the optical limits in the process of photolithographic). The groundbreaking technology at molecular level is inevitable and this triggered, naturally, the birth of Molecular Electronics,<sup>13</sup> which is mainly about the possibilities of constructing devices at molecular level and studying the electronic properties of them. It is also one object of this project--to devise functionally molecular electronic devices.

Regarding the second question: what are the MMBs in the Nano era? Different from the traditional semiconductor/microelectronics industry where silicon is the ubiquitous element, current Molecular Electronics/Moletronics researches are mainly base on Carbon an element which builds biological organs. Numerous researches on carbon base molecular devices have been performed in the past decades; especially, the hydrocarbon molecules which have been regarded as the candidates of MMBs at the launch of researches in nanotechnology.<sup>10, 14</sup> Among them the most reported are Carbon Nano Tubes (CNT), Fullerene C<sub>60</sub>, polymers, DNA and the very subject of this project Diamondoids molecules whose potential as MMBs will be addressed intensively in this thesis.

To answer the third question- The concept of bottom-up fabrication is familiar to chemists, since building molecules is one of the main goals and practices of organic synthesis, molecular modeling and drug design related fields<sup>15</sup>; therefore many research methods in those fields may be directly borrowed to fulfill the third question. From the engineering point of view, however, to productize molecular devices i.e. to manufacture Integrated Circuits (IC) for Molecular Electronics may require not only the traditional methods in any of the current research fields but

also unusual methods that could be rejuvenated or original. The bio-mimicking methods has been suggested<sup>1, 15</sup> and probably it is one of the a few achievable methods when come to complex functional systems. Although the intra- and inter-action mechanisms of the bio-molecules are still not completely revealed, we still in principle can design a scheme which could imitate the bottom-up strategy to build molecular IC from MMBs, as proteins from DNA/RNAs; and this scheme does not have to relate any bio-molecules, it could be small molecules, polymers or inorganic surfaces, as long as it works as the directing molecules as DNA and the MMB can aggregate into functional molecular IC's by self-assembly, chemical synthesis, or other methods. Certainly, 'There's plenty of room at the bottom', and we just need to find where it is.

### 1.1.3 The outline of thesis

This thesis presents my basic understandings and main successful scientific works done so far on the way to build molecular electronic devices; the results are still far from the final products that we may see in the future, but it serves as the milestones and cornerstones to that vision. The layout of this thesis is presented in four chapters and appendices as below:

Chapter 1 introduces the background of Molecular Electronics, diamondoid molecules and comparison of methods, also it implies the purpose of this project; Chapter 2 covers the characteristics of the seven diamondoids and derivatives studied in the course of this research through computational quantum computational methods, which was the first step of treating diamondoids as MMBs; Chapter 3 expounds the electronic properties of diamondoids and the potential for molecular electronic devices; Chapter 4 is the results of the MD simulations of the seven diamondoids and derivatives to demonstrate the probability of building molecular structures with those molecules. The more detailed theories can be found in the Appendices.



## 1.2 Molecular Electronics and Self-assembly

### 1.2.1. The development of Molecular Electronics devices and their theoretical studies

As traditional microelectronic devices, molecular electronics devices (MED) family should include diodes and transistors to form logic gates-- AND, OR, and NOT, and then construct hierarchy devices which are functional as the devices in normal computers, such as CPU, RAM, hard drivers. The first MED reported was molecular rectifier in 1974 by Aviram and Ratner.<sup>16</sup> Since then various MED studies have performed, there are Nano-wire logic gates,<sup>17</sup> Carbon nano-tube transistors,<sup>18, 19</sup> self-assembled monolayers formed Field-effect transistors,<sup>20, 21</sup> molecules formed digital information storage/memory device,<sup>22, 23</sup> quantum interference effect transistor,<sup>24</sup> DNA-based devices<sup>25, 26</sup> and many other related researches.

The transportation theories at molecular scale also have been undergoing ups and downs since 1974.<sup>13</sup> All the theories are about the transportation of electrons in the nanoscale structures. The main evolutions range from traditional Kubo formalism and Landauer approach, currently popular Non-equilibrium Green's function (NEGF) formalism, and the hydrodynamics theory of electron liquid.<sup>27</sup> Computationally, other *ab initio* techniques have also been involved, *e.g.* Density Functional Theory has been used with Landauer method and NEGF formalism in various manners.

### 1.2.2. Towards the fabrication of molecular Integrated Circuits (IC's)

Many chemists, material scientists and biologists, on the other hand, have declared the challenge of building 'anything' from atoms and molecules since the publishing of Drexler's book *Engines of Creation*.<sup>15</sup> Among many ideas of making nanoscale structures, self-assembly has been the most exciting one, since it seems a natural path of building complex structures from

molecules.<sup>10</sup> While still attempting the traditional top-down methods, device physicists also adapt the self-assembly concepts. There are three main categories of bottom-up nanofabrication: a. self-assembly on inorganic substrates to form monolayer or multilayers,<sup>28</sup> b. soft material (such as DNA) directed self-assembly,<sup>29</sup> c. phase transition driven self-assembly.<sup>10, 30</sup>

The goal of constructing molecular IC will ultimately be the overlap of the Molecular Electronics and bottom-up nanofabrication, i.e. using the nanofabrication techniques such as self-assembly to build electronically functional devices productively and effectively. The corresponding studies thus should be based on the requirements of both aspects, which demand the MMBs are i. electrical-transportation controllable, ii. mechanically stable, iii. both structurally and electronically integrateable as traditional IC's, i.e. industrially reproducible.

Diamondoid molecules have highly potential as MMBs,<sup>31</sup> since they have already matched most of the above criteria and the researches of this project further supported it by studying their electronic properties and self-assembly abilities.

### 1.3 Diamondoids as Molecular Building Blocks

#### 1.3.1 Diamondoids family and their applications

Diamondoid molecules are cage-like, ultra-stable, saturated hydrocarbons; also known as cage-hydrocarbons. They are ringed compounds, which have a diamond-like structure consisting of a number of six-member carbon rings fused together and these carbon-carbon framework constitutes the fundamental repeating unit in the diamond lattice structure. Because of this structural characteristic they are called "diamondoids", meaning diamond-like. As in lattice structure diamond, the carbon orbital in diamondoids are  $sp^3$ -hybridized. Depending on the order of the diamondoids, the carbon-carbon bonds vary around 1.5 Å the bond length for those in

diamond.<sup>32, 33</sup> Diamondoids first discovered to exist in petroleum<sup>34</sup> and could be produced through chemical synthesis.<sup>35, 36</sup> More importantly, diamondoids can be purified easily<sup>37</sup> which is one distinguishable advantage superior to CNTs, and this property indicates diamondoids based devices have the potential of lower cost for industrial manufacturing.

Moreover, due to their six or more linking groups, highly symmetrical and strain free structures, controllable nano-structural characteristics and non-toxicity, diamondoids have found major applications as templates and as molecular building blocks (MBBs) in molecular manufacturing, polymer synthesis, drug delivery, drug targeting, DNA-directed assembly, DNA-amino acid nanostructure formation, and host-guest chemistry. In addition to the structural traits, diamondoid derivatives show interesting electronic properties and have excellent potential for building diamondoid-based molecular electronic devices, nano-electro-mechanical systems (NEMS)<sup>38</sup> and micro-electro-mechanic system (MEMS).<sup>39</sup> Diamondoid molecules and their derivatives have been recognized as promising candidate in the field of nanotechnology.<sup>40, 41</sup> It is crucial and necessary to intensively study the physical and chemical properties of diamondoids in order to exploit their applications in nanoscience and nanotechnology; these properties include electronic and structural characteristics, self-assembly abilities, bonding properties, reactivity, etc.<sup>30, 42</sup>

Numerous researches about diamondoids have appeared since 1950's, and diamondoids in the recent years gained more attention of scientific community due to their potential as MMBs.<sup>43-48</sup> Researchers have already been able to investigate single isolated tetramantane molecule the fourth order diamondoids using UHV-STM.<sup>49</sup> The lower order isolated diamondoids STM investigations are also in process.

### 1.3.2 Lower Diamondoids and their Derivatives

In this project, we focus on the theoretical studies of lower diamondoids and their possible applications. The lowest diamondoid Adamantane (ADM)  $C_{10}H_{16}$  has been the starting point, since it has been studied for years and the reference data can be served as the validation of the methods used in this project. We apply those methods to higher order diamondoids and their derivatives including: second order diamondoid named diamantane ( $C_{14}H_{20}$ ); three adamantane derivatives namely amantadine ( $C_{10}H_{17}N$ ), memantine ( $C_{12}H_{21}N$ ), rimantadine ( $C_{11}H_{20}N$ ), these three derivatives have pharmaceutical applications such as antiviral agents; and two organometallic derivative namely: ADM•Na ( $C_{10}H_{15}Na$ ), DIM•Na ( $C_{14}H_{19}Na$ ), designed by substituting one hydrogen ion in adamantane and diamantane with a sodium ion. These seven lower diamondoids are categorized into three groups depending on their functional residuals (shown in Table 1.)

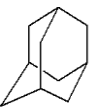
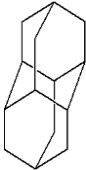
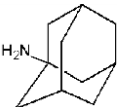
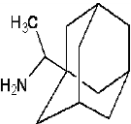
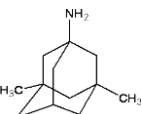
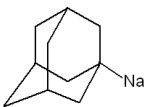
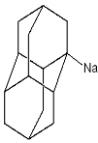
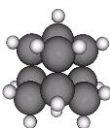
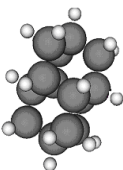
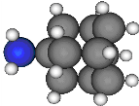
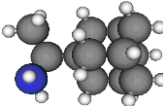

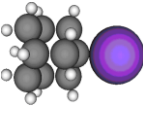
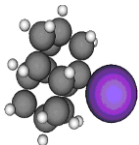
Group 1		Group 2			Group 3	
Adamantane	Diamantane	Amantadine	Rimantadine	Memantine	ADM•Na	DIM•Na
$C_{10}H_{16}$	$C_{14}H_{20}$	$C_{10}H_{17}N$	$C_{11}H_{20}N$	$C_{12}H_{21}N$	$C_{10}H_{15}Na$	$C_{14}H_{19}Na$
						
						

Table 1. Molecular formulas and structures of Adamantane, Diamantane, Memantine, Rimantadine, Amantadine, Optimized ADM•Na and Optimized DIM•Na molecules. In these figures blacks represent – C, whites represent –H, Blues represent –N and purples represent –Na.

Group 1: Adamantane (ADM) and diamantane (DIM), the lowest two diamondoids without any functional residues ‘bare group’. Although these molecules possess all the advantageous mechanical and structural properties, they have negligible electronic transportations which means they are unsuitable as conducting part of electronic devices. Group 2: Memantine, rimantadine and amantadine, the three derivatives of adamantane with nitrogen atoms as functional residues inside the molecules, called the ‘amino group’. Due to nitrogen atoms, these molecules could be used as molecular semiconductors. Group 3: ADM•Na, DIM•Na, the two organometallic derivatives.

#### 1.4 general methods for molecular scale studies

The chief object of this project is to study the applicability of the diamondoids as molecular building blocks in Nanotechnology, especially for the integrated MED. It is natural that some traditional molecular scale methods can be utilized for this purpose. Besides, since the innovative and inter-disciplinary characteristics of nano-systems, many novel methods and theories also emerged and become extremely active research fields. In this project, we attempted several suitable methods and some of them showed highly promising results and possibility as research tools in Nanoscience.

There are many available approaches to study the molecular scale systems both theoretically and experimentally. For the electronic structural and geometrical properties we successfully used the traditional quantum computational methods including Hartree-Fock (HF) theory and the related *ab initio* methods (Post HF) including Configuration Interaction methods (CISD, CASSCF), Many-Body Perturbation Theory (MP2, MP4), Coupled-Cluster method (CCSD), and the popular Density Functional Theory (DFT); and further took advantage of the combined

strategy of DFT and Non-equilibrium Green's Function (NEGF) formalism to investigate the quantum conductance and I-V properties of the seven molecules individually, and the Molecular Dynamics (MD) simulations to study the self-assembly and phase transition properties of seven different ensembles. Experimentally, Ambient and Ultra High Vacuum (UHV) STM/AFM methods were attempted to investigate and prove the theoretical researches.

In addition, we also expected to apply *ab initio* MD methods CPMD and 4-probe system, however they did not show any advantage in the scales of our systems; this issue will be addressed later and we will mainly focus on the discussion of the strategies we utilized.

## Chapter 2 Electronic structures of the Seven Diamondoids-----Quantum

### Computation Studies

#### 2.1 The framework of theories

In order to study objects at molecular level, quantum mechanics is inevitable;<sup>50</sup> and due to the complexity of many-body electronic systems it is impractical to compute the exact solutions by solving Schrödinger Equation, and thus the approximation methods have been used for molecular systems. There are two main branches of approximation approaches. One is the computational methods based on Hartree-Fock (HF) theory or Density Functional Theory (DFT); the other one is the analytical Many-body perturbation method based on Dyson Equation or Feynman diagrams in the quantum field theory by solving Greens functions of the systems. The first type approach is the main player of this chapter while the second one is covered in chapter 3 and their connection is to be discussed briefly.

HF and DFT are methods to approach the many-body Schrödinger equation by solving one-body equations obtained through Variational principal<sup>51</sup> and Honhenberg-Khon theorem,<sup>52</sup> respectively; both of them have been used to study electronic structures of molecules and showed advantages in prediction of molecular properties.

### 2.1.1 Hartree-Fock Theory and Self-consistent method

Hartree-Fock theory has been widely used as a powerful tool to study molecular and condensed matter systems in physics and chemistry communities. Since it is best approximation to ground state, HF method is also the starting point of the related *ab initio* calculation (Post Hartree Fock) methods that include electron correlation energy.<sup>53</sup>

The basic idea of Hartree-Fock theory is to approximate many-body system Schrödinger equation as one particle eigenvalue equation problem, considering the electron-electron interaction at average level, in this sense the HF method is also called mean field theory. The HF theory is outlined below and its detailed deduction procedures in the second quantization<sup>54</sup> language that is more transparent to demonstrate the theory are given in appendix A. Instead of solving the whole many-electron system wave function problem that is practically impossible,  $\hat{H}\Psi = E\Psi$  where  $\Psi$  is total wave function of the system and Hamiltonian is

$$\hat{H} = \sum_i \left[ \frac{\hat{p}_i^2}{2m} + V^{ion}(\vec{r}_i) \right] + \frac{1}{2} \sum_{i,j=1} \frac{e^2}{|\vec{r}_i - \vec{r}_j|}, \quad 2.1$$

we can approximate it to a one particle-like problem as Hartree-Fock equation in compact form, (see Appendix A for deduction)

$$\varepsilon_i \varphi_i(x_1) = \hat{f}(x_1) \varphi_i(x_1), \quad 2.2$$

where the  $\hat{f}$  is the Hartree-Fock operator,  $\varphi(x)$  is the HF wave function (molecular orbital).

$$\hat{f}(x_1) = \hat{h}(x_1) - \sum_{j=1} [J_j(x_1) - K_j(x_1)] \quad 2.3$$

$\hat{h}(x_1)$  is the one particle operator,  $J_j(x_1)$  is the *Coulomb* term:



$$J_j(x_1) = \int dx_2 \varphi_j^*(x_2) h(x_1, x_2) \varphi_j(x_2) = \int dx_2 h(x_1, x_2) |\varphi_j(x_2)|^2, \quad 2.4$$

and  $K_j(x_1)$  is the exchange term:

$$K_j(x_1) = \int dx_2 \varphi_j^*(x_2) h(x_1, x_2) \varphi_i(x_2) \int dx_1' \varphi_j(x_1') \varphi_i^*(x_1'), \quad 2.5$$

which satisfies the exchange relation:

$$K_j(x_1) \varphi_i(x_1) = \int dx_2 \varphi_j^*(x_2) h(x_1, x_2) \varphi_i(x_2) \varphi_j(x_1), \quad 2.6$$

The total ground state energy  $E_0$  can be obtained by using  $\varepsilon$  after performing iterative calculations.

$$E_0 = \sum_{i=1}^N \varepsilon_i - \sum_{j=1}^N [J_j(x_1) - K_j(x_1)], \quad 2.7$$

The energy  $\varepsilon_i$ , according Koopmans' theory,<sup>55</sup> associates with the electron affiliation energy and HF equation is not actual Schrödinger Equation for single electron in molecular orbitals.

To perform self-consistent iteration in practice, however, the basis usually is not orthogonal e.g. the atomic orbital basis, therefore for molecular system it is necessary to expand the basis in the non-orthogonal basis  $\{\chi_\mu\}$ , discussed in next section,

$$\varphi_i(x_1) = \sum_{\mu=1} C_{\mu i} \chi_\mu(x_1), \quad 2.8$$

Plug it back into H-F equation and multiply  $\chi_v^*(x_1)$  from left and integrate both sides, one can obtain Roothaan equation:<sup>56</sup>

$$\varepsilon_i \sum_{\mu=1} C_{\mu i} \int dx_1 \chi_v^*(x_1) \chi_\mu(x_1) = \sum_{\mu=1} C_{\mu i} \int dx_1 \chi_v^*(x_1) f(x_1) \chi_\mu(x_1), \quad 2.9$$

By defining the overlap integrals form so called  $S$  matrix in quantum computation community

$$S_{v\mu} = \int dx_1 \chi_v^*(x_1) \chi_\mu(x_1) \quad 2.10$$

and matrix representation of HF operator  $F$  matrix.

$$F_{v\mu} = \int dx_1 \chi_v^*(x_1) f(x_1) \chi_\mu(x_1) \quad 2.11$$

We can finally get the matrix form of HF:

$$\varepsilon_i \sum_{\mu=1} S_{v\mu} C_{\mu i} = \sum_{\mu=1} F_{v\mu} C_{\mu i}, \quad 2.12$$

or more compactly

$$SC = FC, \quad 2.13$$

With these elements one can solve originally many-particle problem as one-particle problem in the iterative fashion:

1. Input a set of trial coefficients  $C_{\mu i}^0$ 's.
2. Calculate the elements of Fock matrix form by integrations discussed above to form the complete Fock matrix.
3. Diagonalize the Fock matrix and obtain a set of eigenfunctions that contain the new coefficients  $C_{\mu i}^I$ 's.
4. Compare the new coefficients with initial guess. If they are convergent in certain criterion  $|C_{\mu i}^0 - C_{\mu i}^I| < \delta$ , then the Self-consistent-field procedure is done; otherwise,

5. Generate another set of coefficients  $C_{\mu i}^2$ 's based on previous coefficients  $C_{\mu i}^1$ 's depending on specific algorithm, and then return to step 2 until reach the threshold.

Despite HF method is the best single Slater determinants<sup>57</sup> approximation method of one particle to many body problem,<sup>54</sup> the intrinsic deficit of molecular orbital method or say single Slater Determinant method<sup>58</sup> that excludes the electron correlation energy leave the HF method only include 99% of the total energy while the remaining 1% correlation energy is important for chemical properties.<sup>53</sup> Therefore, the electron correlation methods are needed. The typical Post HF methods including configuration interaction (CI), Moller-Plesset Many Body Perturbation Theory (MP-MBPT) and Coupled Cluster (CC) method correct the problem of ignoring electron correlation energy in the HF approximation by including excited molecular states in the constructions of the Molecular orbital (see discussion in section 2.1.3).

### 2.1.2 Introduction to Density functional Theory and exchange-correlation functions

Density functional Theory (DFT)<sup>59-61</sup> is based on the understanding that the one-particle density of a many-particle quantum system determines the ground state energy of that system, i.e. for an N-electron system, there is a one-on-one mapping between the total ground state energy  $E_0$  of the system and the one-electron density  $n(\vec{r})$  which is the integral of the total wave-function square over N-1 electron coordination. Therefore DFT is a method that reveals the relationship between energy and density; however only since Kohn and Sham suggested introducing molecular orbitals into the calculation of density,<sup>52</sup> instead of using density directly, DFT has become one of the most popular quantum calculation methods due to its high accuracy with computational cost as low as HF method. As long as the exchange-correlation functional is determined, the iterative calculation procedure is quite similar as the basic HF method above. The DFT version Schrödinger like eigenvalue function is Kohn-Sham (KS) equation written as:

$$H_{KS}\varphi_i(\vec{r}) = \left[ -\frac{\hbar^2}{2m}\nabla^2 + V^{eff}[n(\vec{r})] \right] \varphi_i(\vec{r}) = \varepsilon_i \varphi_i(\vec{r}) \quad , \quad 2.14$$

which can be considered as a one-particle wave equations like HF equations,

where  $n(\vec{r}) = \sum_i^N |\varphi_i(\vec{r})|^2$  is the electron density,  $\varphi_i(\vec{r})$ 's are the molecular orbital basis, and the

effect potential  $V^{eff}$  is a functional of  $n(\vec{r})$  and divided into three parts as:

$$V^{eff}[n(\vec{r})] = V^{ion}(\vec{r}) + V^H[n(\vec{r})] + V^{xc}[n(\vec{r})] \quad , \quad 2.15$$

The first term is the potential between ions/nuclear and the electron

$$V^{ion}(\vec{r}) = \sum_{\mu=1}^N \frac{Z_{\mu}e^2}{|\vec{r} - \vec{R}_{\mu}|} \quad , \quad 2.16$$

the second term is the Coulomb repulsion usually called Hartree term

$$V^H[n(\vec{r})] = \int \frac{e^2 n(\vec{r}')}{|\vec{r} - \vec{r}'|} d^3\vec{r}' \quad , \quad 2.17$$

which is the solution of the Poisson equation

$$\nabla^2 V^H[n(\vec{r})] = -4\pi n(\vec{r}) \quad , \quad 2.18$$

and the third term is the exchange-correlation (XC) potential in general can be formally written

as:

$$V^{xc}[n(\vec{r})] = f[n(\vec{r}), \nabla n(\vec{r}), \nabla^2 n(\vec{r}), \dots]$$

which could be functional of electron density, gradient of density, second order gradient of density, or even higher order, depending on calculation requirement;

As in the HF method, the molecular orbitals may be expanded in the non-orthogonal Atomic orbitals basis  $\{\chi_\mu\}$ , then  $\varphi_i(x) = \sum_{\mu=1} C_{\mu i} \chi_\mu(x)$

And one can obtain a Kohn-Sham (KS) matrix equation, replace Fock matrix with KS matrix in the Roothaan-equation

$$SC\epsilon = h_{KS}C,$$

and similarly diagonalize it to find out the total energy iteratively.

Another related subject is the functional form of exchange-correlation functions  $V^{xc}[n(\vec{r})]$ . Theoretically, if one can find the exact unknown exchange-correlation functions, then the problems can be solved exactly. In practice, however, there are two kinds of commonly used approximation exchange-correlation functions: Local Density Approximation (LDA) and Generalized Gradient Approximation (GGA).<sup>53, 62, 63</sup> LDA or the spin-included version LSDA is an approximation assuming the density is locally constant or varying slowly, therefore  $V^{xc}[n(\vec{r})] = f[n(\vec{r})]$ . GGA is an improvement of LDA on the form of the functional by adding the gradient of the density to the exchange-correlation function and thus  $V^{xc}[n(\vec{r})] = f[n(\vec{r}), \nabla n(\vec{r})]$ . Higher order gradients of density could be added to the functional, however, they are not included in this project. LDA and B3YLP type GGA exchange-correlation functions are the two main functional used in this project.

### 2.1.3 Basis sets, atomic orbitals, molecular orbitals, and total wave functions

To approximate the infinite complete set in the Hilbert space for the Schrödinger like equations (e.g. HF or KS Equation) of molecular systems, various finite basis sets have to be applied, and these basis sets could be in any mathematical form as long as they are complete basis in the vector/Hilbert space. This also implies that the more complicated the basis set is, the better approximation results one can obtain. The basic procedure is that firstly basis functions form Atomic orbital  $\{ \chi_{\mu} \}$  for each electron on an atom through certain composition method,<sup>53, 63</sup> and then these atomic orbitals approach molecular orbitals (MOs) through a process called Linear Combination of Atomic Orbital (LCAO):  $\varphi_i(x) = \sum_{\mu=1} C_{\mu i} \chi_{\mu}(x)$ . Finally, total ground state wave function  $\Psi$  of the many-body system is the single Slater determinant of all occupied molecular orbitals. In order to include the electron correlation energy into the HF method, the unoccupied MOs are used to form excited wave functions through Slater determinant process, and various schemes can be applied to integrate electron correlation such as CI, MPT and CC. For DFT, electron correlation is already included in the XC functional, thus there is no need to consider excited wave functions. And the basis sets for DFT could be either the same basis as used in HF methods or special basis exclusively for DFT calculations.

Therefore the choice of basis set can eventually determine the quantity of the computation. In general, there are two kinds of basis sets/functions: localized atomic orbital basis and plane wave basis. Atomic orbital basis, including Slater type orbital (STO) and Gaussian type orbital (GTO) are localized basis sets and commonly used for molecular systems,<sup>64</sup> while Plane wave basis are more suitable for periodical solid state systems. We adapted the GTO type atomic orbital basis sets throughout this project for all the molecular systems and GTO's are series of Gaussian functions. In quantum computation, the difference between various basis sets depends on how

they contract primitive GTO (PGTO) for atoms in the element periodic table. Usually more than one set of basis functions are used for one orbital. There could be Double Zeta (DZ) basis, triple Zeta (TZ) basis, etc. and normally polarized functions and/or diffuse functions are augmented to form basis such as Double Zeta Polarized (DZP) basis. Furthermore since the valence electrons are of central importance to chemical properties, basis sets treat core orbitals and valence orbitals differently, i.e. core orbitals are contractions of PGTO's while valence orbitals are split into more than one function which could be contractions of various numbers of PGTO's. The popular basis sets are traditional Pople style basis sets, e.g. 6-311+ + G (d, p) and modern contract basis: correlation consistent basis sets, e.g. aug-cc-pVDZ (which means diffuse function augmented correlation consistent polarized Valence Double Zeta basis). In most of the cases, we applied these two kinds of basis sets.

Moreover, one characteristic about Atomic Orbital (AO) basis is that the functions are non-orthogonal at different atoms and thus the overlap integrals of AO's or matrix form (called S-matrix in quantum computation community) commonly appear in the scenarios, such as the Roothaan equation discussed in the HF theory, the DFT calculation and the matrix form of Green's function discussed in chapter 3.

## 2.2 Quantum computational studies of diamondoid molecules

### 2.2.1 Computation results comparison and methods validation

Diamondoids attract computational researchers' attention largely due to the negative electron affinity (NEA) of Hydrogen-terminated diamond surface, and H-saturated lower diamondoid molecules also have shown NEA feature experimentally<sup>49, 65</sup> and theoretically.<sup>33, 66, 67</sup> NEA means

$EA=E_N - E_{N-1}$  is negative and this property could be used to build NEA photo-emitters, e.g.

Tetramantane has been predicted as the novel materials for LED display/monitors.<sup>49, 68</sup>

We performed systematical electronic structure calculations thoroughly on simplest Adamantane molecule to test how the choices of basis sets can influent the calculation results and the sensitivities of them by using various basis sets and quantum computation discussed above. We first tested various basis sets with DFT calculations through Gaussian 03 package,<sup>69</sup>, and find the highest occupied molecular orbital (HOMO) and the lowest unoccupied molecular orbital (LUMO), and the energy gaps for Adamantane molecule. Different basis set can produce different HOMO/LUMO and their gaps, which range from 7eV to 11eV. The results are list in Table 2:

<i>Basis</i>	<i>cc-pVDZ</i>	<i>6-31++(d,p)</i>	<i>Lanl2dz</i>	<i>cc-pVQZ</i>	<i>6-311++(3df,3pd)</i>
<b>LUMO (eV)</b>	1.0925618	-0.4168878	2.943522	0.197559	-0.4234187
<b>HOMO (eV)</b>	-7.37744532	-7.5801747	-7.37418	-7.61637	-7.6073867
<b>Gap (eV)</b>	8.47000712	7.1632869	10.317702	7.813926	7.183968

Table 2.LUMO and HOMO of adamantane with different basis under DFT calculations.

When HF and Post HF methods are applied, we found even larger discrepancies. The Table 3 below shows the results with different calculation method in the 6-311++G(d, p) basis. The gaps range from 11eV to 16eV.

	<i>CIS</i>	<i>RHF</i>	<i>ROHF</i>	<i>MP2</i>	<i>MP3</i>	<i>HF-pvdz</i>
<b>LUMO(eV)</b>	5.11748872	1.02235484	1.02235484	1.02208272	5.11748872	3.95853
<b>HOMO(eV)</b>	-10.343009	-10.89922236	-10.89922236	-10.8997666	-10.343009	-10.8853
<b>Gap(eV)</b>	15.4604978	11.9215772	11.9215772	11.92184932	15.4604978	14.84387

Table 3 LUMO and HOMO of adamantane in various HF methods with 6-311++G(d, p) basis



### 2.2.2 HOMO and LUMO for seven lower diamondoids

We further calculated the HOMO/LUMO of all the seven molecules using the DZP basis through ATK/VNL package the main quantum conductance calculation platform used in this project. The results are reported in Table 4.

	<i>Group 1</i>			<i>Group 2</i>		<i>Group 3</i>	
	Adamantane	Diamantane	Memantine	Amantadine	Rimantadine	ADM•Na	DIM•Na
<b>LUMO (eV)</b>	1.288	1.097	1.228	1.043	0.974	-1.699	-1.674
<b>HOMO (eV)</b>	-6.554	-6.226	-5.023	-4.956	-4.975	-3.078	-3.435
<b>Gap (eV)</b>	7.842 (7.622 <sup>66</sup> )	7.323 (7.240 <sup>66</sup> )	6.251	5.999	5.949	1.379	1.761

Table 4.HOMO and LUMO of the three groups. (Fermi energy=0 eV)

Our computational results of the first group are generally in agreement with previous calculations reported in literatures.<sup>33,66</sup> The small deviation between our calculations and the literature data are due to different basis and approximation methods applied. The smaller the band gap (the difference between the energies of the HOMO and LUMO) is, the more easily a molecule can be excited. We focused on the changes of HOMO-LUMO gap from Group 1 to Group 3. From Table 4, we see that Group 1 (the lower diamondoids) have the largest band gap, which proves that diamondoids are electrical insulators. The three derivatives in Group2 have smaller band gaps, which indicate that those molecules could be electrical semiconductors. The results also indicate that the -NH<sub>2</sub> (amino) group is electron donating. This is consistent with the fact that -NH<sub>2</sub> has a pair of non-bonded electrons. Group 3 shows not only smaller band gaps than Groups 1 and 2 which indicate high conductance, but also interesting electronic behaviors, such as both the HOMO and LUMO are below Fermi energy which is an indicator of the metallic properties of those molecules. The HOMO and LUMO of molecules are independent of

those of the two-probe systems that will be addressed in Chapter 3. Following these results and directions, we attempt to study the quantum conductance of different groups at different orientations.

It is instructive and convincing to using Gaussian03 to compare HOMO and LUMO of the seven molecules in higher basis set such as cc-pVQZ set.<sup>70</sup> From Table 5, we obtain practically similar conclusions as above, despite the numeric discrepancies, i.e. the functional residues influence the electronic properties of the seven molecules.  $-NH_2$  and  $-Na$  residues change the LUMO/HOMO gaps respectively, and their effects on the conductances can also be seen in Chapter 3.

	<b>Adamantane</b>	<b>Diamantane</b>	<b>Amantadine</b>	<b>Memantine</b>	<b>Rimantadine</b>	<b>ADM•Na</b>	<b>DIM•Na</b>
<b>LUMO (eV)</b>	0.19755912	0.2258596	0.19674276	0.20626696	0.12272612	-1.68387856	-1.64551
<b>HOMO(eV)</b>	-7.6163667	-7.11212832	-6.37958128	-6.36842436	-6.48380324	-3.8681858	-3.88723
<b>Gap (eV)</b>	7.8139258	7.33798792	6.57632404	6.57469132	6.60652936	2.18430724	2.241725

Table 5 HOMO and LUMO of seven molecules in cc-pVQZ basis.

### 2.2.1 Optimized geometries and atomic charge in molecules

By applying DFT, we also obtained the optimized initial structures of all the seven molecules and their atomic electronic charges for the MD simulations that will be discussed in Chapter 4.

The B3YLP exchange-correlation functional<sup>62</sup> method was chosen with cc-pVDZ basis<sup>71</sup>, for all the molecules; NBO (Natural Bond Orbital) analysis<sup>72</sup> was added to calculate the atomic electronic charges which were used as reference to set the atomic charges of nitrogen atom and sodium atom, i.e. -0.76 and 0.65, respectively (in electronic charge units: Coulomb). The atomic charges of carbon and hydrogen atoms were mainly opted from default OPLS-AA force field.

## Chapter 3 Quantum conductance of the seven diamondoids----- *ab initio* NEGF studies

Knowing the properties of diamondoids, then the next question one would ask is: What kinds of molecular electronic devices can diamondoids build? In order to answer this question we should first study the electron transportation of these molecules in two-probe systems under certain potential bias. This is the subject of the rejuvenated research field: Molecular Electronics and one of the mostly applicable methods is non-equilibrium Green's Function (NEGF) formalism that would be discussed below.

### 3.1 Theoretical framework

Before digging into the NEGF, it is interesting to point out some connections between the analytical Green's function methods and computational methods mentioned in Chapter 2 at several levels. As stated before, both of these methods are approximations to exact solutions for various quantum mechanics systems, therefore it is natural they come cross at some points. There are at least three cases: a. they both can be used to study the ground state energy of molecules and there is surprising similarity that two-body interaction problems can be solved in a one-body problem frame in both methods, i.e. from Schrodinger to HF equation or KS equation discussed in chapter 2 and two-body Hamiltonian can be solved by only one-body Green's function (propagator). b. with the help of Green's function formalism one can obtain the densities where the exchange-correlation functional in DFT does not provide accurate results, such as calculating van der Waals forces. This is the motivation of the method that integrates Green's function

method into DFT scheme to form the Generalized Kohn-Sham DFT.<sup>73</sup> c. the third case is for systems that are in non-equilibrium states and the densities are calculated in the NEGF formalism which is integrated with DFT, i.e. DFT provides the functional of equilibrium Hamiltonian.<sup>74, 75</sup>

The molecular systems with bias belong to nonequilibrium systems. Therefore, in principle, NEGF is suitable candidate to calculate the conductance of molecules and to predict reasonable electronic properties for molecular scale systems.

### 3.1.1 Introduction to Non-Equilibrium Green's Functions (NEGF)

In the equilibrium case, Green's Function is defined as:<sup>76, 77</sup>

$$G(\bar{r}, t; \bar{r}', t') = \frac{-i}{\hbar} \frac{\langle \psi_0 | T\{\hat{\phi}_H(\bar{r}, t)\hat{\phi}_H^\dagger(\bar{r}', t')\} | \psi_0 \rangle}{\langle \psi_0 | \psi_0 \rangle} = \frac{-i}{\hbar} \frac{\langle \phi_0 | T\{S(-\infty, \infty)\hat{\phi}_H(\bar{r}, t)\hat{\phi}_H^\dagger(\bar{r}', t')\} | \phi_0 \rangle}{\langle \phi_0 | TS(-\infty, \infty) | \phi_0 \rangle}$$

This S-matrix is the time evolution from  $t = -\infty$  to  $t = \infty$  in the time or complex time axis

formulated by the Wick's time-order operator  $T$ ; the Hamiltonian includes non-interaction and interaction terms  $H = H_0 + H_{\text{int}}$ . With help of Dyson equation and self-energy, one can approximate Green's functions  $G$  using Feynman diagrams technical to desired order theoretically. Dyson equation can be written as:

$$G = G_0 + G_0 \Sigma G, \quad 3.1$$

$G_0$  is the non-interaction Green's function and  $\Sigma$  is the self-energy term that includes all interactions and also can be, in principle, approximated to desired order.

In the non-equilibrium case, however, one uses time-loop/contour to handle the S-matrix from  $(-\infty, t')$  to  $(t', +\infty)$ , so that the positive infinite asymptote is avoided, and therefore the Green's

function can be used even in non-equilibrium cases by changing the time integration path to the time-loop/contour as:

$$G(\bar{r}, t; \bar{r}', t') = \langle T_c \hat{\phi}(\bar{r}, t) \hat{\phi}^+(\bar{r}', t') \rangle,$$

So that one can solve problems with non-equilibrium Hamiltonians  $H = H_0 + H_{\text{int}} + H_{\text{non-equilibrium}}$

The disadvantage of this treatment is that there are four Green's functions and more Dyson's equations, like Eq. (3.1), in non-equilibrium version (called Keldysh Equations). Fortunately, the systematic development of this formalism has been pioneered by Keldysh, Kadanoff, Baym, Lengreth, Caroli, *et al* since 60's and 70's in solve problems of the non-equilibrium states, especially for quantum transportation theories.<sup>78-83</sup> In the past two decades, due to the developing of the computational techniques in the scientific researches and the emerging of nanoscience at molecular level, the non-equilibrium Green's function formalism regained its application by integrating into the quantum computational methods, especially Density Functional Theory method.<sup>27, 82, 84, 85</sup> Numerous researches have been carried out based on NEGF to study molecular and nanoscale systems, such as benzene molecules, CNTs, nanowires, etc.<sup>86-94</sup>

The key motivation or connection between DFT and NEGF methods is that the density in the DFT can also be calculated by Lesser Green's function  $G^<$  in the NEGF, it is defined as:

$$G^<(\bar{r}, t; \bar{r}', t') = \frac{i}{\hbar} \langle \hat{\phi}^+(\bar{r}', t') \hat{\phi}(\bar{r}, t) \rangle \quad 3.2$$

Many useful quantities can be calculated according to it, which will be discussed below.

Since the electron occupation number operator is  $\hat{n}(\vec{r}) = \hat{\phi}^\dagger(\vec{r})\hat{\phi}(\vec{r})$  and the particle density or charge density is defined as  $n(\vec{r}) = \langle \hat{n}(\vec{r}) \rangle = \langle \hat{\phi}^\dagger(\vec{r}, t)\hat{\phi}(\vec{r}, t) \rangle$ , then the link is established as

$$D(\vec{r}, \vec{r}') = -i\hbar \lim_{t \rightarrow t'} G^<(\vec{r}, t; \vec{r}', t') = \frac{1}{2\pi i} \int dE G^<(\vec{r}, \vec{r}'; E) \quad 3.3$$

It is clear that the 1<sup>st</sup> order Reduced Density Matrix  $D(\vec{r}, \vec{r}')$  is the equal time limit of the Less Green's function in time domain and thus the energy integral of Lesser Green's function in energy domain, i.e. Fourier transformation of Lesser Green's function at same time limit.

Then particle density of the system can be found as the diagonal elements of the reduced density matrix.

$$n(\vec{r}) = D(\vec{r}, \vec{r}) = \langle \vec{r} | D(\vec{r}, \vec{r}') | \vec{r} \rangle = \frac{1}{2\pi i} \int dE G^<(\vec{r}, \vec{r}; E) \quad 3.4$$

This is the particle density in DFT that is normally defined as  $n(\vec{r}) = \sum_i^N |\varphi_i(\vec{r})|^2$  in the wave function language, see section 2.2. Therefore, if one can obtain the Lesser GF of the non-equilibrium systems, then, in principle, we can integrate it into DFT calculation. The question is how to calculate  $G^<(E)$  with available technical. This could be done by taking advantage of useful equations in NEGF formalism and projecting them onto computational compatible basis set, and we see the Matrix form of the NEGF. This strategy was developed at the beginning of this century by different groups around the world separately and since then it has become one of the most popular tool in the nanoscale/molecular electronic computations. The computational details might vary at some points, but the fundamental theories and general ideas are the same for all of them.<sup>95</sup>

### 3.1.2 NEGF formalism for transportation in two-probe system

Before explaining the theory, it is necessary to clarify the system first, since several approximations are based on the model. The physical model studied is a two-probe system with two metal leads/electrodes and one molecule in between see Figure 1. This is an infinite open system; when potential bias applied, it is in non-equilibrium state. To attack this problem, the system is ubiquitously split into three parts, the two semi-infinite probes and the central region: the molecule and a few layers from the leads/electrodes that are close to molecule, called ‘Extended Molecule’.

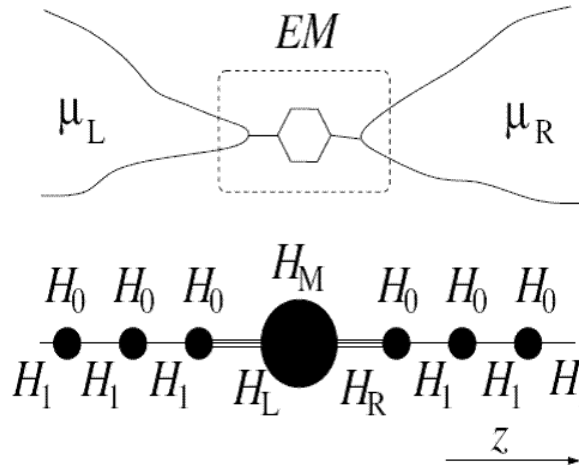


Figure 1. Semi-infinite two probe system

The two leads/electrodes are in their equilibrium states respectively and the mean-field approximation is assumed to the central region in order to apply the NEGF+DFT formalism. One can write the Hamiltonian in a transparent way to demonstrate these ideas

$$H = (H_0 + H_{\text{int}})^{\text{equilibrium}} + H^{\text{non-equilibrium}} \text{ where}$$

$$(H_0 + H_{\text{int}})^{\text{eq}} = H_L^{\text{eq}} + H_R^{\text{eq}} + H_M^{\text{eq}},$$

$$H^{non-equilibrium} = H_L^{non-eq} + H_R^{non-eq}$$

The only non-equilibrium interactions are from the bias applied to the two electrodes and their meanings and explicit forms will be clear later.

Here we outline the most important results actually used in the calculations; other useful equations and deduction are listed in Appendix B. First of all, as mentioned above in the NEGF formalism the Dyson equation is more complicated than equilibrium case, and in the steady state is (see appendix B):

$$G^< = G^R \Sigma^< G^A \tag{3.5}$$

This equation is not simple multiple but is either separate time integral or matrix form in the spectrum/energy representation.  $G^R$  is the Retarded Green's function of the system in general sense and can be calculated based on Hamiltonian operators and retarded self-energy  $\Sigma^R$  (expounded in following sections), while  $G^A$  Advanced Green's function is the Hermitian conjugate of Retarded Green's Function as  $G^{R+} = G^A$ .

The Lesser self-energy  $\Sigma^<$  of a two-probe system represents the non-equilibrium interaction due to the potential bias and thus is the summation of two Lesser self-energy terms  $\Sigma^< = \Sigma_L^< + \Sigma_R^<$ , they are the non-equilibrium source to the system. In the two-probe system problem, when the potential bias applied to the two probe, the system is out of equilibrium overall, however, the two electrodes/leads and reservoir are in their equilibrium states respectively, so one can approximate the total non-equilibrium Lesser Green's function is the summation of the two separate Lesser Green's functions in their equilibrium states, and they are:



$$\Sigma^<(E) = if(E - \mu)\Gamma(E) = -2if(E - \mu)\text{Im}[\Sigma^R(E)] \quad 3.6$$

for each electrode (see Appendix B for details) where

$$\Gamma(E) = i[\Sigma^R(E) - \Sigma^A(E)] = i[\Sigma^R(E) - \Sigma^{R+}(E)] = -2\text{Im}[\Sigma^R(E)], \text{ (using } \Sigma^{R+} = \Sigma^A \text{) and}$$

$$f(E - \mu) = \frac{1}{e^{\beta(E - \mu)} + 1} \text{ is the Fermi-Dirac distribution function at certain energy } E, \text{ and}$$

chemical potential  $\mu$  is Fermi energy at zero temperature in the equilibrium state, it could be

set as zero  $\mu_L(T=0) = \mu_R(T=0) = E_F = 0$ . Finally, the total Lesser Green's function is interpreted

as retarded terms  $G^R$  and  $\Sigma^R$  that can be formulated and obtained through Matrix method

explained in the next section:

$$\begin{aligned} G^< &= \sum_{\alpha \in L, R} iG^R \Gamma_{\alpha}(E) G^A f(E - \mu_{\alpha}) \\ &= iG^R(E) [\Gamma_L(E) f(E - \mu_L) + \Gamma_R(E) f(E - \mu_R)] G^R(E)^+ \end{aligned} \quad 3.7$$

The subscript  $\alpha$ ,  $L$ ,  $R$  represents Left or Right lead/electrode, while the superscript  $R$  or  $A$  indicates Retard or Advanced.

If one can obtain this quantity, then many important quantities can be calculated: the particle density through Eq. (3.2) and Eq. (3.3);

Current is calculated by (see appendix B):

$$I = \frac{e}{\pi \hbar} \int dE [f(E - \mu_L) - f(E - \mu_R)] T(E) \quad 3.8$$

where  $T(E) = \text{Tr}[\Gamma_L(E) G_M^R(E) \Gamma_R(E) G_M^R(E)^+]$  recognized as transmission coefficient/probability.

And the conductance is defined as  $g = g_0 T(E, V)$ , where  $g_0 = \frac{2e^2}{h} = 77.5 \mu S$  is the quantum conductance, or written as

$$g = \frac{2e^2}{h} \text{Tr}[\Gamma_L(E) G_M^R(E) \Gamma_R(E) G_M^R(E)^+] \quad 3.9$$

It is formally product of constant number and transmission coefficient.

### 3.1.3 *ab initio* NEGF with DFT

From the above discussion, we know that if one can calculate the Lesser Green's function  $G^<$  then all the related physics quantities would be obtained, and in order to calculate  $G^<$ , the Retarded Green's function  $G^R$  and Retarded self-energy  $\Sigma^R$  are needed. The next step is to build up practical method suitable for DFT computation in the Atomic Orbital (AO) basis sets that are non-orthogonal as discussed in section 2.1.3.

For the two-probe system, the Retard Green's function satisfies the equation below in energy representation for AO basis:

$$[\varepsilon^+ S - H] G^R(E) = I$$

$S$  represents the overlap matrix (see Chapter 2 and Appendix A) due to the non orthogonal nature of the localized atomic orbital, and they would not cause any problem conceptually and computationally.  $\varepsilon^+ = \lim_{\delta \rightarrow 0^+} E + i\delta$ , makes energy has poles in the low half of energy complex plane to indicate the Green's function is the retarded one.  $H$  is the total Hamiltonian of the system.

The matrix form of this Retarded Green's equation is:

$$\begin{pmatrix} \varepsilon^+ S_{LL} - H_{LL} & \varepsilon^+ S_{LM} - H_{LM} & 0 \\ \varepsilon^+ S_{ML} - H_{ML} & \varepsilon^+ S_{MM} - H_{MM} & \varepsilon^+ S_{MR} - H_{MR} \\ 0 & \varepsilon^+ S_{RM} - H_{RM} & \varepsilon^+ S_{RR} - H_{RR} \end{pmatrix} \times \begin{pmatrix} G_{LL} & G_{LM} & G_{LR} \\ G_{ML} & G_{MM} & G_{MR} \\ G_{RL} & G_{RM} & G_{RR} \end{pmatrix} = \begin{pmatrix} I_{LL} & 0 & 0 \\ 0 & I_{MM} & 0 \\ 0 & 0 & I_{RR} \end{pmatrix} \quad 3.10$$

The subscript  $M$  represents the central region called 'extended molecule' that includes the molecule and a few layers of leads/electrodes. Other subscripts  $L/R$  indicate the interaction between the leads/electrodes and the central region. The  $MM$  stands for mid part of the 'extended molecule', just for consistence reason. Notice that the matrix elements between the left and right leads/electrodes are zero, this means that there is no interaction between two probes, thus the tunneling effect has already eliminated formally from this model.

In general, this matrix equation is infinite, since both  $H_{LL}$  and  $H_{RR}$  are semi-infinite matrices for leads/electrodes, however, one can obtain simple form for central region Retard Green's function  $G_{MM}^R(E)$  that is one element of the inverse matrix of Hamiltonian matrix.

$$G_{MM}^R(E) = [\varepsilon^+ S_{MM} - H_{MM} - \Sigma_L^R(E) - \Sigma_R^R(E)]^{-1} \quad 3.11$$

Define the Retarded self-energies and Green's functions for left and right electrodes

$$\Sigma_L^R(E) = (\varepsilon^+ S_{ML} - H_{ML}) G_{LL}^{0R}(E) (\varepsilon^+ S_{LM} - H_{LM})$$

$$\Sigma_R^R(E) = (\varepsilon^+ S_{MR} - H_{MR}) G_{RR}^{0R}(E) (\varepsilon^+ S_{RM} - H_{RM})$$

$$G_{LL}^{0R}(E) = (\varepsilon^+ S_{LL} - H_{LL})^{-1}$$

$$G_{RR}^{0R}(E) = (\varepsilon^+ S_{RR} - H_{RR})^{-1}$$

From the expression for  $G_{MM}^R(E)$  one find the non-equilibrium interactions  $H^{non-equilibrium}$  are only from the two leads/electrodes due to their electrical potential difference represented by Retarded self-energies  $\Sigma_\alpha^R$ . This again confirms the model that central region is in the mean-field approximation to the whole system, i.e. to the NEGF, the central region is a ‘non-interacting’ zone; the equilibrium interactions inside the central region are handled by the DFT. Furthermore, if one wants to add more contacts to the molecule, formally just add more self-energies to the Hamiltonian to form effective Hamiltonian as  $H_{eff} = H_{MM} - \Sigma_L^R - \Sigma_R^R - \Sigma_\beta^R - \dots$

And the Retarded Green’s function  $G_{MM}^R(E)$  is the inverse of this operator/matrix.

As mentioned before, the central region Hamiltonian  $H_{MM}$  in Eq. 3.10 are basically the Kohn-Sham Hamiltonian of the extended molecule defined in the DFT (Eq.2.in Section 2.1.2) with extra potentials from charge distributions in the two leads/electrodes  $V^{electrode}(\vec{r})$  that depend on both ions and electrons at the contacts, and potential due to applied bias  $V^{bias}(\vec{r})$  that is linearly screened inside the extended molecule. If one defines total external effects  $V^{ext} = V^{electrode} + V^{bias}$ , then effective potential  $V^{eff}[n(\vec{r})]$  can be formally written as the one similar in KS DFT:

$$V_{NEGF}^{eff}[n(\vec{r})] = V^{ion}(\vec{r}) + V^H[n(\vec{r})] + V^{xc}[n(\vec{r})] + V^{ext}(\vec{r})$$

Since the contact parts are neutral as whole, the external effect to the extended molecule are comparatively small, thus the approximation can be made to only calculate a few layers of electrodes. And this effective potential can not be served as ordinary  $V^{eff}[n(\vec{r})]$  in DFT anymore.

Then one can obtain the operator form of Hamiltonian for the extended molecule and it is a functional of electron density as

$$\hat{H}_{MM}[n(\vec{r})] = -\frac{\hbar^2}{2m} \nabla^2 + V^{eff}[n(\vec{r})].$$

The matrix element in the position representation is  $H_{\nu\mu}(\vec{r}) = \int d\vec{r} \chi_\nu^*(\vec{r}) \hat{H}_{MM} \chi_\mu(\vec{r})$ , where  $\{\chi_\mu\}$  represent the Atomic orbital basis for the ‘extended molecule’ central region discussed in Section 2.1.3. One can find that  $H_{MM}$  is similar as Fock matrix in HF theory and KS matrix in DFT, however, in this *ab initio* NEGF calculation, the iteration does not involve the calculation of eigenvalue of this matrix, i.e. no diagonalization of  $H_{MM}$ , since ground state DFT is not suitable to deal with the non-equilibrium state problem; instead, one should use  $H_{MM}$  to calculate electron number density  $n(\vec{r})$  to form the self-consistent loop. But it would be practical to use  $H_{KS} + V^{electrode}$  the unbiased central region Hamiltonian to generate density  $n^0(\vec{r})$  by performing normal DFT iteration as the initial trial density or in practice one can perform any quantum computation of the extended molecule with periodic boundary condition to obtain the ‘equilibrium’ density; it is analogue of taking HF calculation as the starting point for the CI calculation (See chapter 2).

The only unknown quantities now in the formula Eq.3.11 are electrodes’ Green’s functions  $G_{LL}^{0R}(E)$  and  $G_{RR}^{0R}(E)$ , and there are already many available methods for calculating semi-infinite systems, such as transfer matrix technique, two-component matrix elements method by Williams *et al.*, recursive methods and we adapted the method introduced by Sanvito *et al.*<sup>86, 90</sup> Basic ideas of them are using Block’s theorem, since the electrodes are essentially periodic systems and these Green’s functions will be used to calculate self-energies  $\Sigma_{L/R}^R(E)$ , once for all, since they are not included in the iteration. Besides, if the potential bias is applied, in the self-energy calculation, the bias induces a rigid energy shift to the leads/electrodes, thus in non-equilibrium

cases  $\Sigma_{L/R}^R(E) \rightarrow \Sigma_{L/R}^R(E \pm eV_b/2)$ , and consequently the line-width function

$$\Gamma_{L/R}(E) \rightarrow \Gamma_{L/R}(E \pm eV_b/2), \text{ which is defined as } \Gamma = i[\Sigma^R - \Sigma^A] = i[\Sigma^> - \Sigma^<]$$

Therefore the Retarded Green's function  $G_{MM}^R(E)$  can be calculated and Lesser Green's function through Eq.3.7, and thus electron density  $n(\vec{r})$  Eq. 3.4. In the practice, dividing the energy integration ranges can reduce the computation cost, and the electron density becomes (see Appendix B4 for details):

$$n(\vec{r}) = -\frac{1}{\pi} \int_{-\infty}^{\mu_{\min}} dE \text{Im}[G^R(\vec{r}, \vec{r}; E)] + \frac{1}{2\pi i} \int_{\mu_{\min}}^{\mu_{\max}} dE G^<(\vec{r}, \vec{r}; E) \quad 3.12$$

$\mu_{\min} \equiv \min\{\mu_L + \Delta V_L, \mu_R + \Delta V_R\} - V'$ ,  $\mu_{\max} \equiv \max\{\mu_L + \Delta V_L, \mu_R + \Delta V_R\} + V'$ ,  $\Delta V_{L(R)}$  is the electrical

potential energy for each electrode, normally set as the half of total bias times  $e$ ,  $\Delta V_{L(R)} = \pm \frac{eV_b}{2}$ ,

and  $V'$  is the cutoff energy for the range of energy integration.

Similarly, the current  $I$  Eq.3.8 becomes:

$$I = \frac{e}{\pi\hbar} \int_{\mu_{\min}}^{\mu_{\max}} dE [f(E - \mu_L) - f(E - \mu_R)] T(E) \quad 3.13$$

The iteration steps can be outlined as:

1. Initiate density  $n^i(\vec{r})$  by performing DFT iteration of the unbiased extended molecule.
2. Form  $H_{MM}[n]$  and  $S$  matrix with DFT software and compute  $G_{MM}^R(E)$  with pre-calculated self-energy  $\Sigma_{L/R}^R(E)$ .
3. Calculated elements of  $G_{MM}^<(E)$  by Eq. 3.7.

4. Obtain new density  $n^{i+1}(\vec{r})$  by energy integration of  $G^<(E)$  Eq. 3.12. If convergence reaches  $\|n^i(\vec{r}) - n^{i+1}(\vec{r})\| < \delta$ , calculate transmission coefficient, current, conductance.

Otherwise,

5. Generate new density  $n^{i+2}(\vec{r})$  by mixing up  $n^{i+1}(\vec{r})$  and  $n^i(\vec{r})$ , iterate step 2.

All the quantities can be represented in the AO basis. Finally, the whole formalism is established completely and the calculation procedure can be summarized in see Fig. 2.

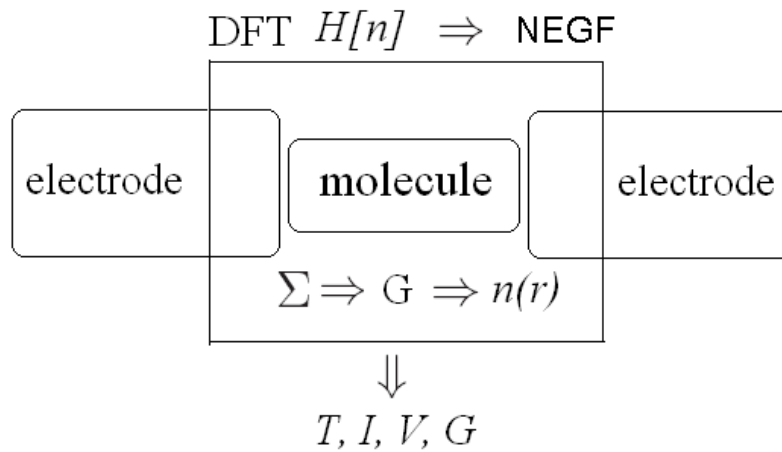


Figure 2. Scheme of Ab initio NEGF for two probe system

At this point, it is interesting and instructive to discuss the three computational methods applied in this project. 1. Technically, they all have self-consistent iterations with differences to certain degree: HF based on wave functions and eigenvalue HF equation, DFT based on density and eigenvalue KS equation, therefore these two bear a process of solving eigenvalue problem i.e. diagonalization of a matrix called Fock matrix, however, *ab initio* NEGF here is based on density and integration of the Lesser Green's function to form iteration. 2. The DFT can conveniently generate initial density and provide basic form of Hamiltonian ( $H_{MM}$ ) for *ab initio* NEGF iteration on the same computational platform, but it is not in the core of the iteration; HF methods also could be applied for the necessary purposes. Therefore the integration of NEGF

and DFT is rather subtle. 3. Normal DFT is only valid for ground state problems, thus in this non-equilibrium case, NEGF is suitable formalism; however, the dynamics DFT is a candidate to cope the transportation problem for nanostructures though it is not included in this project. 4. the *ab initio* NEGF discussed in this project is a commonly used method in the Nano-transportation community, and it is still under developing since there are limits or approximations can be reduced or improved independently, such as construction of self-energy, Hamiltonian, DFT itself, etc. For the purpose of this project, we just need qualitative understanding of conductance and *I-V* characteristics of the seven molecules, therefore, this method is appropriate at this stage, and more rigorous investigations leave to improved computational and experimental methods in the future. The detailed computational setting and procedures are discussed in the next section.

### 3.2 Two probe system with seven Diamondoids

#### 3.2.1 Calculation tools and System setups

In this project, we used the ATK (Atomistix ToolKit) software package ([www.atomistix.com](http://www.atomistix.com)) and the VNL (Virtual Nanolab) software package ([www.virtualnanolab.com](http://www.virtualnanolab.com)). Atomistix ToolKit (ATK) whose predecessor is TranSIESTA-C package<sup>96</sup> an *ab initio* electronic structure program capable of simulating and modeling electrical properties of molecular systems coupled to semi-infinite electrodes. Non-equilibrium Green's functions (NEGF) and density functional theory (DFT) are already integrated in the software. All the *ab initio* NEGF calculations discussed above could be performed in these two software packages. And Virtual Nanolab (VNL) software package provides access to atomic-scale modeling techniques with a graphical interface for simulation and analysis of the atomic scale properties of nanoscale devices.



With the assistance of VNL, we constructed two types of electrodes: first type is semi-infinite linear gold (Au) chains and second one is comprised of Au (100) surface in a  $2 \times 2$  unit cell, as shown in Figure 3. We choose gold as the electrodes since it is more practical and promising as monatomic nano-wire. The constant bond length of Au atom was optimized by ATK. Molecules could be placed in between two electrodes and then each central region/extended molecule as discussed in theoretical part includes one diamondoid molecule and two layers Au atoms from each leads/electrodes.

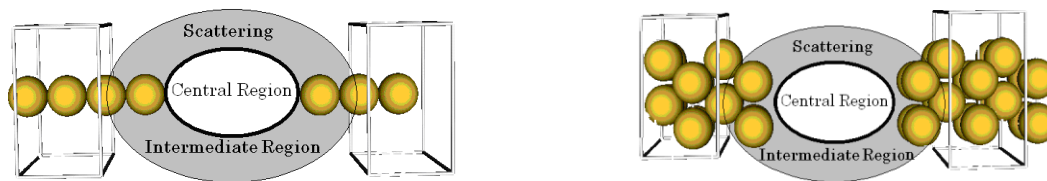


Figure 3. The two semi-infinite linear and  $2 \times 2$  gold (Au) chain electrodes

The distance between the electrodes in the two cases can be freely controlled in VNL graphical interface, however, this setting should be chosen with caution i.e. the distance has to be physically reasonable, can not be too small, while if it is too large, the calculation lose its purpose. There is no standard criterion for this subtle setting. We opted this distance by optimizing the geometry of extended molecule first and using the optimized distance as reference. Thus the distance between the electrodes depends on the orientations and the sizes of the molecules.

In most cases of calculations, the exchange-correlation functional is LDA-PZ, which is the local density approximation (LDA) with the Perdew-Zunger (PZ) parameterization<sup>97</sup> of the correlation energy of a homogeneous electron gas calculated by Ceperly-Alder.<sup>98</sup> We used the Double Zeta Polarization basis set for the *ab initio* NEGF calculations. DZP is sufficient enough to provide serious results while save computation cost. A double-zeta basis set for hydrogen has

two functions, and a true double-zeta basis set for carbon would have ten functions. Additional flexibility is built in by adding higher-angular momentum basis functions. Since the highest angular momentum orbital for carbon is a  $p$  orbital, the “polarization” of the atom can be described by adding a set of  $d$  functions. Besides, the optimal value of the mesh cut-off was found to be 100 Ry, and the optimum  $k$ -point grid mesh number in the  $Z$  direction was found to be 100.

Based on the theory and computation implements, we calculated the energy levels, transmission spectrums and conductance of the seven chosen molecules. We also calculated current-voltage ( $I$ - $V$ ) and conductivity-voltage ( $G$ - $V$ ) characteristics of some of those molecules.

### 3.2.2 Computation settings

We have focused on the exhibition of the results we obtained and the prospective applications in the field of nanotechnology. As a simulation of real experiments, geometrical optimizations using DFT method is necessary. However, since diamondoids are very stable and stiff molecules therefore, the geometrical structures of these molecules would not, and thus the conductance would not, be affected. For these reasons, we do not need to perform geometrical optimizations again. We checked by optimizing adamantane and diamantane with two gold (Au) atoms considered as the two-tips of the electrodes. In both cases, the geometrical structures of these diamondoids did not change significantly. Therefore, we could conclude that due to the stiffness of diamondoids, the electronic properties would not be affected by the two tips that are used as the electrodes. Although we did not optimize the geometrical structures of molecules in Group 1 and Group 2, we indeed optimized geometrical structures of some two-probe systems

which include molecules and electrodes using ATK, and also we did geometrical optimization of the molecules in Group 3. We would like to discuss the results in the following sections.

### 3.3 Calculation procedures, results and discussions

#### 3.3.1 Quantum conductance calculations

In order to study the conductance of diamondoid molecules and their derivatives and to simulate the experimental conditions, the geometrical optimizations of two-probe systems are performed. Applying DFT method, we first optimized the distances between the linear Au electrodes and the Adamantane and Diamantane molecules and the optimal values are 9.06 Å and 11.00 Å respectively. We did not optimize the geometries of derivatives of Diamondoids with electrodes, however, since: a. these molecules are not geometrically symmetrical, and if we optimize the structures of the whole systems including Au electrodes, the orientations of these molecules will change which is not what we expected. b. Our purpose is to point out the potential of building nano scale electronic devices using the diamondoids and their derivatives, not the structures of the devices which could be manipulated in order to obtain useful conductance. Although the geometrical optimization of all the systems are not such necessary, we considered using the optimized distances between the electrodes and Adamantane and Diamantane molecules which are 9.06 Å and 11.00 Å when choosing the distance between the electrodes and molecules inside, i.e. the central region width.

Based on the geometry considerations above, we first calculated the quantum conductance and transmission spectrums of all our systems at zero bias. All the data are reported as in Table 4.

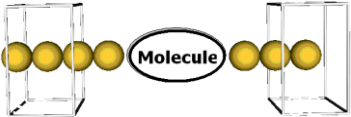
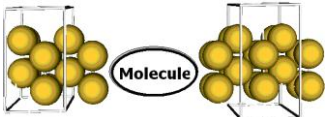

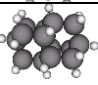
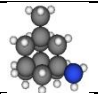
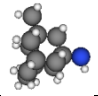
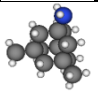
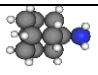
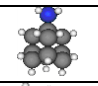
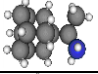
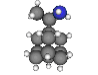

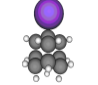
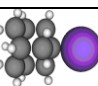
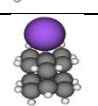
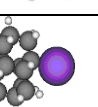

Quantum Conductance( <i>Central Region Width</i> )			
		Au linear Electrodes	Au 2x2 Electrodes
Molecule	Orientation		
Adamantane		<b>0.042</b> (9.06)	<b>2.393</b> (8.15)
Diamantane		<b>0.137</b> (11.00)	<b>10.785</b> (9.76)
Memantine (Orientation 1)		<b>0.850</b> (9.08)	<b>28.668</b> (8.46)
Memantine (Orientation 2)		<b>1.161</b> (8.69)	<b>31.308</b> (8.65)
Memantine (Orientation 3)		<b>0.842</b> (8.53)	<b>3.629</b> (9.64)
Amantadine (Orientation 1)		<b>0.767</b> (8.84)	<b>14.206</b> (8.68)
Amantadine (Orientation 2)		<b>8.072</b> (7.83)	<b>15.039</b> (8.10)
Rimantadine (Orientation 1)		<b>0.020</b> (9.90)	<b>2.837</b> (9.85)
Rimantadine (Orientation 2)		<b>11.818</b> (7.43)	<b>40.817</b> (8.32)
Na		<b>26.107</b> (9.06)	<b>77.494</b> (8.17)
ADM•Na (Orientation 1)		<b>18.078</b> (9.06)	<b>27.790</b> (8.36)
ADM•Na (Orientation 2)		<b>44.54</b> (9.90)	<b>53.60</b> (9.98)
DIM•Na (Orientation 1)		<b>1.37</b> (7.67)	<b>103.41</b> (8.48)
DIM•Na (Orientation 2)		<b>44.32</b> (11.06)	<b>54.24</b> (10.95)
DIM•Na (Orientation 3)		<b>0.578</b> (10.63)	<b>23.654</b> (9.47)

Table 6. Quantum conductance ( $G$ ), in [ $\mu S$ ], and Central Region Width, in [ $\text{\AA}$ ], of the three diamondoids groups under zero bias and the corresponding orientations

### 3.3.2 Adamantane and Diamantane

We began the calculations with adamantane; as expected, the conductance of adamantane reported in Table III is quite small. From the transmission spectrum reported in Figures 2(a) and 3(a) we can conclude that adamantane is an electrical insulator. It shows that our method is pragmatic. For diamantane, we obtained similar results (see Table 4 and Figures 2(a) and 3(a)). However, since the HOMO-LUMO gap of diamantane (Table II) is smaller, we obtained a higher conductance. As mentioned above, we used both Au linear chains and Au (100) 2×2 unit cells as electrodes, and from the results, we found that molecules confined in Au 2×2 electrodes have higher conductance than those confined in Au linear chains. Even with the same central region widths as the linear Au electrodes cases (9.06 Å and 11.00 Å) the conductance of adamantane and diamantane in Au 2×2 electrodes case (1.9375 $\mu S$  and 0.418465 $\mu S$ ) are still greater than those in linear case (0.042 $\mu S$  and 0.137 $\mu S$ ). An explanation could be that the diamondoids are 3-dimensional structures, and when electrodes are also with 3-dimensional structures, the entire systems could have more conductive channels and thus have higher conductance than when electrodes are linear. Nevertheless, this does not mean when we construct molecular electronic structures we have to use 3-dimensional electrodes, we will further discuss this in the next section.

### 3.3.3 Memantine, Rimantadine and Amantadine

When we calculated the conductance of the amino group, we chose various orientations by rotating the molecules between the two electrodes. The two reasons for these rotations are: first, molecules in this group are functionalized and their symmetries are different; second, we wanted to detect the orientations of these molecules that are electronically better which may have

applications for electron transfer or electron capture in their interactions with bio-molecules.

From this part on, the geometrical optimizations of the entire systems was not necessary any more since we were studying the effect of orientation of molecules on their electronic properties. Since the non-optimized structures might influence the accuracy of our calculations, our results for different orientations and various molecules should be used for comparison purposes only.

The conductance obtained for memantine and the central region widths at three different orientations are reported in Table 4. According to this table, in linear electrode case memantine conductance changes slightly when we rotate the molecule. However, in the case of 3-Dimensional electrode we can see significant changes in memantine conductivity with orientation change. When the nitrogen (-N) ion is close to an electrode (Orientation 2), the conductance is the largest.

From the transmission spectrums, Figure 4(b) and Figure 5(b), we can see that the LUMO resonance has more contributions to the conductance of memantine. The above two results also proved that the -NH<sub>2</sub> group has the function of n-donor.

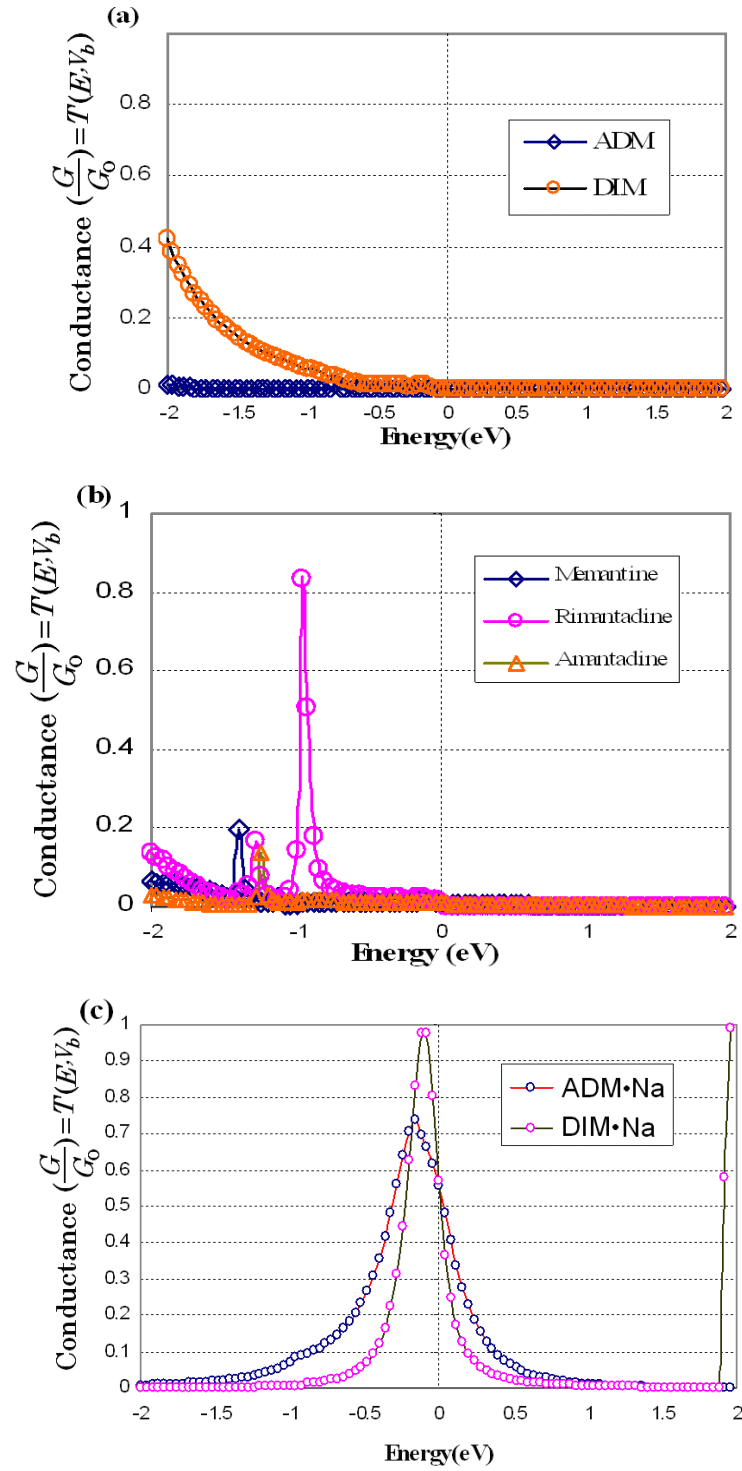


Figure 4. Transmission spectrum in Au Linear electrodes cases. (a) Transmission spectrum of Group 1. (b) Transmission spectrum of Group 2 corresponding to "Orientation 1" in Table 4. (c) Transmission spectrum of Group 3 corresponding to "Orientation 1" in Table 4.

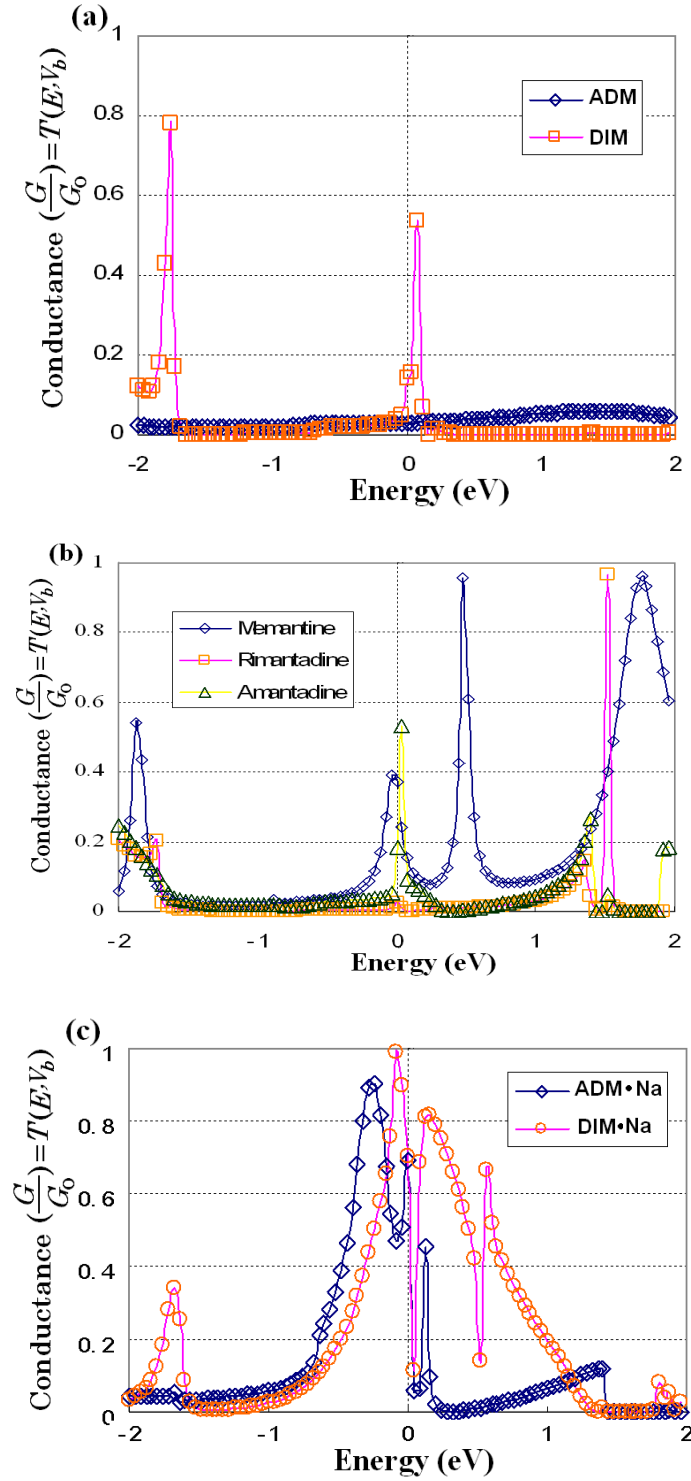


Figure 5. Transmission spectrum in Au 2x2 unit cell cases. (a) Transmission spectrum of Group 1. (b) Transmission spectrum of Group 2 corresponding to “Orientation 1” in Table 4. (c) Transmission spectrum of Group 3 corresponding to “Orientation 1” in Table 4.



Then we studied amantadine at two different orientations as reported in Table 4. From Table III, we can see that the conductance changes significantly with different types electrodes. The transmission spectrums of amantadine, as reported in Figures 4(b) and 5(b), are quite similar in trend to that of memantine.

We performed similar calculations for rimantadine, the last member of this group, at two different orientations as reported in Table III. The nitrogen ion in rimantadine is not directly connected to the adamantane cage, which makes it a bit different from memantine and amantadine. As it is reported in Table 4 the conductances are small in Orientation 1 of this molecule for both kinds of electrodes. However, we obtain high conductances in orientation 2. The Orientation 2 conductances of this molecule are the highest among all the three molecules in all orientations. The transmission spectrums of rimantadine, as reported in Figures 4(b) and 5(b) are quite distinct from those of memantine and amantadine in different ways for linear and for 2×2 electrodes.

### 3.3.4 ADM•Na and DIM•Na

We studied the quantum conductance of ADM•Na and DIM•Na, two artificial diamondoids derivatives as well as the single sodium (Na) atom. As it is reported in Table 4, it is obvious that the various conductances of these artificial molecules are generally higher than those of the lower diamondoids and derivatives reported in Table 4. It is also shown that the conductance is a strong function of the position of the Na ion in the molecule: the closer the Na ion to an electrode, the greater the conductance. The difference is large for the two orientation because from the transmission spectrum the rotation of ADM•Na molecule actually changes the Fermi energy i.e. when the Na ion is close to the electrode, the Fermi energy is close to the peak of the

transmission spectrum, while the Na is far from the electrode, the Fermi energy is above the peak. From this result, we can predict that if we can find a method (electric or magnetic field, or some mechanical force, etc) to rotate the ADM•Na molecule, then we can control the conductance of this nanostructure and we could build a nanoscale transistor.

We also studied DIM•Na and we obtained similar results to ADM•Na. Moreover, there is another interesting result for this molecule: a sharp transmission peak is shown to be close to the Fermi energy, see Figure 4(c). We can predict that as the bias increases, the current would not increase and there should be a peak or plateau on the  $I$ - $V$  characteristics graph, as discussed in the next section. Moreover, in all the Au  $2 \times 2$  electrode cases, conductance is greater than those in the three linear cases, especially, in Orientation 1. Another interesting result is that in Orientation 2 the conductance of DIM•Na with Au  $2 \times 2$  unit cell is much greater than ADM•Na with similar structure in which the conductance is almost zero. In addition, this conductance is much higher than the metallic single sodium atom conductance. This molecular orientation is predicted to be metallic representing a substantial change in electronic properties relative to the non-conducting diamondoids. Similar effects were observed in nano-tubes and fullerene doped with alkali metals.<sup>91, 92</sup>

At the end of this section, we would like to compare the transmission spectrums which demonstrate the electronic properties of our systems. From Figure 4 (a) and Figure 5 (a) we can see that Group 1 is an insulator group, especially, adamantane has very low conductance. According to Figures 4(b) and 5(b) although the conductance of Group 2 is not high but from the transmission spectrum [see Figure 4 (b) and Figure 5 (b)] we find that conductance of Group 2 can approach to  $1G_0 = 77.5\mu S$ . Therefore, we predict that Group 2 has the potential to build molecular electronic devices and the results in Table III may be used to explain the medical

applications of the molecules in this group. From Figure 4(c) and Figure 5(c), we can see the most active transmission spectrums, which show the high conductance of two artificial molecules ADM•Na and DIM•Na.

### 3.3.5 $I$ - $V$ and $G$ - $V$ characteristics

In the last section of this chapter, we applied bias potentials on electrodes and we studied the  $I$ - $V$  and  $G$ - $V$  characteristics of ADM•Na and DIM•Na molecules. Such information can be useful to build nanoscale active devices such as diodes or transistors. By studying the effects of applying various steady voltages or currents; we would find a desired mode of operation. As an example, we report horizontal orientation of these two molecules when placed in between Au linear Electrodes as reported by Figure 6.

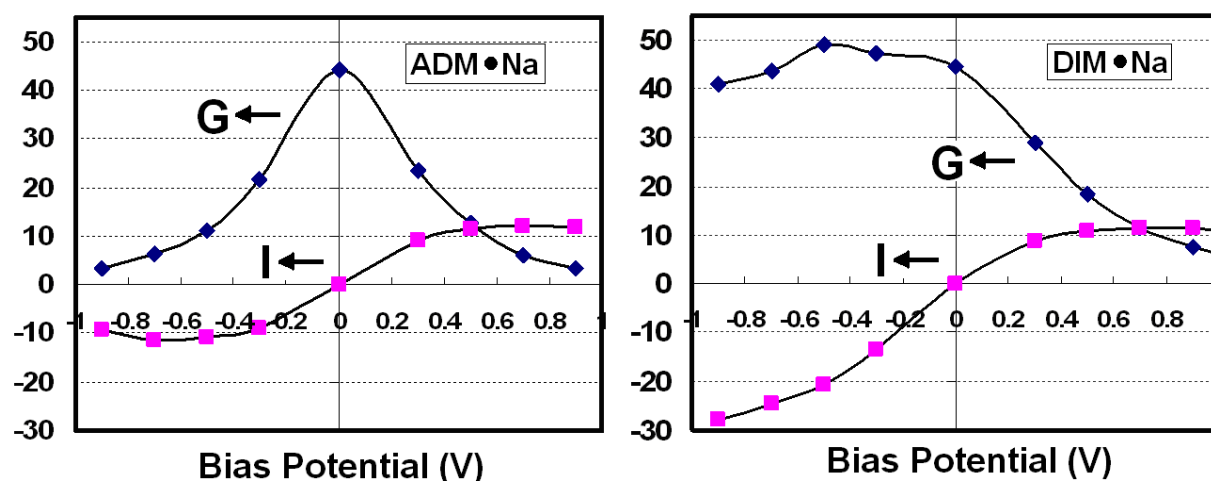


Figure 6.  $G$  [ $\mu$ S] vs.  $V$  [V] and  $I$  [ $\mu$ A] vs.  $V$  [V] characteristics of ADM•Na and DIM•Na in linear electrodes corresponding to their horizontal orientations (Orientations 2 in Table 4).

According to Figure 6, there are plateaus in the  $I$ - $V$  graph between 0.5V and 0.9V for both cases of ADM•Na and DIM•Na molecules and the currents come to maximums of 11.90  $\mu$ A and 11.35  $\mu$ A. Since the current is the integral of transmission over energy as in Eq. (3.13) and when

bias  $V_b$  increases transmission  $T(E, V_b)$  decreases, therefore the integral would come to a maximum, which is the reason there is a plateau in the  $I$ - $V$  characteristic graph. Using this  $I$ - $V$  characteristic, we could build molecular rectifier or surge protector. Furthermore, two characteristics graph are obtained from the linear Au chain since only in the linear electrodes case we found peaks near Fermi energy, which show linear electrodes or atomic nanowire also have possibility to construct nanoscale devices for 3-dimensional molecules.

### 3.4 Conclusions

In this chapter, we first discussed *ab initio* NEGF which is a popular and suitable method for molecular scale electron transportation study. Although approximations and simplification are used in this formalism, researches have showed reliable qualitatively results, furthermore, this formalism could be improved separately, e.g. one can improve the formalism by calculating the self-energy with better algorithm, or/and developing exact exchange-correlation functional, or/and including electron-phonon scattering in the central region. Therefore, all the results here could be refined by improving the calculation methods.

We then applied this method to study seven lower diamondoids; according to the *ab initio* NEGF studies, we could conclude that when different residues are added to diamondoids, the electronic properties of diamondoids can be changed, such as the HOMO-LUMO gap of molecules, the conductance, etc. We also found that the diamondoid derivatives have the potential as molecular building blocks of nanoscale electronic devices due to their considerable conductance. It is also demonstrated that quantum conductance of diamondoids derivatives change significantly for various orientations. The  $I$ - $V$  characteristics of ADM•Na and DIM•Na

show that these molecules have the potential as molecular rectifiers.<sup>16</sup> It is also highly possible to construct more complicated devices with different combinations of these molecules.

The studies on the potential of diamondoids as MMBs in molecular electronics, however, need experimental justification, and this chapter is sufficient as the start point of further researches which can focus on quantitative quantum conductance study both theoretically and experimentally, and the designing of the MED based on diamondoids.

On the other hand, to build functional integrated molecular devices e.g. molecular IC, one needs to understand self-assembly properties of the diamondoids which is the goal of next chapter.

## Chapter 4 Self-assembly and Phase transitions-----MD studies

Understanding the electronic nature of diamondoids is the foundation of building the molecular electronic devices, and finding a suitable process of fabricating is the next question that should be answered. The traditional top-down methods in semiconductor industry, in general, are not suitable for building structures at molecular scale, while the bottom-up methods commonly used in chemistry and drug design communities are more appropriate for this task, especially the self-assembly strategy. In order to adapt bottom-up methods to build molecular structures with diamondoids, one should understand the intermolecular behaviors of these molecules first, i.e. how diamondoids molecules interact with each other. And then one can apply those understandings to control the bottom-up procedures, such as the conditions of self-assembly process. Many related researches have been executed to study the self-assembly properties of diamondoids. We attempted classical molecular dynamics (MD) methods to study the interaction characteristics of diamondoids at molecular level, including the self-assembly behaviors, phase transitions in the freezing process, and to investigate the final structural properties. The systematic MD studies demonstrate the interesting self-assembly properties of those molecules and their potential as molecular building blocks.

### 4.1 Self-assembly and MD simulations of diamondoids

#### 4.1.1 Self-assembly researches of diamondoids

The most studied case for self-assembly of diamondoids is Self-Assembled Monolayer (SAM), either adamantane-thiol (ADM+S) on the metal (such as Au) surface<sup>99, 100</sup> or adamantane molecules on Si surfaces.<sup>65, 101</sup> Since those researches are suitable for experimental studies of diamondoids, such as STM and X-ray studies. The second kind of self-assembly is soft materials directed assembly, e.g. polymers or bio-molecules. This case is similar to the bio-mimic through directing of DNA amino-acid molecules can form proteins and most researches are about DNA directed self-assembly of adamantane.<sup>31, 41</sup>

The other strategy is through freezing of diamondoids to form self-assembled structures, which is this chapter's main goal. We applied MD simulation to study self-assembly properties of the seven diamondoids using the procedure similar to phase transition from vapor state to liquid state and then to solid state, discussed in section 4.3.

#### 4.1.2 Phase transition MD simulations

Diamondoids have attracted attentions of researchers due to their plastic crystal /molecular crystal nature and MD simulations have been common tools to study the phase transitions of lower diamondoids.<sup>102</sup> One interesting properties of adamantane is that in the solid state adamantane molecular crystal has secondary phase transition from FCC to BCC or from disordered state to ordered crystal structure state,<sup>103</sup> which has been studied by various MD simulation methods,<sup>104-107</sup> mainly different force fields.

Self-assembly, on the other hand, involves the transition process from random state to a semi-ordered state i.e. vapors state to solid state. MD simulations have been used to study the freezing-like procedures from hard spheres to clusters<sup>108</sup> and showed that MD method is an appropriate tool to study phase transition process. And there have not been any reports on the

third kind of self-assembly of adamantane by MD simulations or any other methods; therefore we first applied the MD methods to theoretically study one of the most important properties to build molecular devices from the bottom.

## 4.2 Introduction to Molecular Dynamics Simulations

### 4.2.1 Molecular interaction, Quantum mechanics and Force fields in nutshell.

MD simulations is a method to study the dynamics behavior of molecules semi-empirically;<sup>109</sup> it treats molecules or atoms as classical mass points and the molecular interactions that are originated from quantum mechanics effects of electrons and nuclei are represented in one single force field (interacting potential energy) as classical Newton's problem, i.e. instead of solving quantum mechanics expectation value problem:<sup>110</sup>

$$E_{\text{int}}(R_{ij}) = \langle \Psi(r_1, r_2 \dots r_N; R_1, R_2 \dots R_M) | \hat{V}_{\text{int}}(R_{ij}) | \Psi(r_1, r_2 \dots r_N; R_1, R_2 \dots R_M) \rangle,$$

where  $\hat{V}_{\text{int}}(R_{ij})$  is the potential energy term between two nuclei in the Hamiltonian of

Schrödinger equation and  $|\Psi\rangle$  represents the eigenvectors of the many-body practically

insolvable differential-equation  $i\hbar \frac{\partial}{\partial t} |\Psi\rangle = \hat{H} |\Psi\rangle$  or the time-independent version

$\hat{H} |\Psi\rangle = E |\Psi\rangle$  as the one mentioned in the chapter 2, one uses a semi-empirical force field

$E_{\alpha}(R_{ij})$  between two sites  $i, j$  ( that could be real atoms or virtual ones) to imitate the total

quantum effects,  $\alpha$  indicates the type of force fields for the two specific sites or say the

combination rule. The more one can accommodate the quantum effects of electrons in the

simplified the force fields for atomic sites, the better the one can simulate the molecular system.

In reality there is no one force field can truly include all quantum effects just as no exact

solutions to many-body Schrodinger equation and no force field can handle all the simulation



purpose appropriately, but only capable for certain conditions or purposes. That is why there are various types of force fields for the users to choose that depends on the requirements of the simulation.

In classical MD, once the force fields are chosen or assigned to each site in the system, the force fields remain unchanged in the whole simulation process; therefore the quality and choice of force field is crucial for the classical MD simulation; while the *ab initio* MD in which the force fields are evaluated at certain step by quantum method is more flexible about the force fields, but it cost much more computation time, therefore not suitable for large systems. The force fields in classical MD could be derived from experiment data, e.g. the William Force Field for adamantane,<sup>111</sup> perturbation theory calculation and *ab initio* quantum computation, e.g. the OPLS Force Fields,<sup>112</sup> or the mixed methods.

MD simulation methods have been broadly used in studying dynamics of molecules, despite of its classic approximation.<sup>113</sup> The beauty and greatest success of MD is that only assign force fields to a few atoms through certain combination rules for different atoms, one can simulate/predict the dynamics of the whole molecular system which could contain hundreds of those atoms and it provides results that can connect microscopic world and macroscopic world in a way similar as statistic mechanics to thermodynamics.<sup>114</sup> Although MD simulations method is semi-empirical, it is proven a powerful and reliable tool for molecular level problems at many fields, such as molecular biophysics, and it is also a common method for nanoscale researches.

#### 4.2.2 OPLS-AA force field.

In MD simulations, atomic sites (real or virtual) are recognized as the basic elements, since all the effects of electrons are already artificially integrated in the atomic site models. The interaction energy of a whole molecular system usually split into intramolecular interactions and intermolecular interactions. The intramolecular interaction means the potential energies between atomic sites inside molecules, thus it should include bonding energy (stretch), bending energy (angle), torsional energy (dihedral) and non-bonding energies between atomic sites; while the intermolecular interactions are all non-bonded, including van der Waals energy and electrostatic energy; and there is a cross term which means all the remaining effect besides other energies and the coupling (doubt counted) energy parts, this is term in many classical force fields are ignored. Therefore, one can write the total energy as summation of these terms,  $R^N$  here represents distance between two atomic sites of  $N$  body system:

$$E(R^N) = E_{bond} + E_{angle} + E_{dih} + E_{vdw} + E_{el} + E_{cross}$$

We use the OPLS-AA force field as an example to demonstrate the terms individually. In the Optimized Potentials for Liquid Simulations All Atom (OPLS-AA)<sup>112, 115</sup> force field total energy is divided as:

$$E(R^N) = E_{bond} + E_{angle} + E_{dih} + E_{ab}$$

The bonding, bending, torsional parts of intramolecular interactions are treated as usual, while the non-bonding terms share the same form with the intermolecular interaction non-bonding terms but with different scale factor, and  $E_{ab}$  represents the non-bonding energy inside molecule  $a$  (b) individually or between molecule  $a$  and molecule  $b$ , explained below.

The bonding energy is the potential energy between two bonded atomic sites and treated as harmonic oscillation:

$$E_{bond} = \sum_{bonds} k_R (R - R_{eq})^2 ,$$

The bending energy is potential energy between two bonds, similarly as angular harmonic oscillation with angle as variable:

$$E_{angle} = \sum_{angles} k_\theta (\theta - \theta_{eq})^2$$

The torsional (dihedral) energy can be pictured as the energy arising from twisting of two bonds that are not directly connected but have one bond in between them. It is periodic and can be written as Fourier series; in OPLS-AA force field, the first four terms are used as many other force fields.

$$E_{dih} = \frac{V_1}{2} [1 + \cos(\phi)] + \frac{V_2}{2} [1 - \cos(2\phi)] + \frac{V_3}{2} [1 + \cos(3\phi)] + \frac{V_4}{2} [1 - \cos(4\phi)]$$

In the OPLS-AA force field, the non-bonded interactions are represented by the general Lennard-Jones plus Columbic form as:

$$E_{ab} = \sum_i^a \sum_j^b E_{ij} = \sum_{i \in a, j \in b} \left\{ 4\epsilon_{ij} \left[ \left( \frac{\sigma_{ij}}{R_{ij}} \right)^{12} - \left( \frac{\sigma_{ij}}{R_{ij}} \right)^6 \right] + \frac{q_i q_j e^2}{R_{ij}} \right\} f_{ij}$$

where  $E_{ij}$  is the interaction energy of two sites for both intermolecular and intra-molecular non-bonded cases.

$$E_{ij} = \sum_{i,j} \left\{ 4\epsilon_{ij} \left[ \left( \frac{\sigma_{ij}}{R_{ij}} \right)^{12} - \left( \frac{\sigma_{ij}}{R_{ij}} \right)^6 \right] + \frac{q_i q_j e^2}{R_{ij}} \right\} f_{ij}$$

The combining rules used along with this equation are  $\sigma_{ij} = (\sigma_{ii}\sigma_{jj})^{1/2}$  and  $\epsilon_{ij} = (\epsilon_{ii}\epsilon_{jj})^{1/2}$ . For intermolecular interactions (when  $i, j$  corresponds to different molecules)  $f_{ij}=1.0$ . While for intramolecular non-bonded interactions between all pairs of atoms ( $i < j$ ) separated by three or more bonds, the 1, 4-interactions are scaled down by  $f_{ij}=0.5$ .

All the formula above is one demonstration of MD interaction energy, and there are more variations for different force fields, for example, the forms of bonding energy could be Morse potential, the Lennard-Jones potential could be 'Exponential form', etc.

When all the parameters such as  $k_r$ ,  $\sigma_{ij}$  are determined for atomic sites, then one can apply those equations to simulate the molecular systems of interesting. For different force fields the parameters are different since the energy equations would be different and the combination rules also vary, therefore, the force field normally are not directly interchangeable and it is common to use consistent force field for one system. However, there are always exceptions, such as mixing of force fields, hybrid of quantum MD and classical MD, all depend on the actually problems, and new parameterization process might be involved.

#### 4.2.3 Temperature, temperature couplings and simulated annealing in MD.

The basic physics principles behind MD can be simply just classic mechanics, however, since the molecular systems could consist of hundreds even thousands of atomic sites, there are many actually technique problems involved, here we point out a few related in this project. More specific technical issues are explained in the next section.

The macroscopic quantity temperature in MD is defined classically by:

$$\frac{1}{2} N_{df} kT = \frac{1}{2} \sum_{i=1}^N m_i v_i^2 = E_{kinetic}$$

$N_{df}$  is the degree of freedom which can be computed:

$$N_{df} = 3N - N_c - N_{com}$$

$N_c$  is the constraints imposed on the mechanic system by the nature of the problem, while the  $N_{com}$  indicates the removal of freedoms at the center of mass of the whole system in the MD simulation: when consider the simulation box as a whole system the translational motion of the center of mass (COM) can be removed  $N_{com} = 3$ ; when in the vacuum, the rotational motion of COM can be removed  $N_{com} = 6$ .

Temperature coupling is the technique used in MD to control the system temperature  $T$  to a heat bath temperature  $T_0$ . The heat flows into and out of the system by scaling the velocities of each particle at every time step through certain protocol.<sup>116</sup> Simulated annealing means the current reference temperature for temperature coupling changes as time goes by, e.g. one can change the temperature from initially 200K to 100K during certain time steps. The important concern in simulated annealing is that there should be longer coupling time than the system inherent relaxation time, i.e. one need to allow sufficient annealing time or system may crash due to too much temperature difference at each time step.

In our molecular dynamics (MD) simulation study of seven diamondoids self-assembly and phase transition behaviors, we chose Optimized Potentials for Liquid Simulations All Atom (OPLS-AA) force field since the process is similar to condensation transition from gas state to

liquid state, and then freezing transition from liquid state to solid state, which is a border range of phase transitions and OPLS-AA force field has shown excellent capabilities not only in the gas and liquid states but also in crystalline phases in a large range of temperatures; moreover, OPLS-AA is a reliable force field for carbohydrates<sup>115</sup> and, obviously, for hydrocarbons.

## 4.2 MD Simulation Procedures and Results

### 4.2.1 Settings of simulation system and the validations

Our MD simulations are mainly performed based on the Gromacs 4 MD simulation package<sup>117-119</sup> a well-known fast calculation package with flexible characteristics, besides Gromacs package integrates OPLS-AA force fields. The MD results in the chapter are visualized by VMD software.<sup>120</sup> Most of the system setup operations could be done by the commands in Gromacs package; only exceptions, technically, were from the absence of topology files (.top file) of the seven molecules. In order to perform simulations involving small molecules, we added to it the necessary ITFs “included topology files” for the seven molecules we studied which were generated by *x2top* command in Gromacs package and then produced the ‘.top’ file for the seven molecules.

The initial geometrical structures of the seven molecules are from the quantum calculations from Chapter 2. And also the atomic electronic charges are calculated to be -0.76 and 0.65 for nitrogen atom and sodium atom, respectively (in electronic charge units: Coulomb). The atomic charges of carbon and hydrogen atoms were mainly opted from default OPLS-AA force field.

We report a brief summary of our MD simulation scheme: vacuum simulation strategy was used in the first step to determine how many molecules were suitable for our simulation and

obtain equilibrated stable structures. Then we built periodic boundary simulation box; and we used fast PME (Particle-Mesh Ewald) electrostatics method<sup>121</sup> for the preparation of gas state while we chose simpler cutoff technique for electrostatics in the self-assembly/freezing procedure, since the PME cost more computation time while cutoff method is adequate to produce reliable results; we performed both for adamantane system and the difference turned out to be insignificant.

To simulate freezing transition, we applied the annealed simulation technique to gradually decrease the system temperature. V-rescale temperature coupling was applied throughout and in all the simulations. This is a temperature-coupling method using velocity rescaling with a stochastic term. The van der waals force cut-off and neighbor-searching list distance were, both, set to 2.0 nm, which was large enough since above 1.4 nm the van der waals force is negligible.

The first step was to determine the number of molecules in the simulation box which is a canonical (NVT) ensemble. We performed short (20-40 picoseconds) MD simulations of different numbers of adamantane molecules, (i.e. 8, 27, 64, 125, 216, 343, 512, 729 molecules) in vacuum with the temperature set at 100 K, and we successfully obtained all the stable structures as shown in Figure 7.

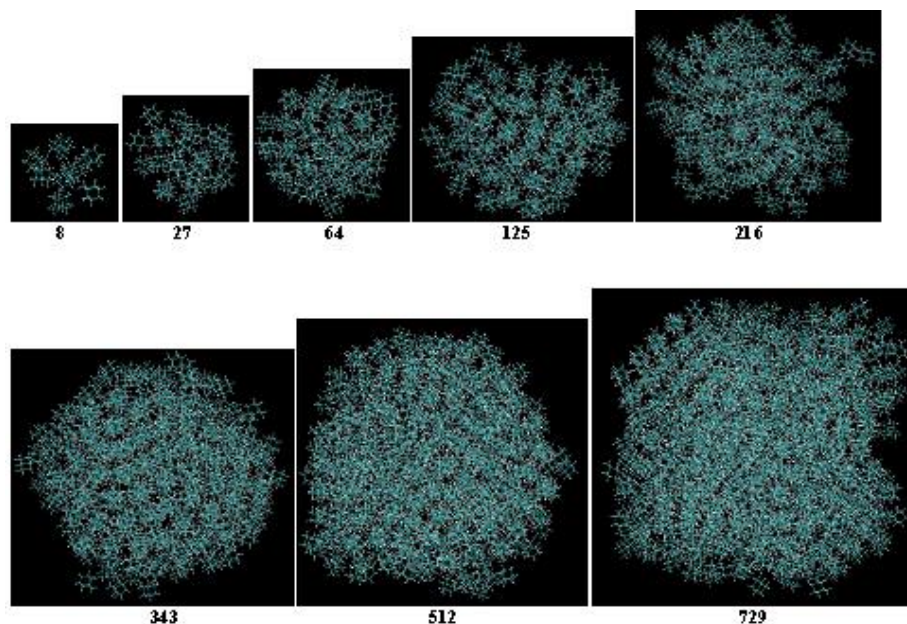


Figure 7 Snapshots from MD simulations using various numbers of adamantane molecules ( $2^3$ ,  $3^3$ ,  $4^3$ ,  $5^3$ ,  $6^3$ ,  $7^3$ ,  $8^3$ ,  $9^3$ )

Although those structures are stable, they may not be used for structural analysis, since the simulations are rather too short. And we found that 125-molecule system is large enough to represent the self-assembly behavior, which also can save calculation cost, therefore, we chose 125 molecules in what is reported in the rest of this paper. From this point on, all the MD simulation systems involved 125 molecules for the seven molecules.

In order to perform self-assembly simulations from gas state to liquid state and eventually solid state, we developed the following procedure for the seven types of molecules:

(a). A MD simulation box with  $5 \times 5 \times 5 = 125$  molecules was built by the intrinsic tools in the Gromacs software as shown in Figure 8-a.



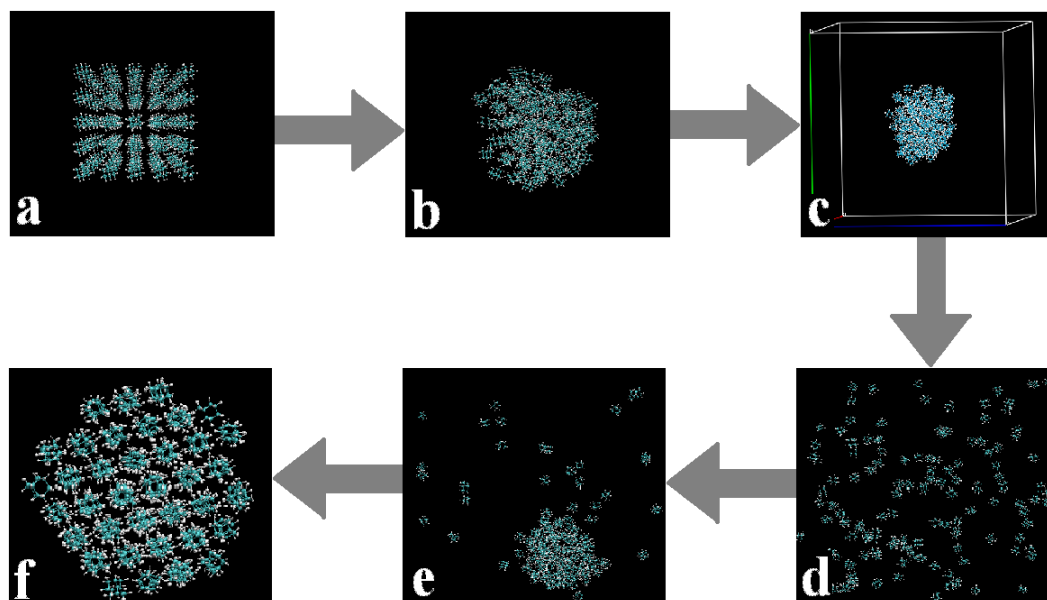


Figure 8. Stages of simulation procedure: (a) Initial 5x5x5 MD simulation box; (b) Molecules relaxed in vacuum at 100 K after a short MD simulation; (c) Boxed simulation system with overall gas density; (d) Gas phase as a result of equilibrating simulation in the NVT ensemble; (e) The liquid state; (f) Final self-assembly of molecules to solid state.

- (b) Then we performed a short MD simulation by letting all the molecules relax in a vacuum at 100 K (like Figure 1) to obtain the stable self-assembled structure as shown in Figure 8-b.
- (c) We boxed those stable structures and set the distances from molecules to the boundaries of simulation boxes to about +3 nm. In this manner we could build simulation systems with reasonable densities which are in the range of their gas states and also make the systems isolated from the adjacent simulation boxes under the periodic boundary conditions as shown in Figure 8-c.
- (d) Longer (more than 1000 picoseconds) equilibrating simulations were performed in the NVT ensembles, and we applied PME method with cut-off at 2.0 nm and high temperatures (in the range of 500 – 700 K) to make sure the entire system went to the gas state, *i.e.* all the molecules separated from each other and distributed randomly in the simulation box as shown in Figure 8-d.

By applying the above four-step procedure we could equilibrate the system in a gas state. As a result, we eliminated the problem due to directly equilibrating the initially prepared molecular system, Figure 8-a, at high temperature. The equilibrated and stable-structure gas state, Figure 8-d, was then ready for cooling down towards the self-assembly.

(e) The next step of the simulation was the cooling down the equilibrated and stable-structure gas state, Figure 8-d, from the gas to the liquid state as shown in Figure 8-e.

(f) Further cooling down of the system resulted in the complete self-assembly of all the molecules (to solid state) as shown in Figure 8-f.

The snapshots of the gas-liquid-solid MD simulations for 125 molecules (stages d, e and f of Figure 2) of each of the seven molecules (*Adamantane*, *Diamantane*, *Amantadine*, *Rimantadine*, *Memantine*, *ADM•Na.*, *ADM•Na*) are reported in Figure 9.

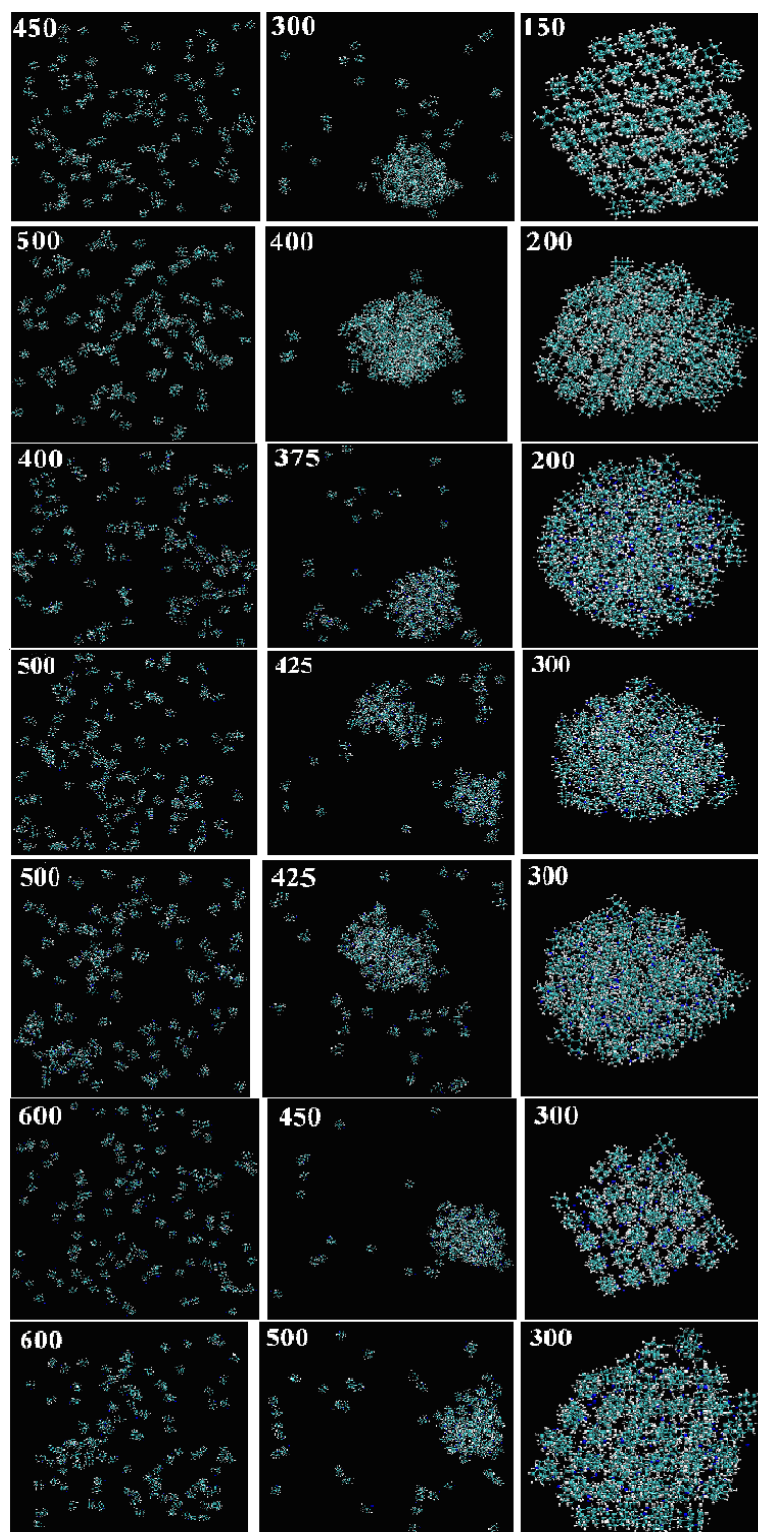


Figure 9. Self-assembly snapshots of 125 molecules of the seven compounds (from top: Adamantane, Diamantane, Amantadine, Rimantadine, Memantine, ADM•Na., ADM•Na) as temperature [K] is decreased.

From these snapshots we can directly observe clear phase transitions for each kind of molecule, from the gaseous state to liquid state, and then their aggregation into a highly condensed solid (self-assembled) state.

In order to find the equilibrium configurations of the collection of the 125 molecules at every given temperature we used the simulated-annealing procedure. Every change of 1 K occurred within 10 picoseconds (5,000 time-steps and each time-step was 0.002 ps). With these settings we could observe the self-assembly behaviors in the cooling steps.

It should be mentioned that we applied the cut-off of 2.0 nm for the electrostatics instead of PME, which was used in step d (Figure 8), in order to 1. make sure all the interactions among molecules are considered, even beyond 1.4nm which is custom cut-off setting, since after 1.4nm there is no significant van der waals force; 2. thus save the computation time as well, since PME requires more computation than cut-off method does.

According to Figure 9 adamantane, diamantane, ADM•Na and ADM•Na form ordered condensed (crystalline) states. However, amantadine, rimantadine and memantine, while they self-assemble, they do not seem to form clear ordered condensed (crystalline) states. We further produced the hydrogen bonds locations of the same self-assembled snapshots of amantadine, memantine and rimantadine as shown in Figure 10 below.

According to this figure we do not observe any ordered format for the location of hydrogen-bonds which is an indication of the non-crystalline self-assembled states of these three kinds of molecules. Obviously the existence of partial hydrogen-bonds between these molecules is the reason for the lack of a clear crystalline state in their self-assemblies.

#### 4.2.2 Hydrogen-bonds distribution of Group 2

Group 2 (amino group) can form Hydrogen bonds due to the interactions between H and N ions. From Figure 10 it is obvious that bonding orientation is rather random even at very low temperature 50K.

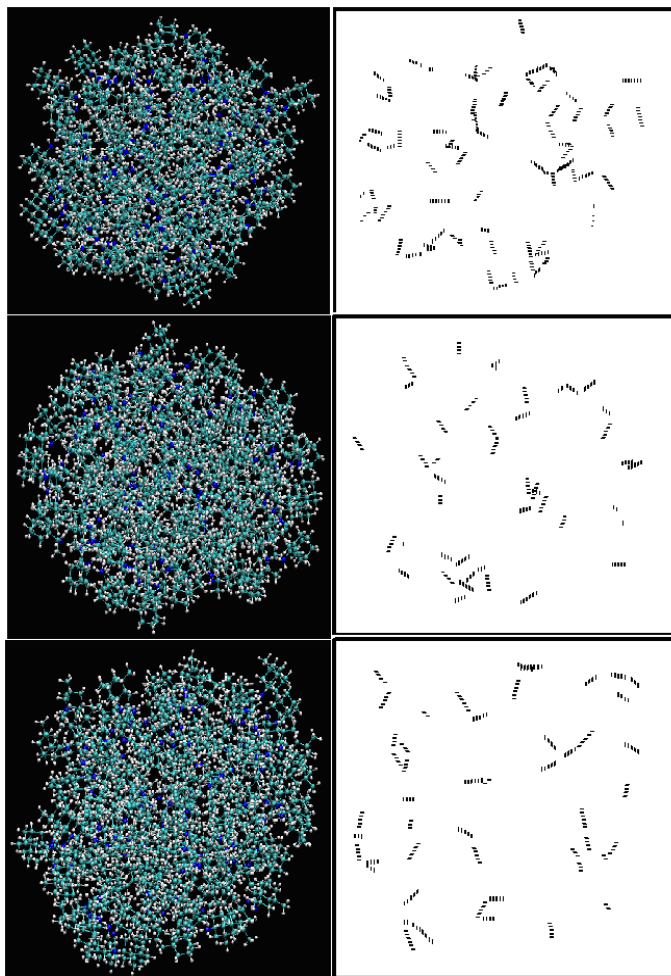


Figure 10. MD snapshots of (from top to bottom) Amantadine, Rimantadine and Memantine and at 50K hydrogen bonds location

We also performed studies in the hydrogen-bonds saturation as a function of temperature as well as hydrogen-bond distribution of the three molecules (amantadine, rimantadine and memantine) as shown in Figures 11 and 12.

According to Figure 11 in the process of phase transition and self-assembly of these three molecules the number of their hydrogen-bonds saturate at relatively low temperatures (below 100K).

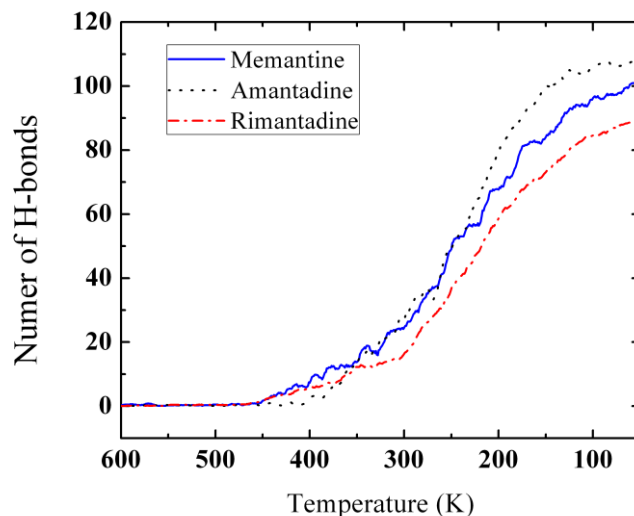


Figure 11. The number of Hydrogen bonds for Amantadine, Memantine and Rimantadine vs. temperature. As temperature decreases the numbers of H-bonds increase, and tend to maximum numbers for the three derivatives.

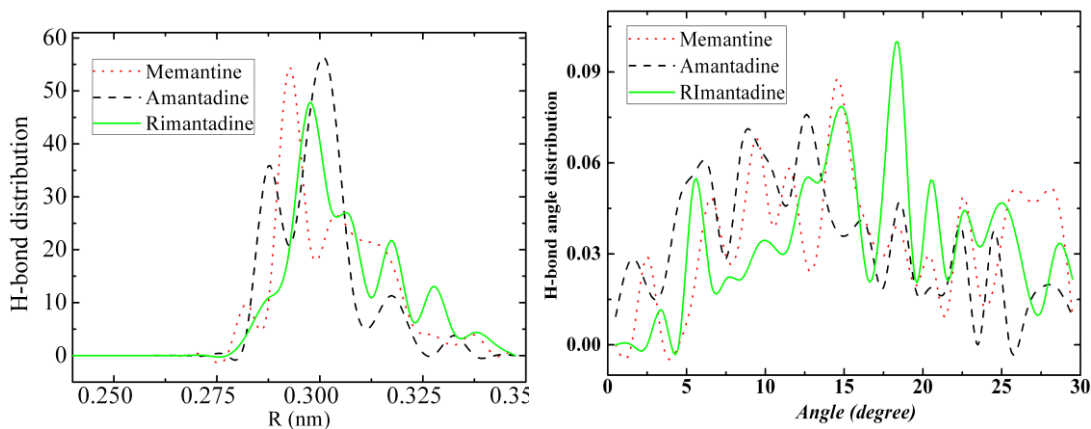


Figure 12. Hydrogen-bond distance distribution (Left) and hydrogen-bond angle distribution (Right) at 60K for Amantadine, Rimantadine and Memantine. The most possible hydrogen-bond lengths are around 0.3 nm for the three molecules. The hydrogen-bond angles seem randomly distributed.

From the hydrogen-bond distance-distribution graph of these three molecules at 60 K (Figure 12-Left), we can find three peaks at about 0.3 nm, which indicate that the structures are close to uniform crystal structures. While the angle distributions (Figure 12-Right) show that the hydrogen-bond angles are rather randomly distributed for all the three molecules. We already mentioned of the hydrogen-bonds of this group at 50 K (Figure 9) which did not show any ordered features. Both Figures 9 and 12 indicate that these structures are not neat crystal structures contrary to adamantane self-assembled state. These three hydrogen-bonded molecules just self-assemble at particular temperatures, but may not form well-organized self-assembled crystal structures. The reason is that the geometry structures of these molecules are not as symmetric as adamantane; and their  $\text{-NH}_2$  and  $\text{-CH}_3$  segments, make them unable to pack orderly as adamantane.

#### 4.3 Radial distribution functions (RDFs) and structure factors (SFs) analysis

We also produced the radial distribution functions (RDFs) and structure factors (SFs) of the seven different molecules as presented and discussed below. Study of the RDFs and SFs also reveal further about these phase transition features as discussed below. The RDFs we studied and report here are for the centers of the geometry of molecules.

##### 4.3.1. Adamantane and $\text{ADM}\cdot\text{Na}$

The main feature of adamantane is that at low temperatures we can observe ordered crystal structures (the top-right image in Figures 9). From the RDF and SF graphs at different temperatures (Figure 13) we can observe gas, liquid and solid characteristics.

In the RDF figures, higher and sharper peaks can be observed as the temperature decreases and for the SF graphs, the intensity increases as phase transits from gas to liquid and to solid state. We observed similar features in the RDF and SF of ADM•Na as shown in Figure 14.

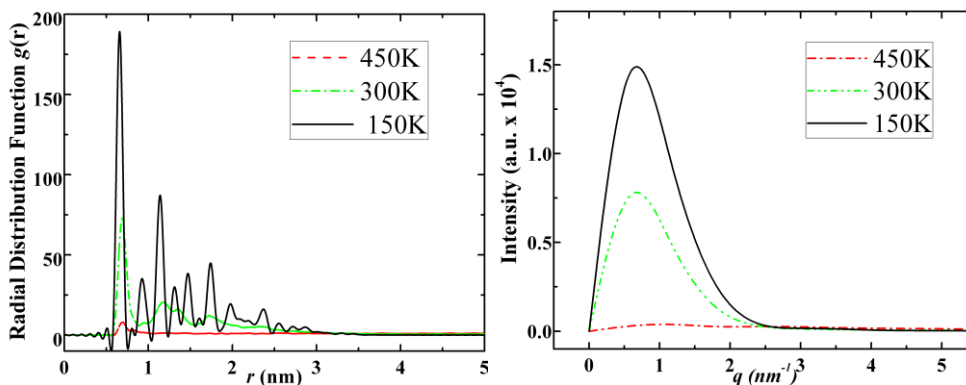


Figure 13. Radial distribution functions (left) and structure factors (right) of adamantane at 450K, 300K and 150K for gas, liquid and solid states, respectively.

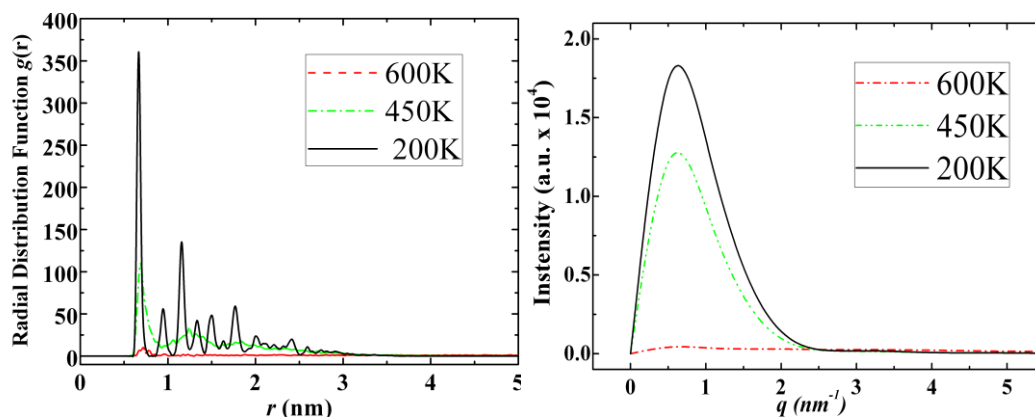


Figure 14. Radial distribution functions (left) and structure factors (right) of ADM•Na at 600K, 450K and 200K for gas, liquid and solid states, respectively.

The phase transition temperatures for ADM•Na are higher than those of adamantane. However, this is attributed to -Na affecting the molecular interactions among adamantane molecules, i.e. -Na ion in the ADM•Na structure causes stronger bonding than that of the respective -H ion in adamantane. We may also conclude that the higher phase transition



temperatures in ADM•Na compared to those of adamantane are due to  $\text{Na}^+$  ion, while the geometry structure is determined by the structure of adamantane.

#### 4.3.2. Diamantane and ADM•Na:

Diamantane molecules can self-assemble to a certain type of solid state structure which can be observed from simulation snapshots (Figure 9), however, its self-assembled structure is not as neat as the crystal structure of adamantane. In Figure 15 we report the RDF and structure factor of diamantane in various phases.

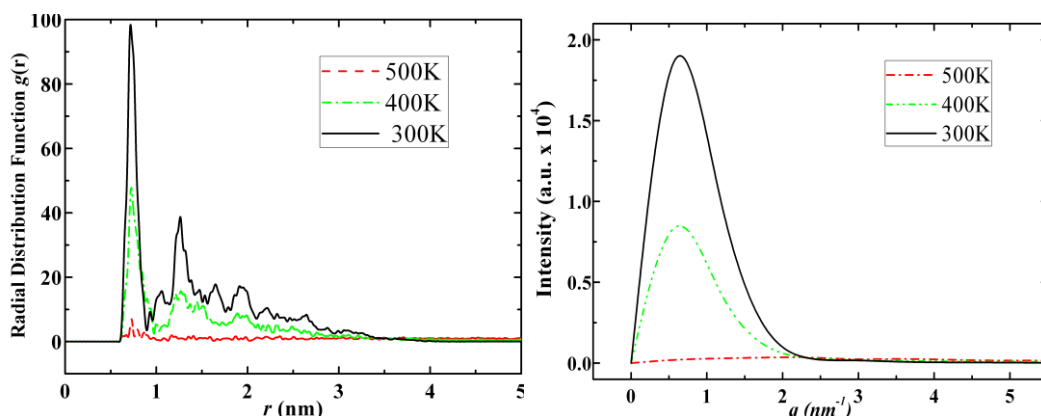


Figure 15. Radial distribution functions (left) and structure factors (right) of diamantane at 500K, 400K and 300K for gas, liquid and solid states, respectively.

From the RDF and structure factor of diamantane, Figures 15, respectively, we may also conclude the same, i.e. at low temperatures diamantane does not have features of neat crystal structure. ADM•Na shows similar relationship to diamantane as ADM•Na to adamantane, i.e. higher phase transition temperatures due to sodium, while similar self-assembled crystal structures as diamantane molecules (See related snapshots in Figure 9, RDFs in and SFs in Figure 16).

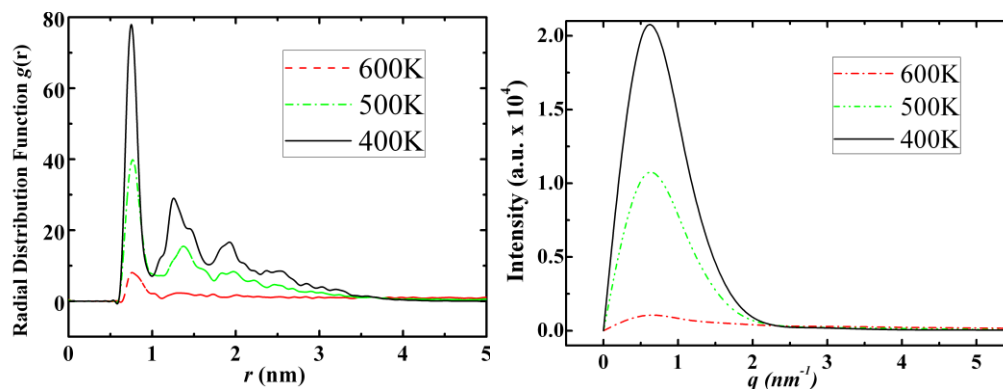


Figure 16. Radial distribution functions (left) and structure factors (right) of ADM•Na at 600K, 500K and 400K for gas, liquid and solid states, respectively.

#### 4.3.3. Amantadine, Rimantadine and Memantine

The three molecules in this group self-assemble at higher temperatures compared with adamantane, but they don't have well-organized crystalline structures as shown in the snapshots in Figure 10. The reasoning for the self-assembly behavior of these three molecules is as follow: Since there are nitrogen ions in the structure of these molecules, which makes the attractive intermolecular forces much bigger than that of diamondoid, higher temperature should be applied to these systems in order to obtain initial gas state structures in the step d of Figure 8 . During the procedure of cooling down these molecules, hydrogen-bonds are formed which, as expected, increases the phase transition temperatures compared to that of adamantane. As it is observed from their self-assembled structures (snapshots in Figure 9) these molecules form certain types of self-assembled structure, however, those structures are much more random than that of adamantane, i.e. no apparent solid state structure as FCC or BCC. There may be two main reasons for this: 1. the  $-\text{NH}_2$  group present in these molecules break some geometrical symmetry of adamantane; 2. we observed that hydrogen bonds are randomly distributed in the bulk

structures which makes the entire structures far from an ordered one. In Figures 17-19 we report the RDFs and SFs of these three molecules for the gas, liquid and solid phases.

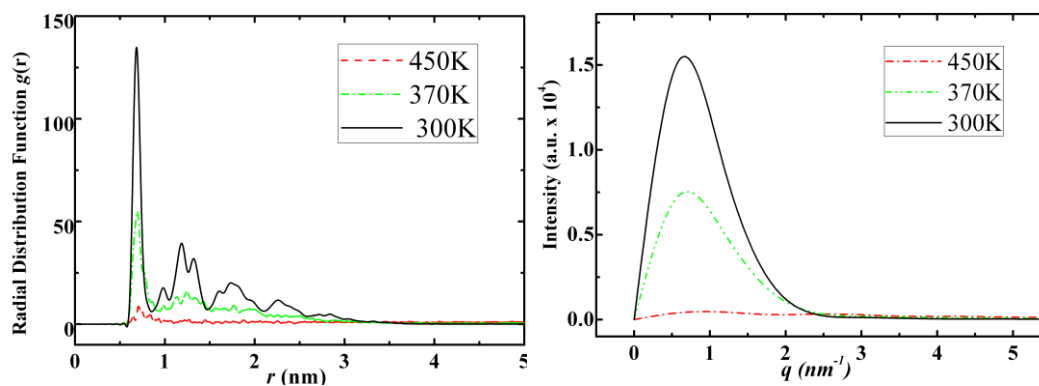


Figure 17. Radial distribution functions (left) and structure factors (right) of amantadine at 450K, 370K and 300K for gas, liquid and solid states, respectively.

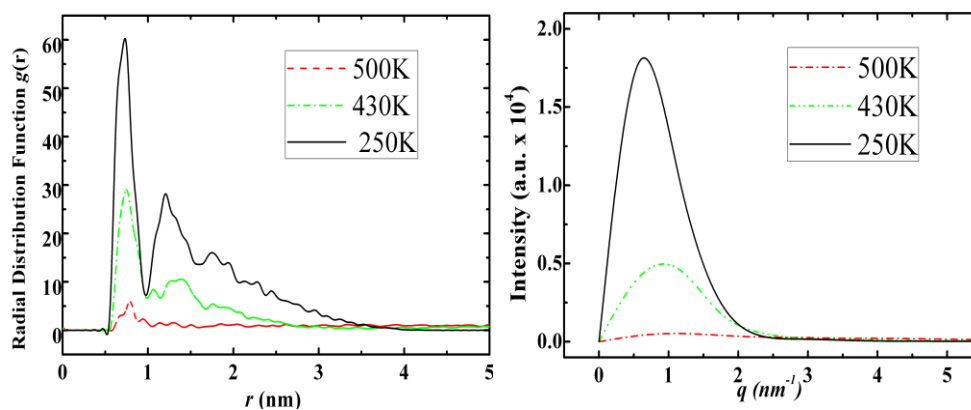


Figure 18. Radial distribution functions (left) and structure factors (right) of rimantadine at 500K, 430K and 250K for gas, liquid and solid states, respectively

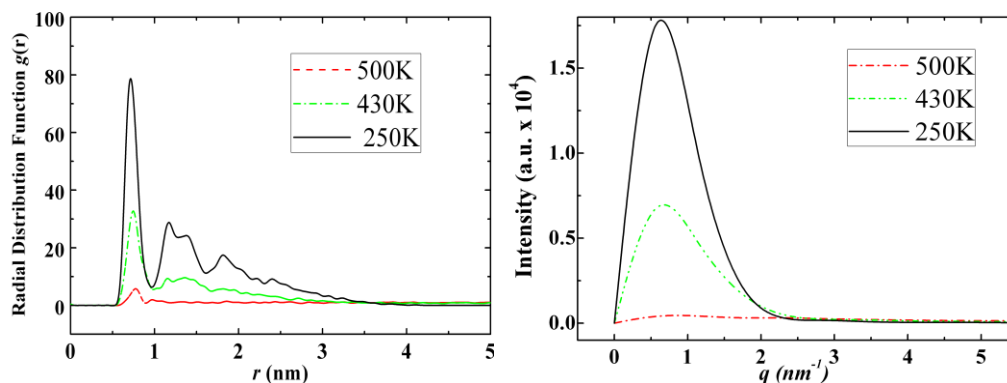


Figure 19. Radial distribution functions (left) and structure factors (right) of Memantine at 500K, 430K and 250K for gas, liquid and solid states, respectively.

According to Figures 17-19 the solid phase RDFs and SFs analysis of these three molecules show that for most part there is less obvious solid state features, i.e. sharp peaks as in adamantane and ADM•Na RDFs. The liquid-state RDF graphs for these three molecules also, for most part, have less obvious liquid-state features either.

In Figure 20 and Figure 15 we summarize the self-assembled (solid-state) radial distribution functions and structure factors, respectively, of the seven molecules with uniform coordinates scales for the purpose of their collective comparison.

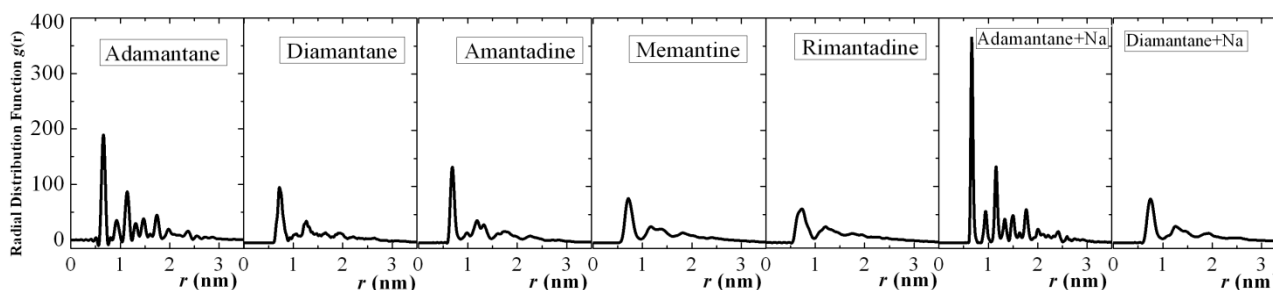


Figure 20. Radial distribution functions of the seven compounds (from left: Adamantane, Diamantane, Amantadine, Rimantadine, Memantine, ADM•Na., ADM•Na) in the self-assembled (solid) state.

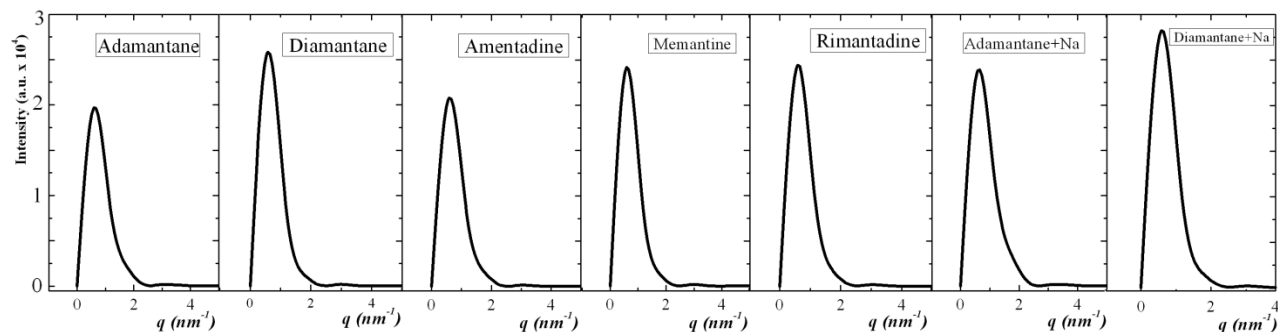


Figure 21. Structure factors of the seven compounds (from left: Adamantane, Diamantane, Amantadine, Rimantadine, Memantine, ADM•Na., ADM•Na) in the self-assembled (solid) state.

From Figure 20 and Figure 21 we can observe that adamantane and ADM•Na have more sharp peaks than other five molecules, which indicate compact solid state structures. Other five molecules also show solid characteristic peaks but they have less number of such sharp peaks than adamantane and ADM•Na. These results match the image observation of simulations (Figure 9), i.e. adamantane and ADM•Na have neater structures in solid state due to their molecular symmetry, which thus proves that self-assembly of those molecules are structure-dependent.

#### 4.3.4 Density dependence studies of phase transition points

We also chose different volumes for 64 and 125 adamantane molecular systems to study the density dependence of phase transition points (Onset and completion of self-assembly) as shown in Figure 22 and Figure 23. It is obvious that transition points vary when the density changes for both 64 and 125 adamantane molecular systems. The transition points, however, are markedly different at low densities for the two systems of 64 and 125 molecules.

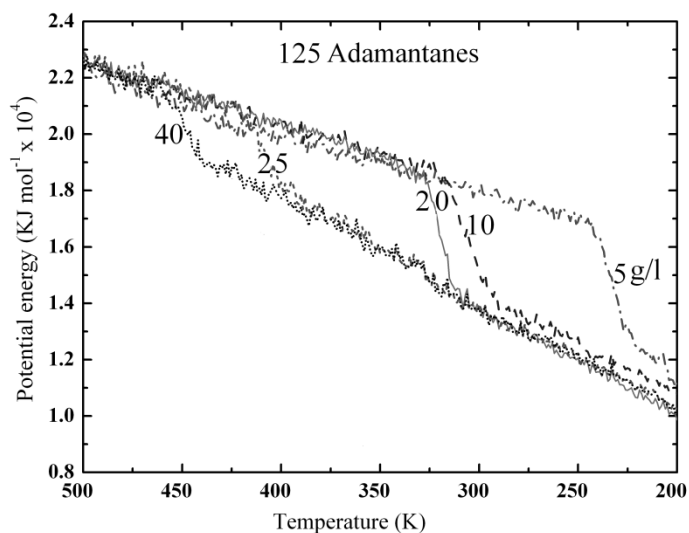


Figure 22. Potential energy vs. Temperature raw simulation data of 125 adamantane molecules ensemble system at different density from 5, 10, 20, 25 and 40g/l simulated annealing from 500K-200K, showing density dependence of phase transition points.

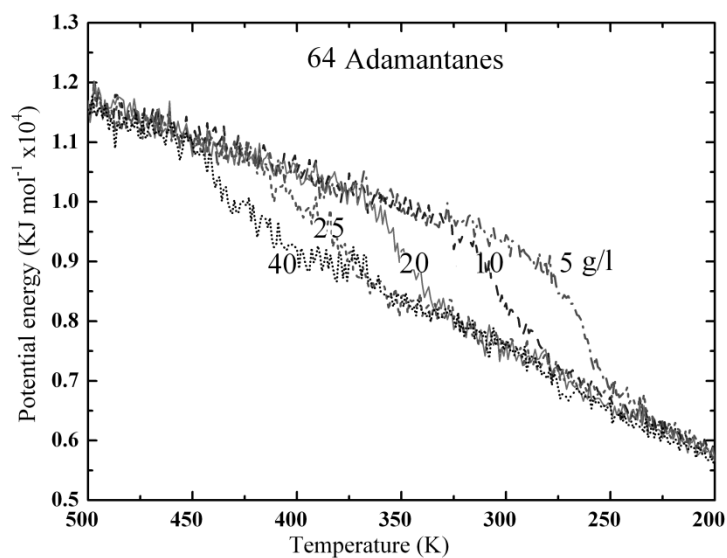


Figure 23. Total potential energy vs. Temperature raw simulation data of 64 adamantane molecules ensemble system at different densities (5, 10, 20, 25 and 40g/l) using simulated annealing technique showing density dependence of phase transition points.

#### 4.4 Conclusion

We have performed a detailed molecular dynamics study of the self-assembly process of seven different diamondoids and derivatives due to temperature variations. From the MD simulation study of the seven molecules, we may conclude the following: 1. The nature of self-assembly in these molecules is a structure-dependent phenomenon. 2. Final self-assembly structures depend on the different bonding types present in the molecular structure of these various molecules. 3. The artificial molecules still hold neat crystal structures. Although -Na ion increases the phase transition temperature, as those the -NH<sub>2</sub> residue in group 2, in a large extent the structural features of diamondoids are retained in adamantane-Na and diamantane-Na. The reasons for the latter might be that: A. the -Na ion has less topology effect than does the -NH<sub>2</sub> residue. B. there is no hydrogen-bonding in the structures of adamantane-Na and diamantane-Na; therefore they can aggregate to ordered structures. This feature is very promising, since it would allow us to build orderly-shaped NEMS and MEMS. The density dependence of phase transition point studies showed that at small scale the transition points depends on the densities of the nanoscale systems; this could assist the controlling of the self-assembly processes of those molecules.

## REFERENCES

1. Feynman, R.P.: There's Plenty of Room at the Bottom. *Caltech Engineering and Science* 23: 22-36, 1960.
2. Landau, L.D. and Lifshitz, E.M.: *Quantum Mechanics (Non-relativistic Theory) 3rd ed.* Butterworth-Heinemann, Reed Educational and Professional Publishing, 1977.
3. Sakurai, J.J.: *Advanced Quantum Mechanics*. New York, Addison-Wesley, 1967.
4. Sakurai, J.J.: *Modern Quantum Mechanics, Revised ed.* New York, Addison-Wesley, 1994.
5. Chen, C.J.: *Introduction to Scanning Tunneling Microscopy 2nd ed.* New York, Oxford University Press, 2008.
6. Binnig, G. and Rohrer, H.: Scanning tunneling microscopy. *IBM Journal of Research and Development* 30:4, 1986.
7. Giessibl, F.J.: Advances in atomic force microscopy. *Reviews of Modern Physics* 75:949, 2003.
8. Alcock, N.W.: *Bonding and structure : structural principles in inorganic and organic chemistry*. New York, Ellis Horwood, 1990.
9. Burkert, U.: *Molecular Mechanics*. Michigan, American Chemical Society, 1982.
10. Mansoori, G.A.: *Principles of Nanotechnology- Molecular-Based Study of Condensed Matter in Small Systems*. NJ, World Scientific Pub. Co. Hackensack, 2005.
11. Moore, G.E.: Progress in digital integrated electronics. *IEEE IEDM Tech Digest*:11-13, 1975.
12. Hutcheson, D.G.: Moore's Law: The History and Economics of an Observation that Changed the World, *The Electrochemical Society INTERFACE* 14:17-21, 2005.
13. Petty, M.C., Bryce, M.R. and Bloor, D.: *Introduction to Molecular Electronics*. New York, Oxford University Press, 1995.



14. Lu, A.J., Pan, B.C. and Han, J.G.: Electronic and vibrational properties of diamondlike hydrocarbons. *Phys. Rev. B* 72:35447, 2005.
15. Drexler, K.E.: *Engines of Creation*. New York, Doubleday, 1986.
16. Aviram, A. and Ratner, M.A.: Molecular Rectifiers. *Chem. Phys. Lett.* 29: 277-283, 1974.
17. Huang, Y., Duan, X., Cui, Y., Lauhon, L.J., Kim, K.-H. and Lieber, C.M.: Logic Gates and Computation from Assembled Nanowire Building Blocks. *Science* 294 2001.
18. Bachtold, A., Hadley, P., Nakanishi, T. and Dekker, C.: Logic Circuits with Carbon Nanotube Transistors. *Science* 294:1317, 2001.
19. Tans, S.J., Vershueren, A.R.M. and Dekker, C.: Room-temperature transistor based on a single carbon nanotube. *Nature* 393:49, 1998.
20. Schön, J.H., Meng, H. and Bao, Z.: Self-assembled monolayer organic field-effect transistors. *Nature* 413:713, 2001.
21. Schön, J.H., Meng, H. and Bao, Z.: Field-Effect Modulation of the Conductance of Single Molecules. *Science* 294: 2138-2140, 2001.
22. Reed, M.A., Chen, J., Rawlett, A.M., Price, D.W. and Tour, J.M.: Molecular random access memory cell. *Appl. Phys. Lett.* 78:3735, 2001.
23. Roth, K.M.e.a.: Molecular approach toward information storage based on the redox properties of porphyrins in self-assembled monolayers. *J. Vac. Sci. Technol. B* 18:2359, 2000.
24. Stafford, C.A., Cardamone, D.M. and Mazumdar, S.: The quantum interference effect transistor. *Nanotechnology* 18:6pp, 2007.
25. Ullien, D., Cohen, H. and Porath, D.: The effect of the number of parallel DNA molecules on electric charge transport through 'standing DNA'. *Nanotechnology* 18:4pp, 2007.
26. Lagerqvist, J., Zwolak, M. and Di Ventra, M.: Fast DNA Sequencing via Transverse Electronic Transport. *NANO LETTERS* 6: 779-782, 2006.
27. Di Ventra, M.: *Electrical Transport in Nanoscale Systems*. New York, Cambridge University Press, 2008.

28. Clay, W.A., Liu, Z., Yang, W., Fabbri, J.D., Dahl, J.E., Carlson, R.M., Sun, Y., Schreiner, P.R., Fokin, A.A., Tkachenko, B.A., Fokina, N.A., Pianetta, P.A., Melosh, N. and Shen, Z.X.: Origin of the monochromatic photoemission peak in diamondoid monolayers. *Nano Lett* 9:57-61, 2009.
29. Linko, V., Leppiniemi, J., Paasonen, S.-T., Hytonen, V.P. and Toppari, J.J.: Defined-size DNA triple crossover construct for molecular electronics: modification, positioning and conductance properties. *Nanotechnology* 22:275610 7pp, 2011.
30. Xue, Y. and Mansoori, G.A.: Self-assembly of diamondoid molecules and derivatives (MD simulations and DFT calculations). *Int J Mol Sci* 11:288-303, 2010.
31. Ramezani, H., Saberi, M.R. and Mansoori, G.A.: Diamondoids and DNA Nanotechnologies. *Int'l J. Nanoscience & Nanotechnology (IJNN)* 3: 21-35, 2007.
32. Zhang, G.P., George, T.F., Assoufid, L. and Mansoori, G.A.: First-principles simulation of the interaction between adamantane and an atomic-force microscope tip. *Phys. Rev. B* 75 2007.
33. Drummond, N.D., Williamson, A.J., Needs, R.J. and Galli, G.: Electron emission from diamondoids: a diffusion quantum Monte Carlo study. *Phys Rev Lett* 95:096801, 2005.
34. Fort, R.C. and Schleyer, P.v.R.: Adamantane: Consequences of the Diamondoid Structure. *Chem. Rev.* 64: 277–300, 1964.
35. Mansoori, G.A.: Diamondoid Molecules. *Advances in Chemical Physics* 136: 207-258, 2007.
36. Marchand, A.P.: Diamondoid Hydrocarbons--Delving into Nature's Bounty. *Science* 299: 52–53, 2003.
37. van Leeuwen, R., Dahlen, N.E., Stefanucci, G., Almladh, C.O. and von Barth, U.: Introduction to the Keldysh Formalism and Applications to Time-Dependent Density-Functional theory.
38. Marsusi, F., Mirabbaszadeh, K. and Mansoori, G.A.: Opto-electronic Properties of Adamantane and Hydrogen-Terminated Sila- and Germa-Adamantane: A Comparative Study. *Physica E* 41: 1151-1156, 2009.
39. Mansoori, G.A., George, T.F., Zhang, G.P., Assoufid, L.: *Structure and Opto-Electronic Behavior of Diamondoids, with Applications as MEMs and at the Nanoscale Level, Chapter I* Nova Pub's 2009.

40. Ramezani, H., Mansoori, G.A. and Saberi, M.R.: Diamondoids-DNA Nanoarchitecture: From Nanomodules Design to Self-Assembly *J. Comput'l & Theor'l Nanoscience* 4:96-100, 2007.
41. Pathak, R. and Marx, A.: An adamantane-based building block for DNA networks. *Chem Asian J* 6:1450-5, 2011.
42. Xue, Y. and Mansoori, G.A.: Quantum Conductance and Electronic Properties of Lower Diamondoids and their Derivatives. *International Journal of Nanoscience* 7: 63–72, 2008.
43. Xue, Y. and Mansoori, G.A.: Phase Transition and Self-assembly of Lower Diamondoids and Derivatives. *MRS Proceedings*:1282, 2010.
44. Drummond, N.D.: Nanomaterials: diamondoids display their potential. *Nat Nanotechnol* 2:462-3, 2007.
45. Schwertfeger, H., Fokin, A.A. and Schreiner, P.R.: Diamonds are a chemist's best friend: diamondoid chemistry beyond adamantane. *Angew Chem Int Ed Engl* 47:1022-36, 2008.
46. Filik, J., Harvey, J.N., Allan, N.L., May, P.W., Dahl, J.E., Liu, S. and Carlson, R.M.: Raman spectroscopy of diamondoids. *Spectrochim Acta A Mol Biomol Spectrosc* 64:681-92, 2006.
47. Fokin, A.A., Tkachenko, B.A., Gunchenko, P.A., Gusev, D.V. and Schreiner, P.R.: Functionalized nanodiamonds part I. An experimental assessment of diamantane and computational predictions for higher diamondoids. *Chemistry* 11:7091-101, 2005.
48. Silvano de Araujo, E., Mansoori, G.A., Xue, Y. and Lopes Barros de Araujo, P.: Diamondoid molecules behavior prediction by ab initio methods. *Physics Express* 1:67-88, 2011.
49. Wang, Y., Kioupakis, E., Lu, X., Wegner, D., Yamachika, R., Dahl, J.E., Carlson, R.M., Louie, S.G. and Crommie, M.F.: Spatially resolved electronic and vibronic properties of single diamondoid molecules. *Nat Mater* 7:38-42, 2008.
50. Simons, J. and Nichols, J.: *Quantum Mechanics in Chemistry*,. New York, Oxford University Press, 1997.
51. Hohenberg, P. and Kohn, W.: Inhomogeneous Electron Gas. *Phys. Rev.B* 136:864, 1964.
52. Kohn, W. and Sham, L.J.: Self-Consistent Equations Including Exchange and Correlation Effects. *Phys. Rev.A* 140:1133, 1965.

53. Jensen, F.: *Introduction to Computational Chemistry*. New York, John Wiley & Sons, 1999.
54. Scheck, F.: *Quantum Physics*. New York, Springer, 2007.
55. Koopmans, T.A.: Ordering of Wave Functions and Eigenenergies to the Individual Electrons of an Atom. *Physica* 1:104, 1933.
56. Roothaan, C.C.J.: New Developments in Molecular Orbital Theory. *Rev. Mod. Phys* 23:69, 1951.
57. Slater, J.C.: Atomic Shielding Constants. *Phys. Rev.* 36:57, 1930.
58. Slater, J.C.: *The Self-Consistent Field for Molecules and Solids: Quantum Theory of Molecules and Solids Vol.4*. New York, McGraw-Hill.Inc., 1974.
59. Baerends, E.J. and Gritsenko, O.V.: A Quantum Chemical View of Density Functional Theory. *J. Phys.Chem.* 101:5383, 1997.
60. Ziegler, T.: Approximate density functional theory as a practical tool in molecular energetics and dynamics. *Chem. Rev.* 91:651, 1991.
61. Parr, R.G. and Yang, W.: *Density-Functional Theory of Atoms and Molecules*. New York, Oxford University Press, 1989.
62. Lee, C., Yang, W. and Parr, R.G.: Development of the Colle-Salvetti correlation-energy formula into a functional of the electron density. *Phys. Rev. B* 37: 785-789, 1988.
63. Helgaker, T., Jorgensen, P. and Olsen, J.: *Molecular Electronic Structure Theory*. New York, Wiley, 2000.
64. Woon, D.E. and Jr., a.D.T.H.: Gaussian basis sets for use in correlated molecular calculations. III. The atoms aluminum through argon. *J. Chem. Phys.* 98:1358, 1993.
65. Meevasana, W., Supruangnet, R., Nakajima, H., Topon, O., Amornkitbamrung, V. and Songsiriritthigul, P.: Electron Affinity Study of Adamantane on Si(111).*Applied Surface Science* 256:934-936, 2009.
66. McIntosh, G.C., Yoon, M., Berber, S. and Tománek, D.: Diamond fragments as building blocks of functional nanostructures.*PHYSICAL REVIEW B* 70:1-8, 2004.

67. Landt, L., Bostedt, C., Wolter, D., Moller, T., Dahl, J.E., Carlson, R.M., Tkachenko, B.A., Fokin, A.A., Schreiner, P.R., Kulesza, A., Mitric, R. and Bonacic-Koutecky, V.: Experimental and theoretical study of the absorption properties of thiolated diamondoids.*J Chem Phys* 132:144305, 2010.
68. Yang, W.L., Fabbri, J.D., Willey, T.M., Lee, J.R., Dahl, J.E., Carlson, R.M., Schreiner, P.R., Fokin, A.A., Tkachenko, B.A., Fokina, N.A., Meevasana, W., Mannella, N., Tanaka, K., Zhou, X.J., van Buuren, T., Kelly, M.A., Hussain, Z., Melosh, N.A. and Shen, Z.X.: Monochromatic electron photoemission from diamondoid monolayers.*Science* 316:1460-2, 2007.
69. Frisch, M.J., Trucks, G.W., Schlegel, H.B. and al., e.: Gaussian 03, Revision D.01, Gaussian, Inc., Wallingford CT,. 2004.
70. Woon, D.E. and Dunning, T.H.: Gaussian basis sets for use in correlated molecular calculations. III. The atoms aluminum through argon.*J. Chem. Phys.* 98:1358-1371, 1993.
71. Dunning, T.H.: Gaussian basis sets for use in correlated molecular calculations. I. The atoms boron through neon and hydrogen.*J. Chem. Phys.*, (1989) . 90:1007-1023, 1989.
72. Reed, A.E., Curtiss, L.A. and Weinhold, F.: Intermolecular interactions from a natural bond orbital, donor-acceptor viewpoint.*Chem. Rev.* 88:899-926, 1988.
73. Godby, R.W. and Garcia-Gonzalez, P.: Density Functional Theories and Self-energy Approaches, Chapter in A Primer in Density Functional Theory. *LNP* 620: 185–217, 2003.
74. Taylor, J., Guo, H. and Wang, J.: Ab Initio Modeling of Quantum Transport Properties of Molecular Electronic Devices. *Phys.Rev.B* 63:245407, 2001.
75. Xue, Y., Datta, S. and Ratner, M.A.: First-Principles Based Matrix Green's Function Approach to Molecular Electronic Devices: General Formalism. *Chem.Phys.* 281: 151-170, 2002.
76. Mahan, G.D.: *Many-Particle Physics. Physics of Solids and Liquids 3rd ed.*New York, Kluwer Academic/Plenum Press, 2000.
77. Haug, H. and Jauh, A.P.: *Quantum Kinetics in Transport and Optics of Semiconductors, vol. 123 of Springer Series in Solid-State Sciences.* New York, Springer, 1996.
78. Keldysh, L.V.: Diagram Technique for Nonequilibrium Processes. *Sov.Phys. JETP* 20:1018, 1965.

79. Kadanoff, L. and Baym, G.: *Quantum Statistical Mechanics*. Menlo Park, W.A. Benjamin, 1962.
80. Caroli, C., Combescot, R., Nozieres, P. and Saint-James, D.: Direct calculation of the tunneling current. *J. Phys. C: Solid State Phys* 4:916-929, 1971.
81. Rammer, J. and Smith, H.: Quantum field-theoretical methods in transport theory of metals. *Rev. Mod. Phys.* 58:323, 1986.
82. Rammer, J.: *Quantum Transport Theory*. Reading, Perseus Books, 1998.
83. Kita, T.: Introduction to Nonequilibrium Statistical Mechanics with Quantum Field Theory. *Prog.Theor. Phys.* 123:581, 2010.
84. Datta, S.: *Electronic Transport in Mesoscopic Systems*. New York, Cambridge University Press, 1995.
85. Ferry, K. and M., G.: *Transport in Nanostructures*. New York, Cambridge University Press, 1997.
86. Sanvito, S.: *Ab-initio methods for spin-transport at the nanoscale level in Handbook of Computational Nanotechnology*. Stevenson Ranch, American Scientific Publishers, 2005.
87. Datta, S.: *Quantum Transport: From Atoms to Transistors. Cambridge*. New York, Cambridge University Press, 2005.
88. Brandbyge, M., Mozos, J.L., Ordejón, P., Taylor, J. and Strokbro, K.: Density-Functional Method for Nonequilibrium Electron Transport. *Phys.Rev.B* 65:165401, 2002.
89. Emberly, E.G. and Kirczenow, G.: Theoretical study of electrical conduction through a molecule connected to metallic nanocontacts. *Phys. Rev. B* 58:10911, 1998.
90. Sanvito, S., Lambert, C.J., Jefferson, J.H. and Bratkovsky, A.M.: General Green's-function formalism for transport calculations with spd Hamiltonians and giant magnetoresistance in Co- and Ni-based magnetic multilayers. *Phys. Rev.B* 59:11936, 1999.
91. Chen, P., Wu, X., Lin, J. and Tan, K.L.: High H<sub>2</sub> Uptake by Alkali-Doped Carbon Nanotubes Under Ambient Pressure and Moderate Temperatures. *Science* 285:91, 1999.
92. Farajian, A.A., Esfarjani, K. and Kawazoe, Y.: Nonlinear Coherent Transport Through Doped Nanotube Junctions. *Phys. Rev. Lett.* 82:5084, 1999.

93. Taylor, J., Brandbyge, M. and Stokbro, K.: Theory of Rectification in Four Wires: The Role of Electrode Coupling. *Phys.Rev.Lett.* 89:138301, 2002.
94. Taylor, J., Guo, H. and Wang, J.: Ab Initio Modeling of Open Systems: Charge Transfer, Electron Conduction and Molecular Switching of a Device. *Phys.Rev.B* 63:121104, 2001.
95. Rocha, A.R., Suarez, V.M.G., Bailey, S.W., Lambert, C.J., Ferrer, J. and Sanvito, S.: Smeagol - non-equilibrium electronic transport. [www.smeagol.tcd.ie](http://www.smeagol.tcd.ie) 2004.
96. Stokbro, K., Taylor, J., Brandbyge, M. and Ordejon, P.: TranSIESTA - A spice for molecular electronics. *Ann.NY Acad.Sci.* 1006:212, 2003.
97. Perdew, J.P. and Zunger, A.: Self-interaction correction to density-functional approximations for many-electron systems. *Phys. Rev. B.* 23:5048, 1981.
98. Ceperley, D.M. and Alder, B.J.: Ground State of the Electron Gas by a Stochastic Method.*Phys. Rev. Lett.* 45:566, 1980.
99. Fujii, S., Akiba, U. and Fujihira, M.: Geometry for self-assembling of spherical hydrocarbon cages with methane thiolates on au(111).*J Am Chem Soc* 124:13629-35, 2002.
100. Kim, M., Hohman, J.N., Morin, E.I., Daniel, T.A. and Weiss, P.S.: Self-assembled monolayers of 2-Adamantanethiol on Au{111}: control of structure and displacement.*J Phys Chem A* 113:3895-903, 2009.
101. Simons, J.K., Frigo, S.P., Taylor, J.W. and Rosenberg, R.A.: X-ray energy dependent photochemistry of the adamantane (C<sub>10</sub>H<sub>16</sub>)/Si(111) - 7×7 surface.*Journal of Vacuum Science & Technology A* 11:2244 - 2249, 1993.
102. Meyer, M. and Ciccotti, G.: Molecular dynamics simulation of plastic adamantane I. Structure properties. *Molec. Phys.* 56 6: 1235-1248, 1985.
103. Rapcewicz, K. and Przystawa, J.: On the order-disorder transition in crystalline adamantane C<sub>10</sub>H<sub>16</sub>.*Physica B, Condensed Matter* 205: 115-120, 1995.
104. Meyer, M., Marhic, C. and Ciccotti, G.: Molecular dynamics simulation of plastic adamantane II. Reorientation motion.*Molec. Phys.* 58:723-733, 1986.
105. Ciccotti, G., Ferrario, M., Memeo, E. and Meyer, M.: Structure Transition on Cooling of Plastic Adamantane: A Molecular-Dynamics Study.*Phy. Rev. Lett.* 59:2574-2577, 1987.

106. Trew, A.S. and Pawley, G.S.: Molecular dynamics simulation of the phase transition in adamantane. *Can. J. Chem.* 66:1018, 1988.
107. Greig, D.W. and Pawley, G.S.: Molecular dynamics simulations of the order-disorder phase transition in adamantane. *Molec. Phys.* 89: 677-689, 1996.
108. Lewis, L.J., Jensen, P. and Barrat, J.-L.: Melting, freezing, and coalescence of gold nanoclusters. *Phys. Rev. B* 56:2248–2257, 1997.
109. Lewis, L.J., Jensen, P. and Barrat, J.-L.: Melting, freezing, and coalescence of gold nanoclusters. *Phys. Rev. B* 56:2248–2257, 1997.
110. Kaplan, I.G.: *Intermolecular Interactions : physical picture, computational methods and model potentials*. Chichester, John Wiley & Sons, 2006.
111. Williams, D.E.: Nonbonded Potential Parameters Derived from Crystalline Hydrocarbons. *J. Chem. Phys.* 47:4680, 1967.
112. Jorgensen, W.L., Maxwell, D.S. and Tirado-Rives, J.: Development and Testing of the OPLS All-Atom Force Field on Conformational Energetics and Properties of Organic Liquids. *J. Am. Chem. Soc.* 118: 11225–11236, 1996.
113. Rapaport, D.: *The Art of Molecular Dynamics Simulation*. New York, Cambridge University Press, 2004.
114. Allen, M.P. and Tildesley, D.J.: *Computer Simulation of Liquids*. Oxford, Oxford University Press, 1987.
115. Damm, W., Frontera, A., Tirado-Rives, J. and Jorgensen, W.L.: OPLS All-Atom Force Field for Carbohydrates. *Journal of Computational Chemistry* 18:1955-1970, 1997.
116. Berendsen, H.J.C., Postma, J.P.M., van Gunsteren, W.F. and DiNola, A.H., J. R. : Molecular-Dynamics with Coupling to an External Bath. *Journal of Chemical Physics* 81:684–3690, 1984.
117. Lindahl, E., Hess, B. and van der Spoel, D.: GROMACS 3.0: A package for molecular simulation and trajectory analysis. *J. Mol. Mod.* 7: 306-317, 2001.
118. van der Spoel, D., Lindahl, E., Hess, B., Groenhof, G., Mark, A.E. and Berendsen, H.J.C.: GROMACS: Fast, Flexible and Free. *J. Comp. Chem.* 26: 1701-1718, 2005.



119. Hess, B., Kutzner, C., van der Spoel, D. and Lindahl, E.: GROMACS 4: Algorithms for highly efficient, load-balanced, and scalable molecular simulation.*J. Chem. Theory Comput.* 4: 435-447, 2008.
120. Humphrey, W., Dalke, A. and Schulten, K.: VMD-Visual Molecular Dynamics.*J. Molec. Graphics* 14: 33-38, 1996.
121. Darden, T., York, D. and Pedersen, L.: Particle mesh Ewald: An Nlog(N) method for Ewald sums in large systems.*J. Chem. Phys.* 98:10089-10092, 1993.

## Appendix A

### Hartree-Fock approximation in second quantization notation

In the second quantization language, quantum states are represented with the help creation operators  $C^+$  and annihilation operations  $C$ : for one particle state, it is written as

$$|\psi_i\rangle = |i\rangle = C_i^+ |0\rangle ,$$

$|0\rangle$  is the vacuum state or ground state in condensed matter physics.

The two particle state is written as:

$$|\psi_{ij}\rangle = |ij\rangle = C_i^+ C_j^+ |0\rangle ,$$

And one-particle operators can be written as:

$$\hat{h}(1) = \sum_{i,j=1} |i\rangle\langle i| \hat{h}(1) |j\rangle\langle j| = \sum_{i,j=1} \langle i| \hat{h}(1) |j\rangle C_i^+ C_j ,$$

since  $I(1) = \sum_i |i\rangle\langle i|$  and  $\sum_{i,j=1} |i\rangle\langle j| = \sum_{i,j=1} C_i^+ C_j$  for one particle in single state.

The energy for one particle states is  $E_0(1) = \langle \psi_0 | \hat{h}(1) | \psi_0 \rangle = \sum_i \langle i | \hat{h}(1) | i \rangle ;$

The two-particle interaction operator is written as:

$$\hat{h}(2) = \frac{1}{4} \sum_{i,j,k,l=1} |ij\rangle\langle ij| \hat{h}(2) |kl\rangle\langle kl| = \frac{1}{4} \sum_{i,j,k,l=1} \langle ij | \hat{h}(2) | kl \rangle C_i^+ C_j^+ C_l C_k ,$$

Since  $I(2) = \frac{1}{2} \sum_{i,j=1} |ij\rangle\langle ij|$  and  $|ij\rangle\langle kl| = C_i^+ C_j^+ C_l C_k$ .

And the energy for one particle states is

$$E_0(2) = \langle \psi_0 | \hat{h}(2) | \psi_0 \rangle = \frac{1}{4} \sum_{i,j,k,l=1} \langle ij | \hat{h}(2) | kl \rangle \langle \psi_0 | C_i^+ C_j^+ C_l C_k | \psi_0 \rangle$$

$$= \frac{1}{4} \sum_{i,j,k,l=1} \langle ij | \hat{h}(2) | kl \rangle (\delta_{ik} \delta_{jl} \pm \delta_{il} \delta_{jk})$$

$$= \frac{1}{4} \sum_{i,j=1} (\langle ij | \hat{h}(2) | ij \rangle \pm \langle ij | V(1,2) | ji \rangle)$$

$$= \frac{1}{2} \sum_{i,j=1} \langle ij | \hat{h}(2) | ij \rangle$$

Therefore for Hamiltonian  $\hat{H} = \sum_{i,j=1} \langle i | \hat{h}(1) | j \rangle C_i^+ C_j + \frac{1}{4} \sum_{i,j,k,l=1} \langle ij | \hat{V}(1,2) | kl \rangle C_i^+ C_j^+ C_l C_k$

the total ground state energy is  $E_0 = \langle \psi_0 | \hat{H} | \psi_0 \rangle = \sum_i \langle i | \hat{h}(1) | i \rangle + \frac{1}{2} \sum_{i,j=1}^N \langle ij | \hat{V}(1,2) | ij \rangle$

now consider the variation theory  $\langle \psi_0 | \hat{H} | \psi_0 \rangle \geq E_0$  for the ground state fermions system with  $N$

particles; we vary the ground state by  $\delta | \psi_0 \rangle = \mathcal{E} C_m^+ C_n | \psi_0 \rangle$  ( $n \leq N < m$ ,  $|\mathcal{E}| \ll 1$ ), or equivalently,

$\delta \langle \psi_0 | = \mathcal{E} \langle \psi_0 | C_n^+ C_m$  we should obtain the result  $\delta \langle \psi_0 | \hat{H} | \psi_0 \rangle = 0$  which indicates that:

$$\mathcal{E} \langle \psi_0 | C_n^+ C_m \hat{H} | \psi_0 \rangle = 0$$

$$\sum_{i,j=1} \langle i | \hat{h}(1) | j \rangle \langle \psi_0 | C_n^+ C_m C_i^+ C_j | \psi_0 \rangle + \frac{1}{4} \sum_{i,j,k,l=1}^N \langle ij | \hat{V}(1,2) | kl \rangle \langle \psi_0 | C_n^+ C_m C_i^+ C_j^+ C_l C_k | \psi_0 \rangle = 0$$

$$\sum_{i,j=1} \langle i | \hat{h}(1) | j \rangle \delta_{nj} \delta_{mi} + \frac{1}{4} \sum_{i,j,k,l=1}^N \langle ij | \hat{V}(1,2) | kl \rangle (\delta_{nk} \delta_{jl} \delta_{mi} - \delta_{nl} \delta_{jk} \delta_{mi} + \delta_{nl} \delta_{ik} \delta_{mj} - \delta_{nk} \delta_{il} \delta_{mj}) = 0$$

$$\begin{aligned}
\langle m | \hat{h}(1) | n \rangle + \frac{1}{4} \sum_{j=1}^N (\langle mj | \hat{V}(1,2) | nj \rangle - \langle mj | \hat{V}(1,2) | jn \rangle) + \frac{1}{4} \sum_{i=1}^N (\langle im | \hat{V}(1,2) | in \rangle - \langle im | \hat{V}(1,2) | ni \rangle) &= 0 \\
\langle m | \hat{h}(1) | n \rangle + \frac{1}{4} \sum_{j=1}^N (\langle mj | \hat{V}(1,2) | nj \rangle - \langle mj | \hat{V}(1,2) | jn \rangle + \langle jm | \hat{V}(1,2) | jn \rangle - \langle jm | \hat{V}(1,2) | nj \rangle) &= 0
\end{aligned}$$

the anti-symmetric relation of the fermion states requires the four terms of the two particle interaction are the same, so we can get:

$$\langle m | \hat{h}(1) | n \rangle + \sum_{j=1}^N \langle mj | \hat{V}(1,2) | nj \rangle = 0, \quad n, j \leq N < m$$

Define one-particle Hartree-Fock operator

$$\hat{h}_{HF} = \sum_{m,n} (\langle m | \hat{h}(1) | n \rangle + \sum_{j=1}^N \langle mj | \hat{V}(1,2) | nj \rangle) a_m^+ a_n$$

if we expect to obtain nonzero results,  $m$  and  $n$  should either both represent occupied states or unoccupied states, i.e. either  $m, n < N$  or  $m, n > N$ , otherwise the expectation values will be zero.

Assume there are eigenstates  $|\sigma\rangle$  and eigenvalues  $\mathcal{E}_\sigma$  for this operator, and these eigenstates are the same as the one-particle states for  $H$ , then the matrix elements are:

$$\langle \alpha | \hat{h}_{HF} | \beta \rangle = \sum_{m,n} (\langle m | \hat{h}(1) | n \rangle + \sum_{\sigma=1}^N \langle m\sigma | \hat{V}(1,2) | n\sigma \rangle) \langle \alpha | a_m^+ a_n | \beta \rangle$$

$$\mathcal{E}_\beta \langle \alpha | \beta \rangle = \sum_{m,n} (\langle m | \hat{h}(1) | n \rangle + \sum_{\sigma=1}^N \langle m\sigma | \hat{V}(1,2) | n\sigma \rangle) \delta_{\alpha m} \delta_{n\beta}$$

$$\mathcal{E}_\beta \langle \alpha | \beta \rangle = \langle \alpha | \hat{h}(1) | \beta \rangle + \sum_{\sigma=1}^N \langle \alpha\sigma | \hat{V}(1,2) | \beta\sigma \rangle \quad \text{A. 1}$$

In order to obtain two-particle interaction in language of one particle, one need to have the representation of two particle states in the one particle state and this could be done with the

assists of tensor products. For bosons one defines  $|ij\rangle = \frac{1}{\sqrt{2}}(|i\rangle_1 \otimes |j\rangle_2 + |j\rangle_1 \otimes |i\rangle_2)$ , fermions

$$|ij\rangle = \frac{1}{\sqrt{2}}(|i\rangle_1 \otimes |j\rangle_2 - |j\rangle_1 \otimes |i\rangle_2)$$

$$\text{Then } \langle ij | \hat{h}(2) | kl \rangle = \frac{1}{2} (\langle i | \otimes_2 \langle j | \pm_1 \langle j | \otimes_2 \langle i | ) \hat{h}(2) (|k\rangle_1 \otimes |l\rangle_2 \pm |l\rangle_1 \otimes |k\rangle_2)$$

$$= \frac{1}{2} [{}_1\langle i | \otimes_2 \langle j | \hat{h}(2) | k \rangle_1 \otimes | l \rangle_2 \pm_1 \langle j | \otimes_2 \langle i | \hat{h}(2) | k \rangle_1 \otimes | l \rangle_2 \pm_1 \langle i | \otimes_2 \langle j | \hat{h}(2) | l \rangle_1 \otimes | k \rangle_2 +_1 \langle j | \otimes_2 \langle i | \hat{h}(2) | l \rangle_1 \otimes | k \rangle_2]$$

$$\text{since } {}_1\langle i | \otimes_2 \langle j | \hat{h}(2) | l \rangle_1 \otimes | k \rangle_2 \underline{\underline{1 \leftrightarrow 2}} {}_1\langle j | \otimes_2 \langle i | \hat{h}(2) | k \rangle_1 \otimes | l \rangle_2$$

$$\text{and } {}_1\langle j | \otimes_2 \langle i | \hat{h}(2) | l \rangle_1 \otimes | k \rangle_2 \underline{\underline{1 \leftrightarrow 2}} {}_1\langle i | \otimes_2 \langle j | \hat{h}(2) | k \rangle_1 \otimes | l \rangle_2$$

$$= \frac{1}{2} [{}_1\langle i | \otimes_2 \langle j | \hat{h}(2) | k \rangle_1 \otimes | l \rangle_2 \pm_1 \langle j | \otimes_2 \langle i | \hat{h}(2) | k \rangle_1 \otimes | l \rangle_2 \pm_1 \langle j | \otimes_2 \langle i | \hat{h}(2) | k \rangle_1 \otimes | l \rangle_2 +_1 \langle i | \otimes_2 \langle j | \hat{h}(2) | k \rangle_1 \otimes | l \rangle_2]$$

thus

$$\langle ij | \hat{h}(2) | kl \rangle = {}_1\langle i | \otimes_2 \langle j | \hat{h}(2) | k \rangle_1 \otimes | l \rangle_2 \pm_1 \langle j | \otimes_2 \langle i | \hat{h}(2) | k \rangle_1 \otimes | l \rangle_2 = \sqrt{2} {}_1\langle ij | \hat{h}(2) | k \rangle_1 \otimes | l \rangle_2$$

and similarly one can get

$$\langle ij | \hat{h}(2) | kl \rangle = {}_1\langle i | \otimes_2 \langle j | \hat{h}(2) | k \rangle_1 \otimes | l \rangle_2 \pm_1 \langle i | \otimes_2 \langle j | \hat{h}(2) | l \rangle_1 \otimes | k \rangle_2 = \sqrt{2} {}_1\langle i | \otimes_2 \langle j | \hat{h}(2) | kl \rangle$$
 For

$$\text{fermions } \langle ij | \hat{h}(2) | kl \rangle = {}_1\langle i | \otimes_2 \langle j | \hat{h}(2) | k \rangle_1 \otimes | l \rangle_2 -_1 \langle i | \otimes_2 \langle j | \hat{h}(2) | l \rangle_1 \otimes | k \rangle_2$$

Equation A.1 becomes:

$$\varepsilon_\beta \langle \alpha | \beta \rangle = {}_1\langle \alpha | \hat{h}(1) | \beta \rangle_1 + \sum_{\sigma=1}^N [{}_1\langle \alpha | \otimes_2 \langle \sigma | \hat{h}(2) | \beta \rangle_1 \otimes | \sigma \rangle_2 -_1 \langle \alpha | \otimes_2 \langle \sigma | \hat{h}(2) | \sigma \rangle_1 \otimes | \beta \rangle_2]$$

$$\varepsilon_\beta | \beta \rangle = \hat{h}(1) | \beta \rangle + \sum_{\sigma=1}^N [{}_2\langle \sigma | \hat{h}(2) | \beta \rangle_1 \otimes | \sigma \rangle_2 -_2 \langle \sigma | \hat{h}(2) | \sigma \rangle_1 \otimes | \beta \rangle_2]$$

Since states  $|\beta\rangle$ 's are treated as the state of the real eigenstates of one particle states, for convention and convenience one can replace  $i$  with  $\beta$  and  $j$  with  $\sigma$ ;

$$\varepsilon_i |i\rangle = \hat{h}(1) |i\rangle + \sum_{j=1}^N [{}_2\langle j | \hat{h}(2) | j \rangle_2 \otimes |i\rangle_1 - {}_2\langle j | \hat{h}(2) | j \rangle_1 \otimes |i\rangle_2]$$

Introduce an  ${}_1\langle i | i \rangle_1$  term and multiple it to the last term,

$$\varepsilon_i |i\rangle = \hat{h}(1) |i\rangle + \sum_{j=1}^N [{}_2\langle j | \hat{h}(2) | j \rangle_2 \otimes |i\rangle_1 - {}_2\langle j | \hat{h}(2) | j \rangle_1 \otimes |i\rangle_2 \bullet {}_1\langle i | i \rangle_1]$$

$$\varepsilon_i |i\rangle = \{\hat{h}(1) + \sum_{j=1}^N [{}_2\langle j | \hat{h}(2) | j \rangle_2 - {}_2\langle j | \hat{h}(2) | j \rangle_1 \otimes |i\rangle_2 \bullet {}_1\langle i | i \rangle_1] \otimes |i\rangle_1$$

For computation reason, one needs to work the problem in the wave function basis. Using the direct product (Hartree product) to approximate tensor product, and define  $|x_1, x_2\rangle = |x_1\rangle |x_2\rangle$  for simplicity using  $\hat{h}(1) = \int dx h(x) |x\rangle \langle x|$ ,  $\hat{h}(2) = \int dx_1 dx_2 h(x_1, x_2) |x_1, x_2\rangle \langle x_1, x_2|$  and  $\langle x_1 | i \rangle = \varphi_i(x_1)$ .

After some algebra, one can get the Hartree-Fock equation in the spatial representation:

$$\varepsilon_i \varphi_i(x_1) = \left\{ \hat{h}(x_1) + \sum_{j=1}^N \left[ \int dx_2 \varphi_j^*(x_2) h(x_1, x_2) \varphi_j(x_2) - \int dx_2 \varphi_j^*(x_2) h(x_1, x_2) \varphi_i(x_2) \int dx_1' \varphi_j(x_1') \varphi_i^*(x_1') \right] \right\} \varphi_i(x_1)$$

It is convention to define some terms. Firstly the *Coulomb* term:

$$J_j(x_1) = \int dx_2 \varphi_j^*(x_2) h(x_1, x_2) \varphi_j(x_2) = \int dx_2 h(x_1, x_2) |\varphi_j(x_2)|^2$$

$$\text{and the exchange term: } K_j(x_1) = \int dx_2 \varphi_j^*(x_2) h(x_1, x_2) \varphi_i(x_2) \int dx_1' \varphi_j(x_1') \varphi_i^*(x_1')$$

$$\text{which satisfies the exchange relation } K_j(x_1) \varphi_i(x_1) = \int dx_2 \varphi_j^*(x_2) h(x_1, x_2) \varphi_i(x_2) \varphi_j(x_1)$$

then the Fock operator can be written in spatial representation as:

$$\hat{f}(x_1) = \hat{h}(x_1) - \sum_{j=1} [J_j(x_1) - K_j(x_1)]$$

Write the H-F equation in compact form:

$$\varepsilon_i \varphi_i(x_1) = \hat{f}(x_1) \varphi_i(x_1)$$

In the real world, however, the basis usually is not orthogonal e.g. the atomic orbital basis, therefore for molecular system it is necessary to expand the basis in the non-orthogonal basis

$$\{ \chi_\mu \}, \text{ i.e. } \varphi_i(x_1) = \sum_{\mu=1} C_{\mu i} \chi_\mu(x_1)$$

Plug it back into H-F equation and multiply  $\chi_\nu^*(x_1)$  from left and integrate both sides, one can obtain Roothaan equation:

$$\varepsilon_i \sum_{\mu=1} C_{\mu i} \int dx_1 \chi_\nu^*(x_1) \chi_\mu(x_1) = \sum_{\mu=1} C_{\mu i} \int dx_1 \chi_\nu^*(x_1) f(x_1) \chi_\mu(x_1)$$

$$\text{Define } S_{\nu\mu} = \int dx_1 \chi_\nu^*(x_1) \chi_\mu(x_1) \text{ and } F_{\nu\mu} = \int dx_1 \chi_\nu^*(x_1) f(x_1) \chi_\mu(x_1)$$

We can finally get the matrix form

$$\varepsilon_i \sum_{\mu=1} S_{\nu\mu} C_{\mu i} = \sum_{\mu=1} F_{\nu\mu} C_{\mu i},$$

or more compactly SCF=FC

With this equation one can solve originally many-particle problem as one-particle problem in the iterative fashion:

6. Input the trial coefficients  $C_{\mu i}$ 's.

7. Form matrix form of Fock operator  $F$  with the assists of necessary integral terms.
8. Diagonalize the Fock matrix and obtain new sets of eigenfunctions that contain the new coefficients.
9. Compare the new coefficients with initial guess. If they are convergent in certain criterion, then the Self-consistent-field procedure is done; otherwise,
10. Generate new set of coefficients base on previous trials and go back to step 2 until reach the threshold.

Some points should be discussed:

1. The summation of the eigenvalues  $\varepsilon_i$  of Hartree-Fock operator is not in the sense of the ground state energy  $E_0$  of the many-particle system instead by comparing the ground state energy they have certain relation as:

$$E_0 = \sum_{i=1}^N \varepsilon_i - \frac{1}{2} \sum_{i,j=1}^N \langle ij | \hat{V}(1,2) | ij \rangle = \sum_{i=1}^N \varepsilon_i - \sum_{j=1}^N [J_j(x_1) - K_j(x_1)]$$

According Koopmans' theory,  $\varepsilon_i$  should associate with the electron affiliation energy.

2. Alternatively, one can define the  $H$  in another way. If one defines the two particle interaction as  $V_{ijkl} = {}_1\langle i | \otimes {}_2\langle j | \hat{h}(2) | k \rangle_1 \otimes | l \rangle_2$ , and in the definition the Hamiltonian becomes

$$\hat{H} = \sum_{i,j=1} \langle i | \hat{h}(1) | j \rangle C_i^+ C_j + \frac{1}{2} \sum_{i,j,k,l=1} V_{ijkl} C_i^+ C_j^+ C_l C_k$$

This is common form used in literatures and can be checked that it has the same matrix elements as form 1 or directly obtained by using more elegant anti-symmetric operator method.

For deduction reason we still define Hamiltonian  $H = h(1) + V(1, 2)$  in the form 1.



## Appendix B

### Non Equilibrium Green's Function formalism

B1 Six Green's functions and some useful identities:

$$1. \text{ Lesser Green's function } G^<(t, t') = \frac{i}{\hbar} \langle \hat{\phi}^+(t') \hat{\phi}(t) \rangle$$

$$2. \text{ Greater GF: } G^>(t, t') = -i \langle \phi(t) \phi^+(t') \rangle$$

$$3. \text{ Causal GF: } G(t, t') = \theta(t - t') G^>(t, t') + \theta(t' - t) G^<(t, t')$$

$$4. \text{ Anti-causal GF: } G'(t, t') = \theta(t' - t) G^>(t, t') + \theta(t - t') G^<(t, t')$$

$$5/6. \text{ Retarded/Advanced GF: } G^{r,a} = \pm \theta(\pm t' \mp t) [G^>(t, t') - G^<(t, t')]$$

Relations between the Green's functions:

$$1. G^R - G^A = G^> - G^< \quad \text{B.1}$$

$$2. \Sigma^R - \Sigma^A = \Sigma^> - \Sigma^< \quad \text{B.2}$$

$$3. [G^R]^+ = G^A, [G^>]^+ = G^<$$

$$4. [\Sigma^R]^+ = \Sigma^A, [\Sigma^>]^+ = \Sigma^<$$

$$1^*. G^R - G^A = G^R - G^{R+} = -2i \text{Im}[G^R] \quad \text{B.1}^*$$

$$2^*. \Sigma^R - \Sigma^A = \Sigma^R - \Sigma^{R+} = -2i \text{Im}[\Sigma^R] \quad \text{B.2}^*$$

Two important Keldysh equations:

$$1. G^{<>} = [1 + G^R \Sigma^R] G_0^{<>} [1 + G^A \Sigma^A] + G^R \Sigma^{<>} G^A, \quad \text{B.3}$$

The first term on the right hand-side of (B.3) accounts for the initial conditions. One can show that this term vanishes for steady-state systems, if the system was in a non-interacting state in the infinite past, and if the system is in the non-interaction or interacting at a mean-field level.<sup>76</sup> For the two-probe system, the central region using the DFT calculation experiences mean field treatment, thus it is legitimate to only consider the second term.

$$2. \Sigma^{<>} = [1 + G^R \Sigma^R] \Sigma_0^{<>} [1 + G^A \Sigma^A] + \Sigma^R G^{<>} \Sigma^A \quad \text{B.4}$$

For impurity scattering case, the unperturbed terms equal zeros, only the second terms survive,<sup>76</sup> in the two-probe system with different potential bias it is legitimate to say  $\Sigma_0^{<>} = 0$ , therefore equations B.3 and B.4 become:

$$G^{<>} = G^R \Sigma^{<>} G^A, \quad \text{B.5}$$

$$\Sigma^{<>} = \Sigma^R G^{<>} \Sigma^A, \quad \text{B.6}$$

If plugging B.5 back into B.1, one can obtain expression

$$G^R - G^A = G^R (\Sigma^> - \Sigma^<) G^A \quad \text{B.7}$$

More expression could be revealed but not relevant to this project.

B2 Lesser self-energy  $\Sigma_a^<$  at each lead.

The Lesser self-energy term  $\Sigma^<$  is function of  $G^<$  and can be calculated with help of retarded self-energy  $\Sigma^R$  and advanced self-energy  $\Sigma^A$  of the electrode-molecule interactions. In the steady

state and  $(\mathbf{k}, E)$  representation, the non-interaction Lesser Green's function can be calculated by defining the line-width function  $\Gamma = i[\Sigma^R - \Sigma^A] = i[\Sigma^> - \Sigma^<]$ , and spectral function

$$A(k, E) = i \frac{G^R - G^A}{2\pi} = i \frac{G^> - G^<}{2\pi} = i \frac{G^R \Gamma G^A}{2\pi} \quad \text{B.8}$$

According to fluctuation-dissipation theorem in the grand canonical equilibrium with chemical potential  $\mu$ , the equilibrium Lesser Green's function can be written as:

$$G_\alpha^< = 2\pi i f(E - \mu_\alpha) A_\alpha(k, E) = -f(E - \mu_\alpha) (G_\alpha^R - G_\alpha^A) = -f(E - \mu_\alpha) (G_\alpha^> - G_\alpha^<) \quad \text{B.9}$$

The subscript  $\alpha$  means the equilibrium left or right electrodes separately. Plug it into Eq. B.6, using Eq. B.2; one can obtain the Lesser self-energy for the equilibrium case, the subscript  $\alpha$  omitted.

$$\begin{aligned} \Sigma^< &= \Sigma^R G^< \Sigma^A = -f(E - \mu) (\Sigma^R G^> \Sigma^A - \Sigma^R G^< \Sigma^A) = -f(E - \mu) (\Sigma^> - \Sigma^<) \\ &= i f(E - \mu) \Gamma \end{aligned} \quad \text{B.10}$$

This is the equation Eq.3.6 used in section 3.1.2. And use B.9 one can find the final expression for Lesser Green's function Eq. 3.6 for each electrode/lead. The only question is to handle the Retarded self-energy at the lead/electrode  $\Sigma_R^R$  and  $\Sigma_L^R$  as in Eq.3.6. Keep in mind that Eq. B.9 and Eq.B.10 are only valid in equilibrium cases; we can not use them directly to the non-equilibrium two-probe system, but the summation of  $\Sigma_L^<$  and  $\Sigma_R^<$  the self energies of left and right leads/electrodes which are in equilibrium separately.

### B3. The expression for current

Here we outline some important points about the current definition and details can be found in Di Ventra<sup>27</sup> Page237-242, and Haug<sup>77</sup> Page162-165. For the Left electrode, current is defined as expectation value of the time derivative of occupation number operator  $\hat{n}_L$ :

$$I_L = -e \left\langle \frac{d\hat{n}_L}{dt} \right\rangle = -\frac{ie}{\hbar} \langle [\hat{H}, \hat{n}_L] \rangle$$

After working on the two-probe system Hamiltonian  $\hat{H}$  and  $\hat{n}_L$  which is related to Lesser Green's function, one can find the final result in energy representation:

$$I_L = \frac{ie}{\hbar} \int \frac{dE}{2\pi} \text{Tr} \{ \Gamma_L(E) G^<(E) + \Gamma_L(E) f(E - \mu_L) [G^R(E) - G^A(E)] \}$$

The right electrode current expression is just change subscript  $L$  to  $R$ , and in steady state total current is the same from either side except the direction thus  $I = I_L = -I_R$  and  $I = \frac{I_L - I_R}{2}$

And the total current can be formally written with spin included (multiple by 2) as:

$$I = \frac{ie}{\hbar} \int \frac{dE}{2\pi} \text{Tr} \{ [\Gamma_L(E) - \Gamma_R(E)] G^<(E) + [\Gamma_L(E) f(E - \mu_L) - \Gamma_R(E) f(E - \mu_R)] [G^R(E) - G^A(E)] \}$$

B.11

This is the general form for current and starting point for many calculations.

If one assume  $\Gamma_L(E) = c\Gamma_R(E)$  with  $I = xI_L - (1-x)I_R$  then B.10 can be simplified as

$$I = \frac{2ie}{\hbar} \int \frac{dE}{2\pi} [f(E - \mu_L) - f(E - \mu_R)] \times T_\Delta(E), \quad \text{B.12}$$

$$T_{\Delta}(E) = Tr \left\{ \frac{\Gamma_L(E)\Gamma_R(E)}{\Gamma_L(E) + \Gamma_R(E)} [G^R(E) - G^A(E)] \right\}$$

This is another form of NEGF current.

In the non-interaction or mean field approximation, the current expression B.11 can be simplified further. Substitute the expression for Lesser Green's function  $G^<$  in Eq. 3.7 back Eq. B.11, and in the two-probe model the total line-width function only includes left and right effects  $\Gamma = \Gamma_L(E) + \Gamma_R(E)$ , then Eq. B.7 reads

$$G^R - G^A = G^R(\Sigma^> - \Sigma^<)G^A = G^R\Gamma G^A = G^R[\Gamma_L(E) + \Gamma_R(E)]G^A \quad \text{B.13}$$

Plug this back B.11 too, after some algebra with trace cyclic property one can finally obtain the NEGF-DFT version current:

$$I = \frac{e}{\pi\hbar} \int_{-\infty}^{+\infty} dE [f(E - \mu_L) - f(E - \mu_R)] T(E), \text{ where } T(E) = \text{Tr}[\Gamma_L(E)G_M^R(E)\Gamma_R(E)G_M^A(E)]$$

This is the current defined in Eq. 3.8 and also is the equilibrium current without applying NEGF, i.e. Landauer approach. By comparing it with Eq. B.12, one may tend to recognize  $T_{\Delta}(E)$  as NEGF transmission coefficient/probability like  $T(E)$  in Eq.3.8. However, this is only true in non-interaction or mean field case and assumption  $\Gamma_L(E) = c\Gamma_R(E)$ , i.e. in general non-equilibrium cases there are no transmission coefficient/probability.

At last, it is better to reemphasize that the two-probe model is mean-field model in the central region and the only non-equilibrium interactions are from two leads/electrodes. With these assumptions, one applies the short versions of NEGF equations to calculate relevant physical quantities.

#### B4. Another form of Lesser Green's function and electron density

Lesser Green's function is written as Eq. 3.7

$$G^<(E) = iG^R(E)[\Gamma_L(E)f(E - \mu_L) + \Gamma_R(E)f(E - \mu_R)]G^R(E)^+$$

By adding and subtracting  $iG_{MM}^R(E)\Gamma_R(E)f(E - \mu_L)G_{MM}^R(E)^+$  to it and rearrange the terms, one can obtain

$$\begin{aligned} G^<(E) &= iG^R(E)[\Gamma_R(E) + \Gamma_L(E)]G^R(E)^+ f(E - \mu_L) \\ &+ iG^R(E)\Gamma_R(E)[f(E - \mu_R) - f(E - \mu_L)]G^R(E)^+ \end{aligned}$$

By recalling Eq. B.13, and Eq. B1\*, we can write,

$$G^<(E) = -2i \text{Im}[G^R(E)]f(E - \mu_L) + iG^R(E)\Gamma_R(E)G^{R+}(E)[f(E - \mu_L) - f(E - \mu_R)]$$

If the system is in equilibrium, then  $f(E - \mu_L) = f(E - \mu_R)$  and we have the equilibrium Lesser Green's function:

$$[G^<(E)]^{eq} = -2i \text{Im}[G^R(E)]f(E - \mu_L)$$

This is essentially Eq. B.9 fluctuation-dissipation theorem in equilibrium state a genuinely equilibrium state.

There is another case the system can reach a semi-equilibrium state when energy is low.

From Eq. 3.4 we know that electron density is the energy integration of diagonal elements of Lesser Green's function and if the energy is sufficiently small, say  $E < \mu_{L(R)} - 10/\beta$ , even if there

is potential difference between two electrodes, i.e. non-equilibrium, then

$$f(E - \mu_L) = f(E - \mu_R) \approx 1,$$

$$n(\vec{r}) = \frac{1}{2\pi i} \int dE G^<(\vec{r}, \vec{r}; E) \text{ becomes}$$

$$n(\vec{r}) = -\frac{1}{\pi} \int_{-\infty}^{\mu_{\min}} dE \text{Im}[G^R(E)] + \frac{1}{2\pi i} \int_{\mu_{\min}}^{\mu_{\max}} dE G^<(\vec{r}, \vec{r}; E) \quad \text{B.14}$$

$\mu_{\min} \equiv \min\{\mu_L + \Delta V_L, \mu_R + \Delta V_R\} - V'$ ,  $\mu_{\max} \equiv \max\{\mu_L + \Delta V_L, \mu_R + \Delta V_R\} + V'$ ,  $\Delta V_{L(R)}$  is the electrical

potential energy for each electrode, normally set as the half of total bias times  $e$ ,  $\Delta V_{L(R)} = \pm \frac{eV_b}{2}$ ,

and  $V'$  is the cutoff energy for the range of energy integration, say  $10/\beta(\text{eV})$ .

Formally, the electron density splits into ‘equilibrium’ part and ‘non-equilibrium’ part depending on the energy integration ranges:

$$n(\vec{r}) = n^{eq}(\vec{r}) + n^{non-eq}(\vec{r})$$

## VITA

# Yong Xue

University of Illinois at Chicago, Department of Physics (M/C 273)  
 845 West Taylor St., Chicago, IL 60607  
 Tel: 312-823-0879 E-mail: [yxue4@uic.edu](mailto:yxue4@uic.edu)

## Academic Interests and Expertise

Nanoscience  
 Molecular Self-Assembly  
 Molecular Electronics  
 Classic and Quantum Molecular Dynamics (MD) Simulations  
 Non-equilibrium Green's Function (NEGF) based Quantum Conductance Calculations  
*ab initio* and Density Functional Theory(DFT) quantum Calculations  
 Ambient AFM/STM Experiments

## Education

- 2008-2012 *University of Illinois at Chicago (UIC)*  
 Doctor of Philosophy, Physics  
 Specified in computational and experimental studies of nanoscale systems  
 Dissertation entitled "Lower Diamondoids as Molecular Building Blocks"
- 2005-2008 *University of Illinois at Chicago*  
 Master of Science, Physics  
 GPA 3.3/4.0
- 2001-2005 *Sichuan University (SCU)*  
 Bachelor of Science, Microelectronics  
 GPA 3.5/4.0

## Theoretical and Computational Research Experience

- Research Assistant*, University of Illinois at Chicago  
 Advisor: G Ali Mansoori  
 Concentration: theoretical studies of lower diamondoids and their derivatives.
- 2011- 2012 Investigated *ab initio*/Classic MD simulation studies of chemical reaction properties of the derivatives of adamantane to form electronic-conducting paths
- 2008- 2011 Examined MD simulations and DFT calculation to study the self-assembly and phase transition properties of lower diamondoids and their derivatives



2007- 2008      Analyzed the First Principal studies of the properties of single molecular lower diamondoids and their derivatives, including electronic and geometrical properties, quantum Conductance

## Experimental Research Experience

*Student User*, Center for Nanoscale Materials (CNM)  
Argonne National Laboratory (ANL)  
Supervisor: Lashen Assauid

2011              Inspected 4-probe system study of adamantane on Si substrate

2010-2011        Devised UHV-STM single molecular study of adamantane on Cu substrate and collaborated with UHV group at UIC and X-ray group at ANL

2008-2009        Inspected ambient AFM/STM studies of adamantane-thiol monolayer on Au/Mica

## Teaching Experience

2005-2012      *Teaching assistant*, Department of Physics, UIC

- Conducted and designed two-hour problem-solving workshop for calculus based physics for three semesters
- Taught undergraduate level physics labs and discussion courses
- Tutored undergraduate students physics for 7 years

2009-2012      *Tutor*, Trio Academic Support Program, UIC

- Tutored undergraduate level physics, mathematics
- Helped students prepare for physics section on MCAT

2010              *Instructor*, SALC Summer Program, UIC

Taught freshman mathematics, resulting in college readiness and level achievement through preparation assistance

## Honors and Activities

2010              Best Student Poster Presenter Award, MRS 2010 Fall Meeting symposium A  
GSC Travel Award, Graduate Student Council, UIC

2009              Student Presenter Award for oral presentation in Nanotech 2009, UIC

2007              Vice Present of Chinese Student and Scholars Association, UIC

2004              Second prize for *The Red Ribbon*, a national Chinese college student poem contest

2003              Outstanding Student, Second Prize Scholarship, SCU  
Team leader of top-rated student volunteer program, SCU

2002              Outstanding Student, First Prize Scholarship, SCU

## Presentations and Conferences

- 2012      10th Annual CNST Workshop, UIUC  
             1<sup>st</sup> Frontiers of Diamondoids Science Symposium, Stanford University
- 2011      UIC Science Engineering South (SES) Building Science Exhibition, UIC
- 2010      Material Research Society (MRS) 2010 Fall Meeting, Boston
- 2009      Nanotech 2009, Houston

## Language Skills

Chinese Mandarin

## Computer Abilities

- Proficient in Quantum computation and MD simulation packages: Gaussian03, Gromacs, VMD, ATK-VNL package, CPMD
- Familiar with Molecular construction software: Mercury, Encifer, Avogadro, OpenBabel
- Experienced in MATLAB, C-programming language, Linux commands

## Publications

Elmo Silvano de Araujo, G. Ali Mansoori, Yong Xue and Patricia Lopes Barros de Araujo: Diamondoid molecules behavior prediction by *ab initio* methods. *Physics Express*, 2011, 1(2), 67-88

Yong Xue and G. Ali Mansoori: Phase Transition and Self-assembly of Lower Diamondoids and Derivatives. *MRS Proceedings*, 2011, 1282

Yong Xue and G. Ali Mansoori: Self-Assembly of Diamondoid Molecules and Derivatives (MD Simulations and DFT Calculations) *Int. J. Mol. Sci.* 2010, 11, 288-303

Yong Xue and G. Ali Mansoori: Quantum Conductance and Electronic Properties of Lower Diamondoids and Their Derivatives. *Int. J. of Nanoscience*, 2008, 7(1), 63-72